P-11-01

Site investigation SFR

Fracture mineralogy and geochemistry of borehole sections sampled for groundwater chemistry and Eh

Results from boreholes KFR01, KFR08, KFR10, KFR19, KFR7A and KFR105

Björn Sandström, WSP Sverige AB

Eva-Lena Tullborg, Terralogica AB

January 2011

Svensk Kärnbränslehantering AB
Swedish Nuclear Fuel
and Waste Management Co

Box 250, SE-101 24 Stockholm
Phone +46 8 459 84 00

ISSN 1651-4416
SKB P-11-01

Site investigation SFR

Fracture mineralogy and geochemistry of borehole sections sampled for groundwater chemistry and Eh

Results from boreholes KFR01, KFR08, KFR10, KFR19, KFR7A and KFR105

Björn Sandström, WSP Sverige AB

Eva-Lena Tullborg, Terralogica AB

January 2011

Keywords: SFR, Forsmark, Geology, Fracture mineralogy, Hydrogeochemistry, Borehole, AP SFR-10-009.

Abstract

This report is part of the complementary site investigations for the future expansion of SFR. The report presents the results obtained during a detailed mineralogical and geochemical study of fracture minerals in drill cores from borehole section sampled for groundwater chemistry and where down-hole Eh measurements have been performed. The groundwater redox system comprises not only the water, but also the bedrock/fracture mineral system in contact with this water. It is thus important to gain knowledge of the solid phases in contact with the groundwater, i.e. the fracture minerals. The samples studied for mineralogy and geochemistry, here reported, were selected to represent the fracture surfaces in contact with the groundwater in the sampled borehole sections and will give input to the hydrogeochemical model (SFR SDM).

The mineralogy was determined using SEM-EDS and XRD and the geochemistry of fracture filling material was analysed by ICP-AES and ICP-QMS. The most common fracture minerals in the samples are mixed layer clay (smectite-illite), illite, chlorite, calcite, quartz, adularia and albite. Other minerals identified in the borehole sections include laumontite, pyrite, barite, chalcopyrite, hematite, Fe-oxyhydroxide, muscovite, REE-carbonate, allanite, biotite, asphaltite, galena, sphalerite, arsenopyrite, uranium phosphate, uranium silicate, Y-Ca silicate, monazite, xenotime, harmotome and fluorite.

There are no major differences between the fracture mineralogy of the investigated borehole sections from SFR and the fracture mineralogy of the Forsmark site investigation area. The four fracture mineral generations distinguished within the Forsmark site investigation are also found at SFR. However, some differences have been observed: 1) Barite and uranium minerals are more common in the SFR fractures, 2) clay minerals like mixed layer illite-smectite and illite dominates in contrast to Forsmark where corrensite is by far the most common clay mineral and, 3) REE-carbonates which were not identified in the samples from the Forsmark site investigation occur on many of the analysed fracture surfaces.

Sammanfattning

Denna rapport är en del av de kompletterande platsundersökningarna för den framtida utbyggnaden av SFR. I rapporten presenteras resultaten från detaljerade mineralogiska och geokemiska studier av sprickfyllnadsmaterial i borrkärnor från borrhålssektioner där grundvattenprovtagning med avseende på redox-systemet har genomförts. Redox-systemet i berggrunden består av grundvattnet och mineralen i kontakt med grundvattnet, därför är det viktigt att ha kunskap om sprickmineralogin för att förstå grundvattnets hydrogeokemi. De mineralogiska och geokemiska data som presenteras i denna rapport är representativa för de sprickytor som är i kontakt med grundvattnet i de provtagna borrhålssektionerna och har till syfte att bidra till den hydrogeokemiska modellen (SFR SDM).

Mineralogin bestämdes med hjälp av SEM-EDS och XRD och geokemiska analyser utfördes med ICP-AES/QMS. De vanligaste sprickmineralen i de provtagna sektionerna är blandskikts-lemineral (illit-smektit), illit, klorit, kalcit, kvarts, adularia och albit. Andra mineral som har identifierats är laumontit, pyrit, baryt, hematit, arsenopyrit, kopparkis, järnoxyhydroxid, muskovit, REE-karbonat, allanit, biotit, asfaltit, blyglans, zinkblände, uranfosfat, uransilikat, Y-Ca silikat, monazit, xenotim, harmotom, fluorit.

Generellt är det inte några stora skillnader mellan sprickmineralogin i de provtagna sektionerna från SFR och sprickmineralogin som observerades vid platsundersökningarna i Forsmark. De fyra generationerna av sprickmineral identifierade under platsundersökningarna i Forsmark återfinns även i proverna från SFR. Några skillnader kan dock urskiljas: baryt och uranmineral är vanligare i SFR-proverna, andra sprickmineral dominerar (blandskikts-lermineralet illit-smektit samt illit). REE-karbonat som inte identifierats i några prover från platsundersökningarna i Forsmark har hittats på flera sprickytor från SFR.

Contents

1 Introduction

During 2008, SKB initiated an investigation for the future expansion of the final repository for low and middle level radioactive operational waste, SFR. This document reports the results gained by a detailed fracture mineralogy investigation of drillcore material. The study is part of complementary site investigations for the SFR-extension project.

The investigation is limited to studies of borehole sections where redox-data (downhole Eh-measurements and geochemistry) are available from the groundwater. The sampled sections are presented in Table 1-1 and the location of the boreholes in Figure 1-1.

Original data from the reported activity are stored in the primary database Sicada. Data are traceable in Sicada by the activity plan number (AP SFR-10-009). Only data from Sicada are accepted for further interpretation and modelling. The data presented in this report are regarded as copies of the original data. Data in the database may be revised, if needed. However, such revision of the database will not necessarily result in a revision of this report.

Controlling documents for performing this activity are given in Table 1-2. Both the activity plan and the method description are SKB's internal controlling documents.

Table 1-1. SFR borehole sections included in the detailed fracture mineralogy study.

Borehole (Idcode)	Secup (m)	Secup (m)	Elevation Secmid (m.a.s.l.)
KFR01	44.5	62.3	–94.23
KFR08	63.0	104.0	–80.94
KFR10	87.0	107.3	–146.99
KFR19	95.0	110.0	–56.35
KFR7A	48.0	74.7	–134.43
KFR105	120.0	134.0	–128.38
KFR105	265.0	306.8	–153.59

Table 1-2. Controlling documents for performance of the activity.

Activity plan	Number	Version
Sprickmineralogiska undersökningar i SFR. Provtagningar och studier av borrkärnor från utvalda borrhålssektioner i sex borrhål.	AP SFR-10-009	1.0
Method description		
Sprickmineralogi	SKB MD 144.000	1.0

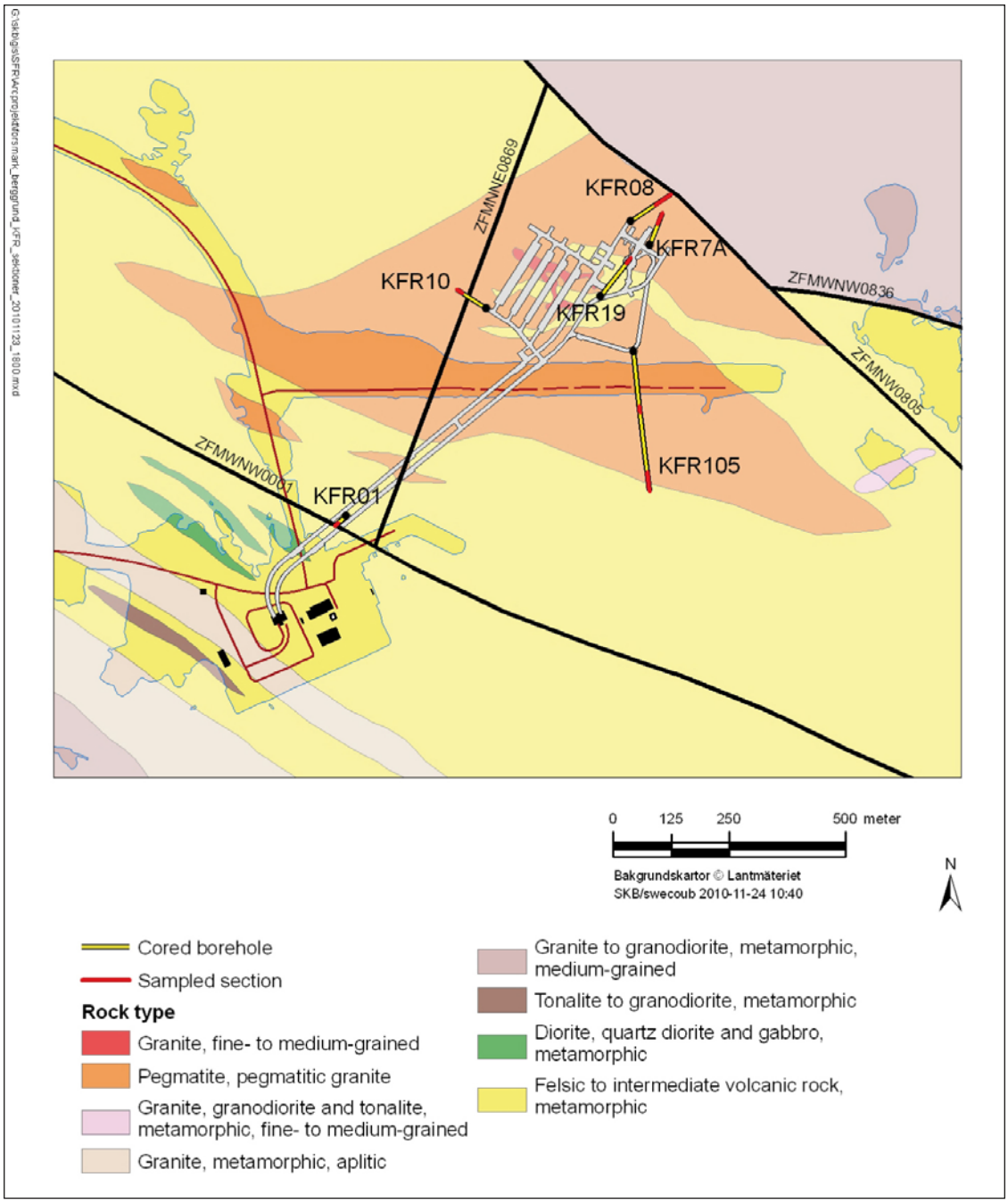

Figure 1-1. *Bedrock geology of the SFR area with surface projections of the sampled boreholes. The sampled borehole sections are showed by red colour on the projections. Surface intercepts of major deformation zones and zones intersecting the sampled sections are also presented in the map.*

2 Background

Detailed studies of fracture mineralogy and wall rock alteration were carried out during the site investigations for a deep repository of spent nuclear fuel in Forsmark (PLU) between 2002 and 2007 /Sandström and Tullborg 2009, Sandström et al. 2006, 2008, 2009, 2010/. During these studies, a sequence with four major events of fracture mineralisation was distinguished based on e.g. cross-cutting relations, stable isotopes and $^{40}Ar/^{39}Ar$ dating. The sequence of events are summarised below.

Generation 1: Precipitation of epidote, chlorite and quartz under hydrothermal conditions at temperatures between ca. 200° and 300°C in preferably sub-horizontal to gently-dipping fractures and fracture zones but also in steep WNW-ENE to NW-SE fractures. The wall rock was hydrothermally altered and red-stained by hematite dissemination during this event. The minerals precipitated during the Proterozoic between 1.8 and 1.1 Ga. It is suggested that precipitation occurred close upon 1.8–1.7 Ga as a result of fracturing and fluid circulation during the waning stages of the Svecokarelian orogeny at conditions close to the ductile-brittle transition.

Generation 2: Hydrothermal precipitation of a sequence of fracture minerals at temperatures between 150° and 250°C. The fracture mineral generation is dominated by hematite-stained adularia and albite, prehnite, hematite-stained laumontite, calcite and chlorite which precipitated along preferably steep ENE-WSW to NNE-SSW and NNW-SSE fractures. $^{40}Ar/^{39}Ar$ ages of adularia and K-feldspar in breccias indicate that, at least, the last event of precipitation of what is considered generation 2 minerals occurred as a response to far-field effects from the Sveconorwegian orogeny around 1,107±*7* to 1,034±*3* Ma. Both reactivation of older structures and formation of new fractures and breccias are inferred during this period. The wall rock was hydrothermally altered, causing red-staining by hematite dissemination. After precipitation of these fracture minerals, a period with some dissolution of fracture minerals occurred, the age and cause of this dissolution is uncertain.

Generation 3: Fracture minerals were precipitated at temperatures between 60° and 190°C during several episodes in the Palaeozoic. $^{40}Ar/^{39}Ar$ ages of adularia indicate that the main stage of precipitation occurred after 460 Ma and before 277±1 Ma. Generation 3 is dominated by quartz, calcite and pyrite with minor occurrences of e.g. asphaltite, analcime, corrensite, galena, adularia and fluorite. Downward penetration of fluids emanating from an organic-rich sedimentary sequence overlying the basement during this period, and mixing with a deep basinal brine, is suggested to have promoted the precipitation of generation 3 minerals. The orientation of fractures lined with these minerals indicates significant reactivation of older fractures during the Palaeozoic, preferably steep ENE-WSW to NNE-SSW and sub-horizontal to gently-dipping fractures. However, formation of new fractures during this period is also inferred. Far-field effects from the Caledonian orogeny and/or elevated hydrostatic pressure due to the overburden of the Caledonian foreland basin is suggested to have caused reactivation and formation of fractures and associated migration of fluids.

Generation 4: Predominantly clay minerals and thin precipitates of calcite in hydraulically conductive fractures and zones and in open fractures in the upper part of the bedrock were formed. Minor occurrences of pyrite and goethite are also found. Precipitation has probably occurred at low temperatures (<50°C) during a prolonged period, possibly since the late Palaeozoic until present by groundwater circulation. Generation 4 minerals are mostly found in sub-horizontal to gently-dipping fractures, but also in steep NNE, ENE and NW trending fractures indicating that most of these fracture minerals have precipitated in older Proterozoic to Palaeozoic fractures. Some formation of sub-horizontal to gently-dipping fractures is also likely in the upper part of the bedrock due to stress release during loading and unloading cycles related to sedimentation episodes during the late Palaeozoic to Mesozoic and to glaciations during the Quaternary.

It is concluded that the majority of the fractures at Forsmark formed during at least two events prior to 1.0 Ga. Substantial reactivation of these fractures, and also formation of new fractures, occurred during the Palaeozoic (>277 Ma). Since then, formation of new fractures has been limited, and groundwater has preferably migrated along older fractures and zones. However, some new fractures have probably formed during later episodes due to loading and unloading cycles, preferably in the upper part of the bedrock /Claesson Liljedahl et al. 2011/.

Due to the proximity between the area investigated during the Forsmark site investigations and SFR, the areas have experienced similar geological evolution. However, some differences may exist between the two areas, possibly due to that SFR is situated outside the “tectonic lens” that borders the Forsmark site investigation are a /Stephens et al. 2007/.

3 Objective and scope

During the hydrogeochemical investigation for the future expansion of SFR, a description of the present redox system is important for the SFR site description as well as the safety assessment. The redox system in the bedrock comprises of the groundwater and the minerals in contact with the groundwater. In order to understand the groundwater hydrogeochemistry, knowledge of the solid phases in contact with the groundwater, i.e. the fracture minerals, are important.

The objective of this P-report is to present data of the mineralogy and geochemistry of fracture filling material from borehole sections where redox-data from the groundwater are available. Fracture minerals have been identified using SEM-EDS and XRD. Geochemical data of fracture filling material have been obtained by ICP-AES and ICP-QMS.

The samples selected during the work with this report and the performed analyses are presented in Table 3-1.

Table 3-1. Selected samples and performed analyses. Elevation data have been extracted from SICADA (data delivery SICADA_10_124, dated 2010-11-17).

Borehole	SecUp (m)	SecLow (m)	Elevation SecUp (m.a.s.l.)	Elevation SecLow (m.a.s.l.)	Performed Analyses		
					SEM-EDS	ICP-AES/ QMS	XRD
KFR01	45.18	45.42	–87.11	–87.32	X	X	X
KFR01	47.09	47.46	–88.76	–89.08	X	X	
KFR01	49.37	49.47	–90.74	–90.82	X		
KFR01	49.99	50.03	–91.27	–91.31	X		
KFR01	61.10	61.12	–100.90	–100.91	X		
KFR7A	49.60	50.04	–134.02	–134.03	X	X	X
KFR7A	68.80	68.90	–134.69	–134.69	X	X	
KFR7A	70.05	70.12	–134.73	–134.74	X	X	X
KFR7A	70.47	70.52	–134.75	–134.75	X	X	X
KFR7A	73.74	73.91	–134.86	–134.87	X		
KFR08	69.22	69.50	–92.05	–92.08	X		
KFR08	76.77	77.27	–92.71	–92.75	X	X	X
KFR08	79.13	79.41	–92.92	–92.94	X		X
KFR08	85.96	86.13	–93.51	–93.53	X		
KFR08	95.29	95.54	–94.33	–94.35	X	X	X
KFR10	95.65	95.80	–145.94	–146.04	X	X	X
KFR10	101.85	101.92	–150.32	–150.37	X		
KFR10	106.30	106.50	–153.47	–153.61	X	X	
KFR19	90.56	90.74	–59.22	–59.18	X	X	X
KFR19	91.05	91.17	–59.10	–59.07	X		X
KFR19	96.97	97.26	–57.69	–57.62	X		
KFR19	98.56	98.71	–57.31	–57.28	X		
KFR105	124.05	124.32	–127.90	–127.94	X		
KFR105	126.90	127.08	–128.37	–128.40	X	X	X
KFR105	133.50	133.75	–129.46	–129.50	X		
KFR105	267.80	268.05	–150.86	–150.90	X		
KFR105	280.07	280.13	–152.72	–152.73	X	X	X
KFR105	283.38	283.57	–153.22	–153.25	X	X	X
KFR105	298.35	298.46	–155.42	–155.43	X		

4 Execution

4.1 Sampling

The drill cores sampled for this study includes drill cores obtained during the construction of SFR facility during the nineteen-eighties, these boreholes were drilled with conventional core-drilling technique and includes boreholes KFR01, KFR7A, KFR08, KFR10 and KFR19. One of the sampled drill cores (KFR105) was drilled during 2009 within the programme for future expansion of SFR and was drilled with the triple tube technique /Curtis et al. 2010/. It is therefore likely that more fracture filling material is missing in the older drill cores due to flushing during the drilling process. The handling of the older drill cores is also more uncertain and exposure of the fracture surfaces to HCl during the drill core mapping and subsequent exposure to air for more than two decades may have affected the fracture minerals. Nevertheless, upon inspection, it was inferred that the drill core quality was sufficient for detailed fracture mineralogical studies.

The sections selected for detailed fracture mineralogical studies are sections where Eh measurements have or will be carried out /Nilsson 2011/.

During the sampling campaign, carried out 2010-10-04, the total length of the drill core sections corresponding to the borehole sections sampled for Eh were available for visual inspection at the Lentab hall at Forsmark.The entire sections were inspected and fractures interpreted to be in contact with the groundwater were sampled. This interpretation was made by inspection of the fracture surface and aided by the flow log data.

4.2 Preparations

Where enough fracture filling material was available for ICP-AES/QMS and XRD analysis, the material was scraped off using a chisel, packed in plastic sample bags and sent for analysis. If there only was enough material for one of these analyses, the method considered to acquire the most valuable data for that specific fracture sample was prioritised. One or more intact fracture surface from each sample was preserved for subsequent SEM-EDS analysis.

A rock saw was used if required for fitting the sample into the SEM-EDS sample chamber. Samples were mounted on a sample stub for the SEM-EDS analyses.

4.3 Analytical work

4.3.1 SEM-EDS

The fracture surfaces were examined by scanning electron microscopy at the University of Gothenburg, Sweden. The microscope is a Hitachi S-3400N scanning electron microscope (SEM) equipped with an INCADryCool energy dispersive X-Ray spectrometer (EDS). The instrument was operated using low-vacuum mode (15 Pa). Mineral identification was aided by EDS-spectrums and quantitative mineral analyses.

4.3.2 ICP-AES/ICP-QMS

ICP-AES/ICP-QMS analyses were carried out by ALS Scandinavia AB in Luleå, Sweden. 0.1 g sample was fused with 0.375 g $LiBO_2$ and dissolved in dilute HNO_3. LOI (Loss on ignition) is carried out at 1,000°C. Analyses are carried out according to EPA methods (modified) 200.7 (ICP-AES) and 200.8 (ICP-QMS).

4.3.3 XRD analyses

The analyses were carried out by the Geological Survey of Sweden (SGU) at Uppsala, Sweden, according to the following procedure. The samples were milled in an agate mortar before identification of major minerals. For major mineral identification, the sample powder was randomly orientated in the sample holder (and very small sample volumes on a piece of glass). Subsequently, the samples were dispersed in distilled water and treated with ultrasound for at least 45 minutes. Some of the samples had to be treated with sodium hexametaphosphate to prevent flocculation. The samples were then filtered and oriented according to /Drever 1973/. For samples of small volumes the suspension was repeatedly put on a glass plate and dried. Three measurements were carried out on each sample for clay mineral identification; 1) dried samples, 2) saturated with ethylene glycol for two hours, and finally 3) after heating to 400°C in two hours.

XRD analyses were carried out with a Siemens D5000 teta-teta diffractometer with cupper radiation (CuK α) at 40 kV and 40 mA. The X-rays were focussed with a graphite monochromator. Scans were run from 2°–65° (2-theta) or from 2°–35° (samples with preferred crystal orientation). The analyses were performed with a fixed 1° divergence, a 2 mm receiving slit and a 0.6 mm receiving slit. Clay mineral analyses were carried out using a 0.1 mm receiving slit.

The XRD raw files were taken up in the Bruker AXS software DIFFRAC PLUS v. 2.2., and evaluated in the programme EVA. The minerals were identified by means of the /ICDD 1994/ computer database. Identification was also aided by clay mineral data from /Brindley and Brown 1984, Starkey et al. 1984, Jasmund and Lagaly 1993/.

5 Results

5.1 Fracture mineralogy

A summary of the fracture mineralogy of the analysed drill core samples are presented in Table 5-1 and the identified minerals are described below. Each sample is described in more detail in Appendix 1.

Table 5-1. Fracture mineralogy of the analysed samples as determined by binocular microscope, SEM-EDS and XRD analysis.

Sample, Secup	Illite	MLC[1]	Chlorite	Quartz	Adularia	Albite	Calcite	Pyrite	Galena	Barite	U-mineral	Fe-oxide	REE-carb.	Other
KFR01 44.5–62.3 m														
KFR01 45.18 m	X		X	X				X						Allanite, muscovite
KFR01 47.09 m	X	X(i–s[2])			X		X	X		X	X(p[4])			asphaltite
KFR01 49.37 m							X	X	X					Y-Ca silicate
KFR01 49.99 m		X(i–s[2])		X	X		X	X	X	X(c[5])				Y-Ca silicate
KFR01 61.10 m				X			X	X		X				asphaltite
KFR7A 48.0–74.7 m														
KFR7A 49.60 m	X	X(i–s[2])	X	X	X	X						X(OH[7])		
KFR7A 68.80 m		X(i–s[2])			X	X					X(p[4])		X	
KFR7A 70.05 m	X			X	X	X				X		X(OH[7])		biotite
KFR7A 70.47 m	X			X	X	X	X							
KFR7A 73.74 m				X	X	X				X	X(p[4])		X	
KFR08 63.0–104.0 m														
KFR08 69.22 m		X(i–s[2])				X			X	X		X(Hm[8])	X	xenotime
KFR08 76.77 m	X	X(i–s[2])	X	X	X	X	X	X			X(p[4])	X(Hm[8])		
KFR08 79.13 m		X(corr[3])		X	X	X	X	X		X		X(Hm[8])		fluorite, REE-silicate, ChPy[9]
KFR08 85.96 m	X	X(i–s[2])		X			X	X				X(Hm[8])		monazite, AsPy[10], Sph[11]
KFR08 95.29 m		X(i–s[2])		X	X	X	X					X(Hm[8])	X	apatite
KFR10 87.0–107.3 m														
KFR10 95.65 m	X		X	X	X	X		X				X(Hm[8])		biotite, laumontite, allanite
KFR10 101.85 m				X			X	X	X					
KFR10 106.30 m		X(i–s[2], corr[3])		X	X	X		X		X				allanite
KFR19 95.0–110.0 m														
KFR19 90.56 m	X	X(i–s[2])		X	X	X	X				X(Si[6])	X(Hm[8])		
KFR19 91.05 m	X	X(i–s[2])		X	X	X	X				X(Si[6])			
KFR19 96.97 m		X(i–s[2])	X	X	X		X							allanite
KFR19 98.56 m	X			X	X	X	X			X		X(OH[7])	X	ChPy[9]
KFR105 120.0–134.0 m														
KFR105 124.05 m		X(i–s[2])	X	X	X			X		X				fluorite
KFR105 126.90 m	X	X(i–s[2])	X	X	X	X				X		X(Hm[8])		biotite
KFR105 133.50 m		X(i–s[2])		X	X	X				X(c[5])				Y-Ca silicate
KFR105 265.0–306.8 m														
KFR105 267.80 m										X			X	laumontite, muscovite, allanite
KFR105 280.07 m	X			X	X	X			X					laumontite, biotite, harmotome
KFR105 283.38 m	X	X(corr[3])	X	X	X		X					X (Hm[8])		biotite, laumontite
KFR105 298.35 m											X(Si[6])			laumontite

[1]MLC = mixed layer clay, [2](i–s) = smectite-illite
[3]corr = corrensite
[4](p) = phosphate
[5](c) = barite-celestine
[6](Si) = silicate
[7](OH) = Fe(oxy)hydroxide
[8](Hm) = hematite
[9]ChPy = chalcopyrite
[10]AsPy = arsenopyrite
[11]Sph = sphalerite

5.1.1 Description of identified fracture minerals

Mineral formulas according to /Deer et al. 1992/.

Adularia ($KAlSi_3O_8$) is usually a low temperature form of K-feldspar. The colour can be brick-red due to hematite-staining, but also greenish varieties occur in fine-grained mixtures with quartz.

Albite ($NaAlSi_3O_8$) is commonly found in fracture fillings together with hydrothermal K-feldspar (adularia). The fillings can be brick-red due to hematite-staining.

Allanite $(Ca,Mn,Ce,La,Y,Th)_2(Fe^{2+},Fe^{3+},Ti)(Al,Fe^{3+})_2O.OH[Si_2O_7][SiO_4]$ is a REE-rich epidote group member.

Arsenopyrite ($AsFeS_2$) has been identified in one fracture as a small crystal.

Asphaltite ("bergbeck" in Swedish). The term is used in a broad sense, meaning black, highly viscous to solid hydrocarbons.

Barite ($BaSO_4$) occurs as small euhedral crystals on the fracture surfaces. A Sr rich mineral (Ba,Sr) SO_4, probably solid solution between barite and celestine, has also been identified in a few samples.

Biotite $(K_2(Mg,Fe^{2+})_{6-4}(Fe^{3+},Al,Ti)_{0-2}Si_{6-5}Al_{2-3}O_{20}(OH,F)_4)$occurs in the fractures but is from the wall rock.

Calcite ($CaCO_3$) occurs abundantly and as several generations.

Chalcopyrite ($CuFeS_2$) occurs as small grains together with pyrite, galena and sphalerite.

Chlorite $((Mg,Fe,Al)_3(Si,Al)_4O_{10}(OH)_2)$ occurs abundantly and is a dark-green mineral found in several associations. XRD identifies the chlorite as clinochlore but large variations in FeO/MgO ratios are indicated from SEM-EDS analyses. The occurrence of K, Na and Ca in many of the chlorite samples indicates ingrowths of clay minerals, mostly corrensite.

Epidote $(Ca_2Al_2Fe^{3+}(SiO_4)(Si_2O_7)(O,OH)_2)$ occurs as a green filling, mainly in sealed fractures.

Fevoxyhydroxide (FeOOH), probably goethite, is found as a brownish to rust-red precipitate and is normally formed under oxidising conditions.

Fluorite (CaF_2). Violet fluorite is found in a few, mostly sealed, fractures.

Galena (PbS) occur in small amount and is generally found together with pyrite.

Goethite, see Fe-oxyhydroxide.

Harmotome $(Ba_2Al_4Si_{12}O_{32}\cdot 12H_2O)$ is a barium zeolite and has been identified in one fracture at SFR.

Hematite (Fe_2O_3) is common in the fractures but the amount is relatively low (does not often turn up in the X-ray diffractograms). However, micro-grains of hematite cause intense red-staining of many fracture coatings.

Illite $(K,H_2O)Al_2[(Al,Si)Si_3O_{10}](OH)_2)$ occurs as micro – to cryptocrystalline, micaceous-flakes, and is usually light grey in colour.

Laumontite $(CaAl_2Si_4O_{12}\cdot 4H_2O)$ is zeolite mineral. It is brittle and the crystals show prismatic shapes. The mineral itself is white, but, at Forsmark, it is stained-red due to micro-grains of hematite, although white varieties are also present.

Mixed layer clays:

Corrensite is a chlorite-like mixed-layer clay with layers of chlorite and smectite/vermiculite, usually with a ratio of 1:1. XRD analyses indicate a poorly ordered crystalline structure.

Smectite-illite is a mixed layer clay consisting of layers of smectite and illite. XRD analyses indicate a poorly ordered crystalline structure.

Pyrite (FeS_2) is found in many fractures as small euhedral, cubic crystals grown on mostly open fracture surfaces, but also together with calcite in sealed fractures.

Quartz (SiO_2) generally occurs as small and occasionally hematite-stained, euhedral crystals covering the fracture walls. They often have a greyish sugary appearance but can also be transparent and then appear to have the colour of the wall rock.

REE-carbonate (REE,Y)CO_3 occurs sparsely as small crystals on the fracture surfaces.

Smectites are a group of swelling clay minerals containing different proportions of Ca and/or Na together with Mg and Fe.

Sphalerite (ZnS) has been found in a few fractures and is commonly associated with galena and pyrite.

In addition to the minerals described above, two uranium minerals and an unidentified calcium-yttrium silicate were detected by SEM-EDS. The uranium phases consist of one poorly crystallised uranium phosphate and an unidentified uranium silicate.

5.1.2 Depth distribution of fracture minerals.

Data of the depth distribution of all open fractures and PFL-anomalies from SFR obtained during the drill core mapping are showed in Figure 5-1 and Figure 5-2. The data were extracted from Sicada (data delivery Sicada-10-083 (0:1), dated 2010-06-28). Fractures omitted from the data set are fractures from KFR24 down to SecUp 147.50 m where no core was available and fractures from the re-mapped drill-cores where no BIPS-logging have been carried out (KFR04, KFR08, KFR09, KFR13, KFR35, KFR36, KFR54, KFR55, KFR7A, KFR7B, KFR7C) /Petersson J 2010, pers. comm./.

No significant depth trends can be seen when selected redox-sensitive minerals and calcite in the sampled borehole sections are plotted against depth (Figure 5-3).

Based on these figures, it is notable that iron hydroxides occur at all depths. However, the age and origin of these occurrences are not known. It is also possible that at least some of these mapped occurrences are iron oxides, which can be difficult to distinguish macroscopically from iron hydroxides during routine drill core mapping. Asphaltite is in general only found in the upper 70 meters of the bedrock, although occurrences at greater depths have also been recorded during the drill core mapping. Pyrite is present at most depths, the absence of pyrite in PFL-anomalies in the upper 10 meters of the bedrock probably represents dissolution during events of intrusion of oxygenated fluids, but the amount of data from the upper part of the bedrock is limited. A lower frequency of hematite in the conductive fractures (PFL) is noted in the upper 500 m (compared with the frequency using all fractures). This supports the interpretations that most of the hematite is old and not related to recent low temperature oxidation.

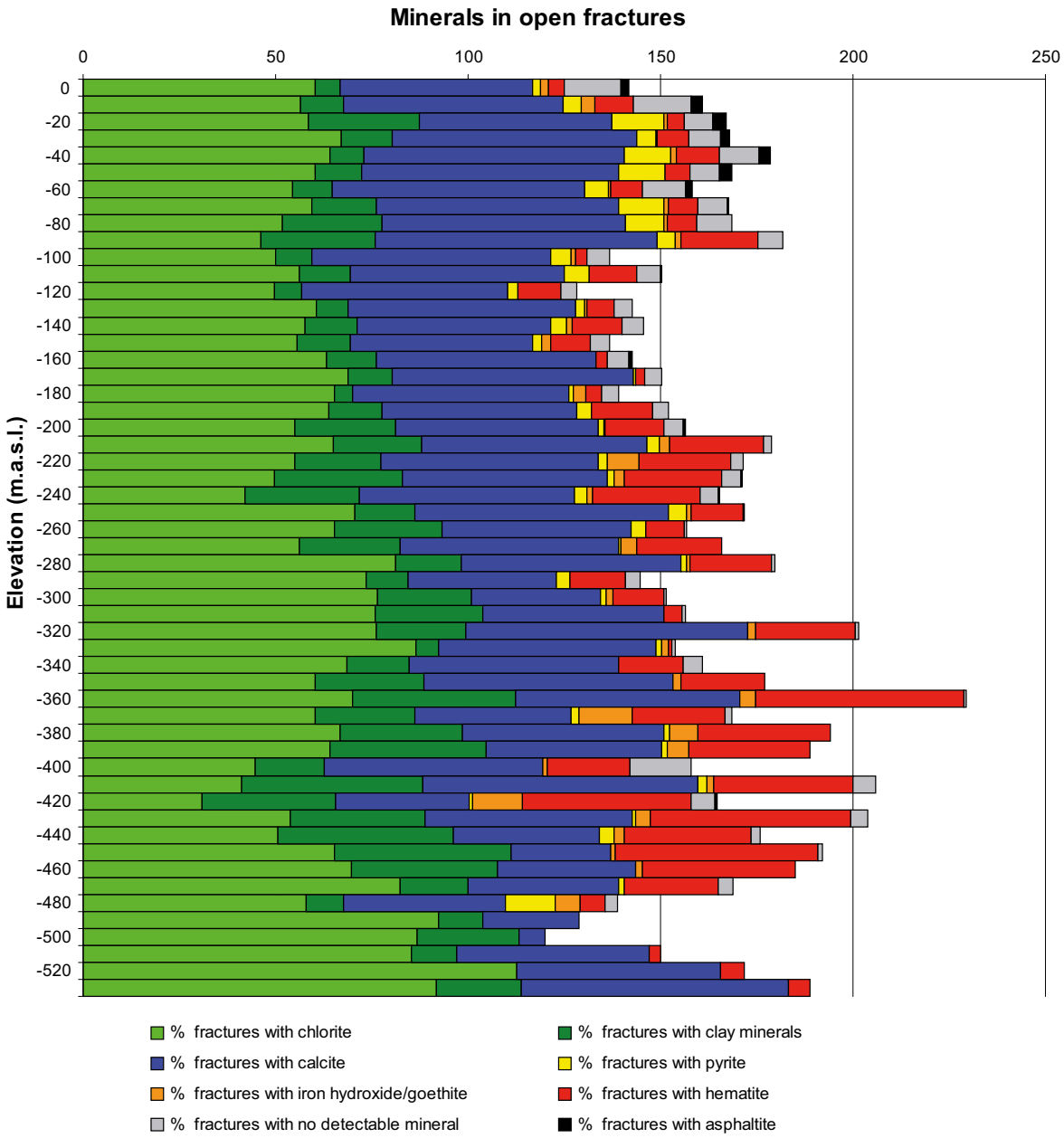

Figure 5-1. *Depth distribution of fracture minerals in all mapped open fractures from SFR.*

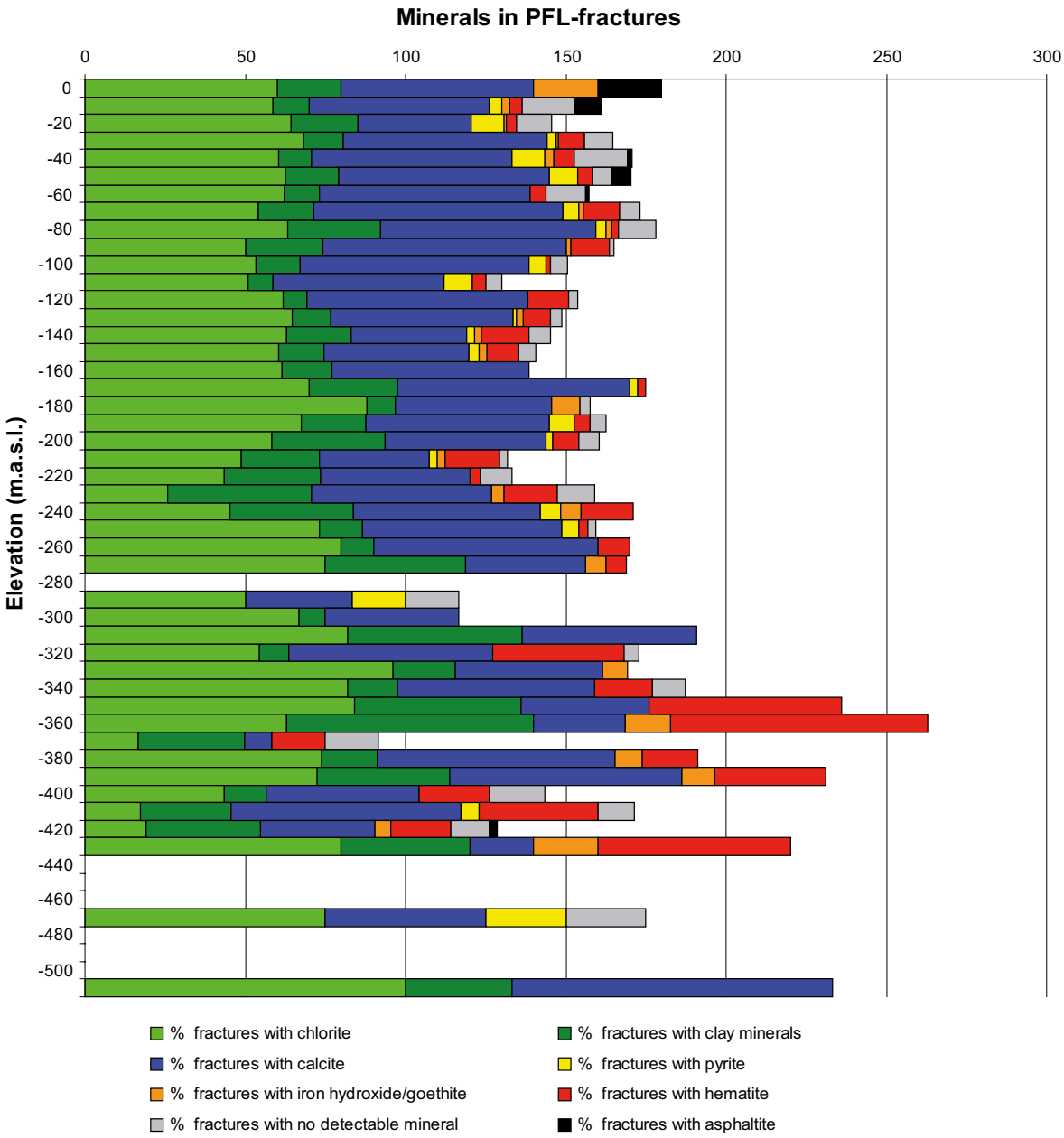

Figure 5-2. *Depth distribution of the fracture mineralogy in all mapped fractures classified as a PFL-anomaly from SFR.*

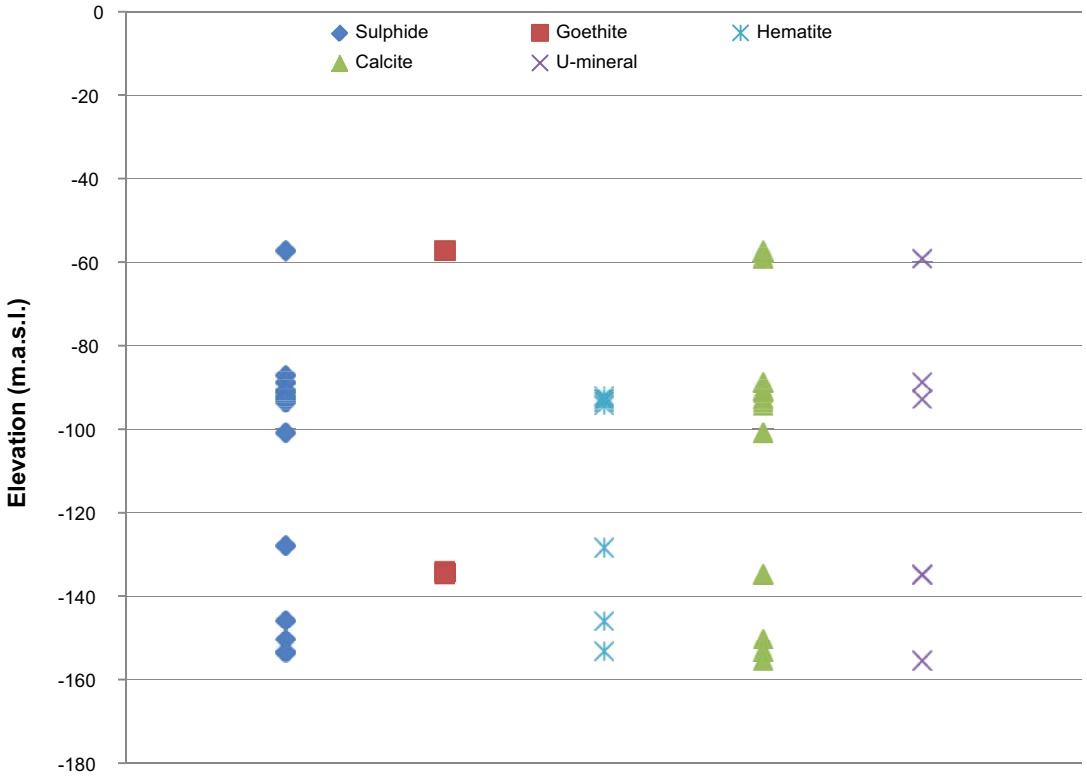

Figure 5-3. *Depth distribution of selected fracture minerals in the analysed samples. Sulphide includes pyrite, galena, chalcopyrite, sphalerite and arsenopyrite.*

Borehole section KFR1: 44.5–62.3 m

The sampled part of the drill core intercepts deformation zone ZFMWNW0001 (the Singö DZ) /Curtis et al. 2010/ and the groundwater found in this borehole section starts with a Transition type groundwater with a large Littorina component which subsequently moves towards more diluted composition with inmixing of Baltic water due to draw-down caused by the tunnel /Nilsson et al. 2010/.

Sealed fractures are frequent in the entire section. The red-stained granite is heavily fractured and open fractures coated with clay minerals and calcite are common (Figure 5-4). Asphaltite is found in several fractures.

Identified fracture minerals:

Dominating

Mixed layer clay (poorly ordered, smectite-illite), illite, chlorite, calcite.

Common

Adularia (hematite stained), pyrite, quartz.

Accessory

Allanite, barite, barite-celestine, asphaltite, uranium phosphate, galena.

Other common minerals in open and partly open fractures in deformation zone ZFMWNW0001 according to the drill core mapping /Curtis et al. 2010/ are laumontite and epidote.

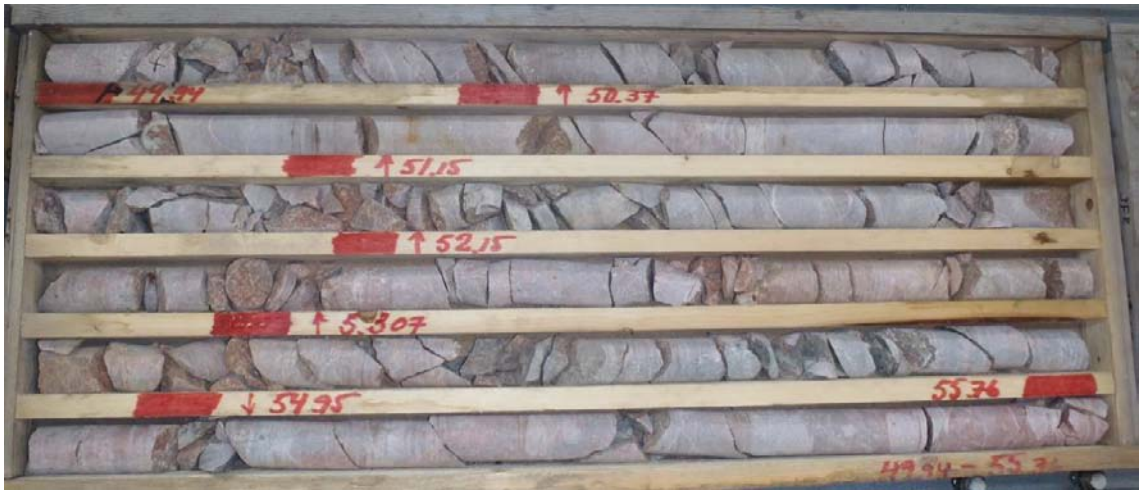

Figure 5-4. *Photograph of drill core box from part of the sampled borehole section KFR1: 44.5–62.3 m.*

5.1.3 Borehole section KFR7A: 48.0–74.7 m

The sampled part of the drill core intercepts deformation zone ZFMNW0805a /Curtis et al. 2010/ and the groundwater found in this borehole section is of Littorina type water /Nilsson et al. 2010/.

The entire section is a cross zone (Figure 5-5). Fractures subparallel with the core axis sealed with epidote and laumontite occur abundantly.

Identified fracture minerals, based on SEM-EDS and XRD analysis:

Dominating

Mixed layer clay (poorly ordered, smectite-illite).

Common

Chlorite, adularia (often hematite stained), albite, quartz, biotite, Fe-oxyhydroxide.

Accessory

Hematite, barite, REE-carbonate, uranium phosphate.

Other common minerals in open and partly open fractures in deformation zone ZFMNW0805a, according to drill core mapping, are calcite, chlorite, laumontite, epidote /Curtis et al. 2010/.

Figure 5-5. *Photograph of drill core box from part of the sampled borehole section KFR7A: 48.0–74.7 m.*

5.1.4 Borehole section KFR08: 63.0–104.0 m

The sampled part of the drill core intercepts with three intercepting zones, ZFMNW0805a, ZFMNNW099, ZFMWNW0836 /Curtis et al. 2010/ and the groundwater type found in this borehole section is Baltic /Nilsson et al. 2010/.

A fracture network sealed with laumontite and calcite (generation 2) occurs between 72 and 80 m. Younger generation 3 minerals such as euhedral quartz have precipitated in voids where partial dissolution of generation 2 minerals has occurred. Open fractures are common at 64–67 m and 67.5–69.5 m (Figure 5-6).

Identified fracture minerals, based on SEM-EDS and XRD analysis:

Dominating

Mixed layer clay (poorly ordered, smectite-illite and corrensite), albite, adularia, quartz.

Common

Hematite, calcite, pyrite.

Accessory

Barite, REE-carbonate, xenotime, galena, chalcopyrite, uranium phosphate, allanite, monazite, arsenopyrite, sphalerite, apatite, arsenopyrite.

Figure 5-6. *Photograph of drill core box from part of the sampled borehole section KFR08: 63.0–104.0 m.*

5.1.5 Borehole section KFR10: 87.0–107.3 m

The sampled part of the drill core intercepts or are close to deformation zone ZFMNNE0869 /Curtis et al. 2010/ and the groundwater found in this borehole section is of Littorina type /Nilsson et al. 2010/.

The section is dominated by clay minerals and calcite. Fractures sealed with laumontite and especially younger calcite, pyrite and quartz belonging to generation 3 are common (Figure 5-7), see Chapter 2.

Identified fracture minerals, based on SEM-EDS and XRD analysis:

Dominating

Mixed layer clay (poorly ordered, smectite-illite), illite, calcite, adularia, (often hematite stained), albite, quartz.

Common

Pyrite, hematite, corrensite, laumontite.

Accessory

Galena, barite, allanite.

Other common minerals in broken fractures in deformation zone ZFMNNE0869, according to drill core mapping, are chlorite, asphaltite, laumontite, epidote /Curtis et al. 2010/.

Figure 5-7. *Photograph of drill core box from part of the sampled borehole section KFR10: 87.0–107.3 m.*

5.1.6 Borehole section KFR19: 95.0–110.0 m

This section is not modelled as a deformation zone in the geological model /Curtis et al. 2010/. The groundwater type in this borehole section is Baltic /Nilsson et al. 2010/.

Clay minerals and calcite are common in open fractures (Figure 5-8).

Identified fracture minerals, based on SEM-EDS and XRD analysis:

Dominating

Mixed layer clay (poorly ordered, smectite-illite), illite, calcite, quartz, adularia.

Common

Hematite.

Accessory

Allanite, uranium-silicate, REE-carbonate, barite, chalcopyrite, Fe-oxyhydroxide.

Figure 5-8. *Photograph of drill core box from part of the sampled borehole section KFR19: 95.0–110.0 m.*

5.1.7 Borehole section KFR105: 120.0–134.0 m

This section is not modelled as a deformation zone in the geological model /Curtis et al. 2010/. The groundwater in this borehole section is of Transition type /Nilsson et al. 2010/.

Hematite-stained laumontite and adularia in sealed fractures. Water conductive fractures are dominated by clay minerals and chlorite (Figure 5-9).

Identified fracture minerals, based on SEM-EDS and XRD analysis:

Dominating

Mixed layer clay (poorly ordered, smectite-illite), illite, chlorite, quartz, calcite, adularia.

Common

Hematite, biotite.

Accessory

Pyrite, barite, barite-celestine, fluorite, Y-Ca silicate.

Figure 5-9. *Photograph of drill core box from part of the sampled borehole section KFR105: 120.0–134.0 m.*

5.1.8 Borehole section KFR105: 265.0–306.8 m

This section is not modelled as a deformation zone in the geological model /Curtis et al. 2010/. The groundwater in this borehole section is of Brackish-Glacial type /Nilsson et al. 2010/.

Sealed fractures with hematite-stained laumontite and adularia dominate the sampled section (Figure 5-10).

Identified fracture minerals, based on SEM-EDS and XRD analysis:

Dominating

Illite, Mixed layer clay (corrensite), chlorite, quartz, calcite, adularia.

Common

Calcite, laumontite, muscovite, biotite, hematite.

Accessory

Allanite, galena, harmotome, REE-carbonate.

Figure 5-10. *Photograph of drill core box from part of the sampled borehole section KFR105: 265.0–306.8 m.*

5.2 Geochemistry of fracture filling material

The obtained geochemical data of fracture filling material are presented in Table 5-2. One sample, KFR105 283.38–283.57 m, has been probably contaminated by steel fragments during the drilling or subsequent handling of the drill core, this is inferred from the anomalously high content of cobolt, chromium and vanadium in the sample.

Table 5-2. Geochemistry of bulk fracture filling material.

ELEMENT	SAMPLE	KFR01 45.18	KFR01 47.09	KFR7A 49.6	KFR7A 68.8	KFR7A 70.05	KFR7A 70.47	KFR08 76.77	KFR08 95.29	KFR10 95.65	KFR10 106.3	KFR19 90.56	KFR105 126.9	KFR105 280.07	KFR105 283.38
	ELEVATION	–87.11	–88.76	–134.02	–134.69	–134.73	–134.75	–92.71	–94.33	–145.94	–153.47	–59.1	–128.37	–152.72	–153.22
	SECTION	KFR01: 44.5–62.3 m		KFR7A: 48.0–74.7 m				KFR08: 63.0–104.0 m		KFR10: 87.0–107.3m		KFR19: 95.0–110.0 m	KFR105: 120.0–134.0 m	KFR105: 265.0–306.8 m	
SiO_2	wt%	41.6	57.7	72.0	64.2	64.8	72.9	65.7	73.9	49.2	60.0	67.7	50.2	63.0	38.9
Al_2O_3	wt%	24.4	16.4	10.6	20.0	18.4	15.4	7.0	9.0	18.1	17.6	15.8	16.8	16.7	10.8
CaO	wt%	0.557	8.86	4.30	0.911	1.08	0.363	11.8	4.35	0.701	0.274	0.614	1.24	6.03	2.28
Fe_2O_3	wt%	7.77	1.16	7.21	0.89	2.24	0.307	2.35	3.15	15.8	7.25	4.07	8.33	0.832	33.1
K2O	wt%	4.48	6.19	1.77	9.26	9.83	9.42	3.00	3.75	4.99	8.96	5.75	7.24	5.30	2.41
MgO	wt%	13.1	0.45	2.39	0.478	0.623	0.0512	0.833	0.973	3.39	1.52	0.849	9.41	0.475	6.73
MnO	wt%	0.14	0.0262	0.207	0.0176	0.0327	0.0128	0.0679	0.0282	0.124	0.0252	0.0262	0.152	0.0105	0.201
Na_2O	wt%	0.36	4.41	0.462	3.26	2.52	2.38	0.791	0.172	1.75	0.202	2.9	0.3	0.358	<0,05
P_2O_5	wt%	0.1070	0.0226	0.0648	0.0240	0.1040	0.0159	0.0362	0.0091	0.3310	0.0464	0.0198	0.2230	0.0203	0.243
TiO_2	wt%	0.5120	0.0697	0.2070	0.0249	0.1920	0.0131	0.1150	0.0091	1.0600	0.0451	0.0184	0.4230	0.0299	0.8870
Summa	wt%	93.0	95.3	99.2	99.1	99.8	100.9	91.7	95.3	95.4	95.9	97.7	94.3	92.8	95.6
LOI	wt%	7.3	6.4	2.6	2.0	1.0	0.2	8.8	5.2	4.4	4.1	2.6	5.1	6.5	4.0
Ba	ppm	715	728	337	1,480	1,350	706	593	389	417	779	815	923	3,570	144
Be	ppm	3.35	1.35	3.92	2.97	1.93	1.24	1.55	1.73	7.37	5.33	6.39	5.02	3.18	2.43
Co	ppm	<6	<6	<6	<6	<6	<6	<6	<6	<6	<6	<6	<6	<6	39.3
Cr	ppm	17.1	13.0	23.6	<10	15.1	<10	50.0	22.0	32.3	<10	12.7	24.3	<10	43.6
Ga	ppm	35.7	17.2	24.6	23.7	20.2	11.6	13.1	11.7	44.6	38.4	30.3	30.7	11.8	26.4
Hf	ppm	11.3	5.64	4.64	2.33	6.09	3.26	3.98	2.03	5.69	10.2	2.9	3.21	1.71	2.63
Mo	ppm	<2	<2	<2	<2	<2	<2	<2	<2	<2	<2	<2	<2	<2	<2
Nb	ppm	3.15	1.48	1.96	0.412	1.76	<0.2	0.813	<0,2	2.71	0.637	0.544	0.898	0.542	0.643
Ni	ppm	19.0	<10	14.1	<10	<10	<10	15.7	13.8	15.0	<10	<10	<10	<10	38.7
Rb	ppm	201	148	99.9	234	219	181	69.8	175	423	390	271	297	195	172
Sc	ppm	19.7	12.3	5.71	4.24	5.38	<1	3.74	<1	49.5	15.1	1.25	16.9	1.61	38.3
Sr	ppm	34.7	135	139	96.6	87.1	73.1	126	54.1	53.1	47.2	71.6	63.3	146	62.8
Ta	ppm	3.59	0.987	1.54	1.59	1.27	0.35	0.725	0.0722	2.31	0.225	0.889	0.765	0.845	0.615
Th	ppm	27.5	14.4	13.0	10.9	40.7	15.4	9.12	2.78	17.7	24.3	10.0	9.96	4.08	3.47
U	ppm	12.6	14.9	10.8	23.8	22.2	10.4	8.12	4.86	44.2	19.9	25.0	24.7	6.85	32.4
V	ppm	57.5	11.1	12.4	42.1	11.9	5.81	22.8	4.96	71.7	33.0	3.81	79.3	3.9	1,030
W	ppm	5.60	7.12	3.95	1.88	1.85	1.05	1.55	2.47	11.0	4.25	16.0	2.59	1.17	3.44
Y	ppm	66.3	661	27.7	16.4	50.0	18.8	32.5	43.8	109	40.4	51.2	33.3	10.0	31.3
Zr	ppm	368	95.2	149	41.3	219	53.2	96.2	8.59	200	180	32.9	97.0	8.27	56.9
La	ppm	70.7	21.3	59.2	10.6	59.9	14.2	22.4	96.3	388	140	11.8	28.9	12.5	40.1
Ce	ppm	134	44.9	118	24.8	121	63.9	51.5	150	861	287	28.7	68.0	27.4	81.1
Pr	ppm	15.7	4.80	12.5	1.75	12.7	2.40	4.69	20.0	86.6	31.0	2.01	5.97	1.85	8.75
Nd	ppm	60.6	25.2	42.4	6.54	44.1	8.80	17.4	73.7	315	94.1	7.53	23.2	6.93	34.6
Sm	ppm	11.9	13.0	7.69	1.51	8.94	2.10	4.12	14.3	58.5	16.3	2.69	5.21	1.46	7.96
Eu	ppm	1.73	2.75	0.975	0.15	1.13	0.301	0.582	1.33	9.74	1.93	0.591	1.05	0.262	1.40
Gd	ppm	11.1	39.4	6.01	1.71	8.21	2.42	5.18	13.1	43.9	11.4	5.49	5.52	1.40	7.32
Tb	ppm	1.71	9.14	0.872	0.339	1.35	0.417	0.78	1.59	4.90	1.45	1.16	0.884	0.244	1.18
Dy	ppm	10.8	77.1	5.21	2.40	8.66	2.98	4.94	8.04	23.1	7.79	8.86	5.52	1.58	6.64
Ho	ppm	2.36	19.8	1.06	0.571	1.92	0.72	1.11	1.49	4.01	1.55	2.10	1.21	0.371	1.28
Er	ppm	6.96	66.2	3.20	1.91	6.13	2.49	3.29	4.01	10.5	4.66	6.78	3.55	1.25	3.55
Tm	ppm	1.11	10.3	0.517	0.334	1.06	0.413	0.472	0.522	1.48	0.671	1.11	0.520	0.229	0.482
Yb	ppm	7.24	68.9	3.60	2.69	7.72	3.08	2.95	3.05	9.74	4.34	7.41	3.15	1.85	3.08
Lu	ppm	1.11	10.7	0.622	0.448	1.31	0.532	0.457	0.484	1.51	1.00	1.39	0.666	0.638	0.522

6 Discussion

In this section, the geochemical data are discussed based on the identified fracture minerals in the sampled borehole sections.

Potassium, sodium, calcium, rubidium, strontium

Potassium is preferably hosted in adularia and illite, both in pure illite and in illite interlayered with smectite as a mixed layer clay. The large rubidium ion is also preferably hosted in clay minerals. Sodium is mainly hosted in albite but small amounts are also found in smectite.

Calcium is mainly hosted in calcite but also in smectite. There are other calcium-bearing minerals present in the fractures but they are only present as minor phases and have no significant effect on the overall calcium content. No correlation can be seen between calcium and strontium (Figure 6-1). Although calcium and strontium have similar ionic size and charge, studies during the Forsmark site investigation showed that Palaeozoic calcite (generation 3), which is the most abundant calcite generation in the area, has a low strontium content /Sandström et al. 2008/. This explains the low correlation between calcium and strontium. Instead the fracture filling material from the Forsmark site investigation with the highest strontium content was rich in laumontite and/or corrensite (a smectite mineral). The presence of strontium in laumontite and corrensite is supported by the analyses of the SFR samples, where all samples with more than 100 ppm strontium contain smectite (interlayered with illite) or laumontite. A few strontium-rich barite crystals were also identified in the SFR drill cores, the mineral is a solid solution between barite ($BaSO_4$) and Celestine ($SrSO_4$).

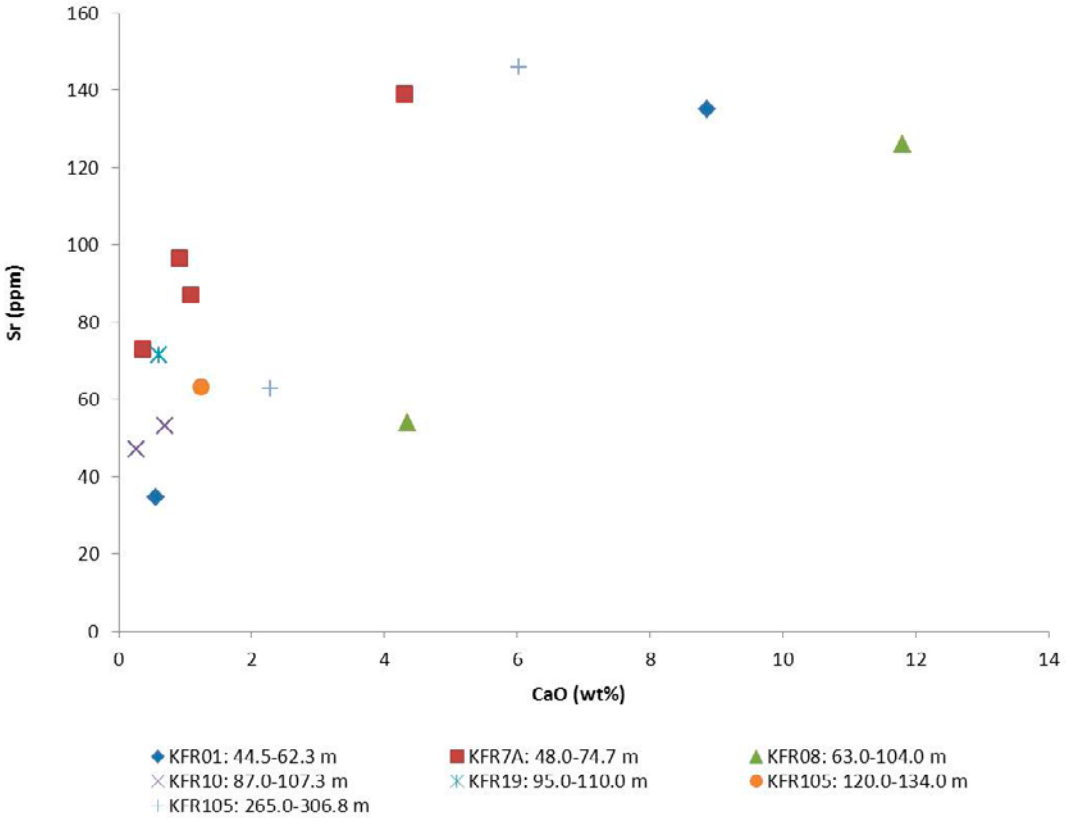

Figure 6-1. *Bivariate plot of CaO (wt%) versus Sr (ppm) in fracture filling material.*

Iron, magnesium, manganese

Iron is mainly hosted in chlorite and mixed layer clay (smectite-illite). These minerals generally have a low Mg/Fe ratio as seen in Figure 6-2. One sample deviates and show a very high MgO content (13.1 wt%), the sample consists of an altered amphibolite. Analyses of amphibolite in the Forsmark area shows a MgO content between 3 and 9 wt% /Sandström and Stephens 2009/, probably explaining the high MgO content in the fracture filling.

Iron is also present as hematite and Fe-oxyhydroxide. Hematite occurs finely disseminated within and on other fracture minerals such as adularia, albite, chlorite and clay minerals and is inferred to have precipitated under oxidising conditions during hydrothermal events during the Precambrian (cf. /Sandström et al. 2010/). However, some of the Fe-oxyhydroxide occurrences could also be of more recent origin.

No depth trends can be seen when the iron, magnesium or manganese content in bulk fracture filling material is plotted against elevation (Figure 6-3).

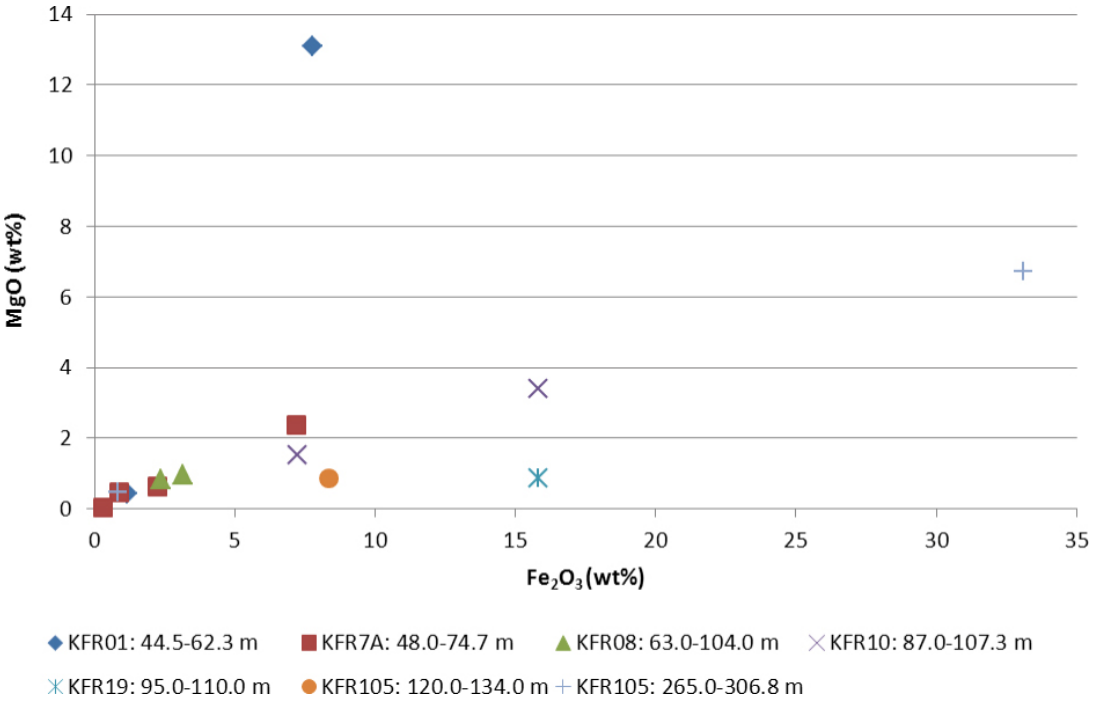

Figure 6-2. *Bivariate plot of Fe(total) presented as Fe_2O_3 (wt%) versus MgO (wt%) in bulk fracture filling material.*

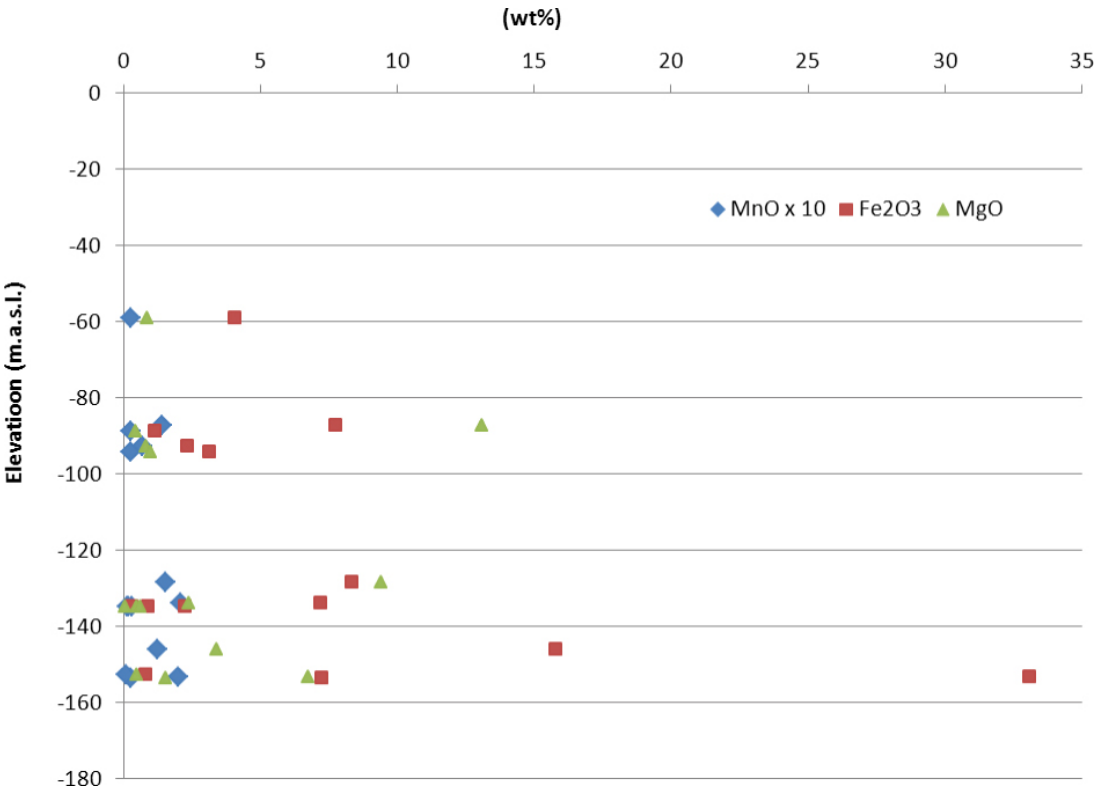

Figure 6-3. *MnO, Fe_2O_3 and MgO versus elevation in bulk fracture filling material.*

Rare earth elements (REE)

Chondrite normalised REE-patterns for the analysed bulk fracture filling material are shown in Figure 6-4. In general, the fracture filling material show enrichment of light REEs compared to the heavy REEs, the same signature is seen in the samples from the Forsmark site investigation and the most common rock types in the area /Sandström and Stephens 2009, Sandström et al. 2008/. The Eu anomaly seen in most samples is probably inherited from the wall rock.

The positive Ce anomalies seen in a few samples (Figure 6-5) indicate oxidation of Ce^{3+} to $Ce^{4+}$and subsequent deposition of the less soluble Ce^{4+} ion by sorption and/or coprecipitation on fracture surfaces. However, the age of the oxidation event cannot be determined by the available geochemical data and it is likely that, at least, some of the observed Ce anomalies are due to oxidation under hydrothermal conditions during the Precambrian and do not represent recent (post-glacial) oxidation (cf. /Sandström et al. 2008/).

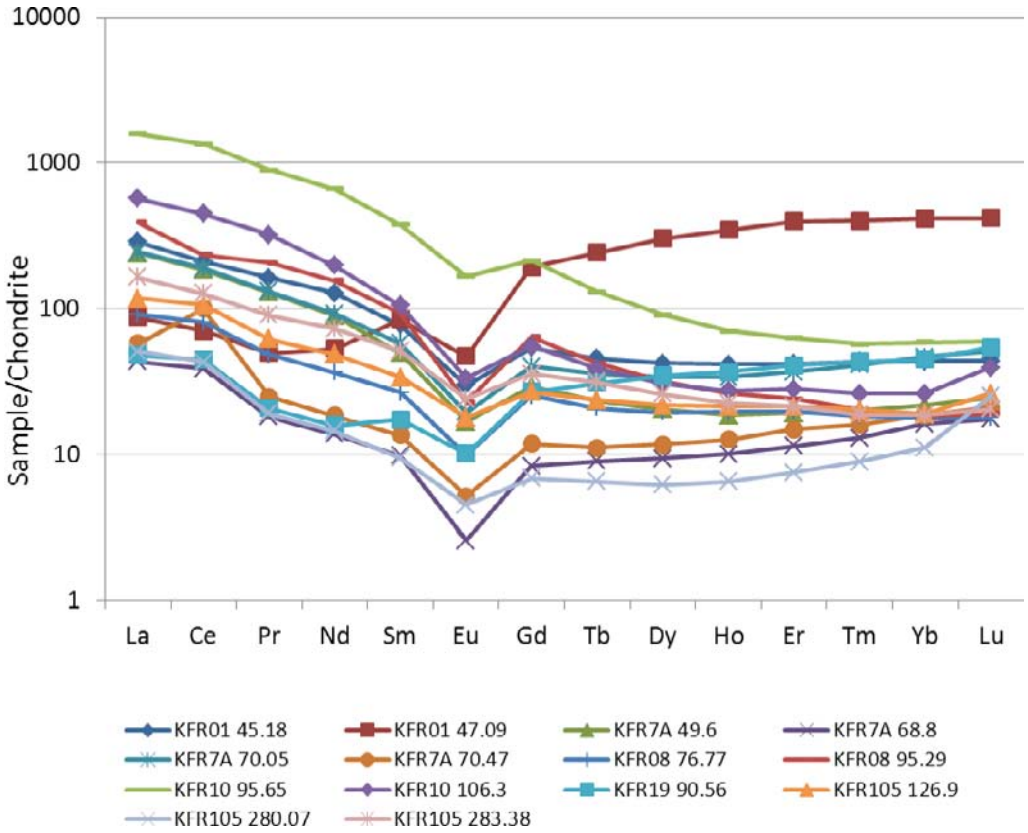

Figure 6-4. *Chondrite normalised REE patterns of bulkfracture filling material. Chondrite values from /Evansen et al. 1978/.*

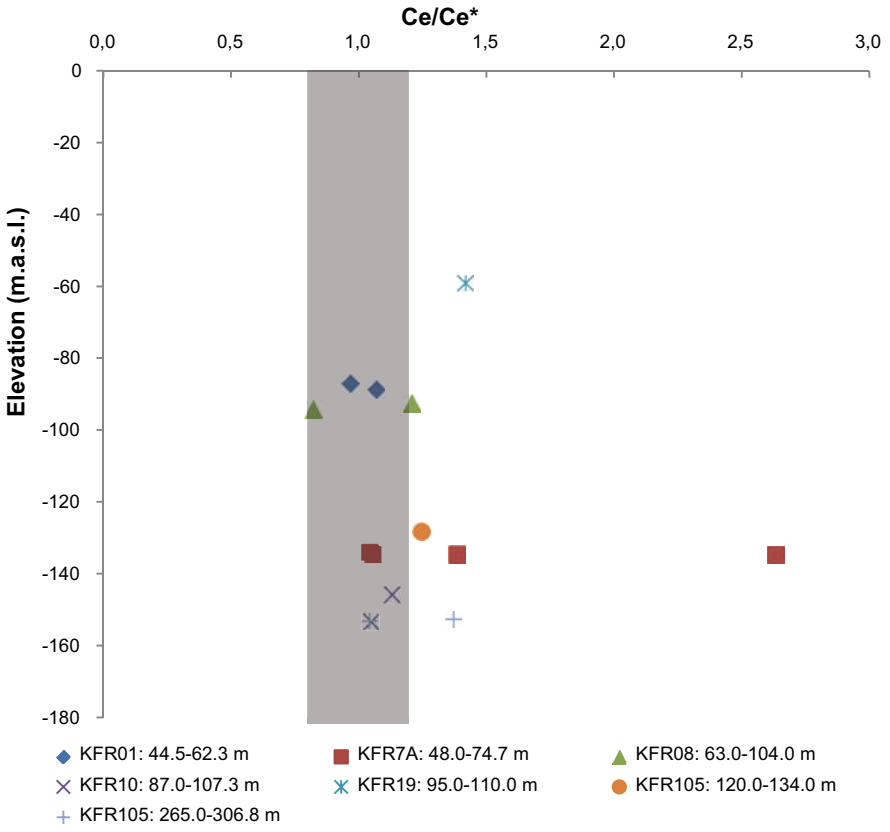

Figure 6-5. *Ce anomalies in bulk fracture filling material versus elevation, given as chondrite normalized Ce/Ce* values where Ce* = $(La \times Pr)^{½}$. Significant anomalies are here considered to be >20%, i.e. values outside the grey field. Chondrite values from /Evansen et al. 1978/.*

Uranium, thorium

Based on the SEM-EDS analyses, at least two different uranium minerals are present in the fracture system at SFR. No quantitative geochemical data were obtained by SEM-EDS due to the uneven surfaces of the samples. The mineral found most frequently is inferred to be a uranium phosphate. The uranium occurs in a poorly crystallized phase cogenetic with asphaltite, pyrite, calcite and adularia (Figure 6-6), typical generation 3 minerals of Palaeozoic age (cf. /Sandström et al. 2008/). The interpretation of the EDS-spectra is not obvious, the phosphorus and yttrium energy peaks are very close and therefore difficult to distinguish by the EDS technique (Figure 6-7). However, based on the good correlation between uranium and phosphorus in the bulk fracture filling material (Figure 6-8) it is inferred that it is a uranium phosphate. However, it cannot be excluded that it also contains significant amounts of yttrium. According to the EDS-spectra, the uranium phase also contains silicon and small amounts of calcium and aluminum. Since the X-rays obtained during EDS-analysis come from a volume with a depth of about 5 µm (the interaction volume), it is possible that both the silicon and aluminum peaks are effects from silicates underneath the uranium-phosphate. The uranium minerals occur as small (<1 mm), unevenly distributed precipitates on the fracture surfaces.

The samples with identified uranium minerals are not the samples with the highest uranium content in the bulk fracture fillings. However, it is plausible that similar uranium minerals are present in the samples with the higher uranium contents, although not on the specific part of the fracture studied by SEM-EDS.

The Th/U ratio is below 2 in all but one of the analysed bulk fracture fillings (Figure 6-10), this is significantly lower than the Th/U ratio in all rock types analysed in the area /Sandström and Stephens 2009/, indicating uranium deposition at some period in the past. Based on the paragenesis of the uranium minerals detected by SEM-EDS, it is inferred that precipitation of uranium has occurred at several events. Many of the uranium-minerals found on the fracture surfaces in the water conductive fractures at SFR are cogenetic with generation 3 pyrite and asphaltite (see Chapter 2). It can, therefore be assumed that precipitation of uranium phosphate occurred during the same period (cf. /Sandström et al. 2008/). However, during the Forsmark site investigation, uranium oxide was found associated with older chlorite and hematite /Sandström et al. 2008/ and uranium appears to have been remobilized and precipitated during several events during the geological evolution of the Forsmark area, starting already during the Precambrian (cf. /Welin 1964, Sandström et al. 2008/).

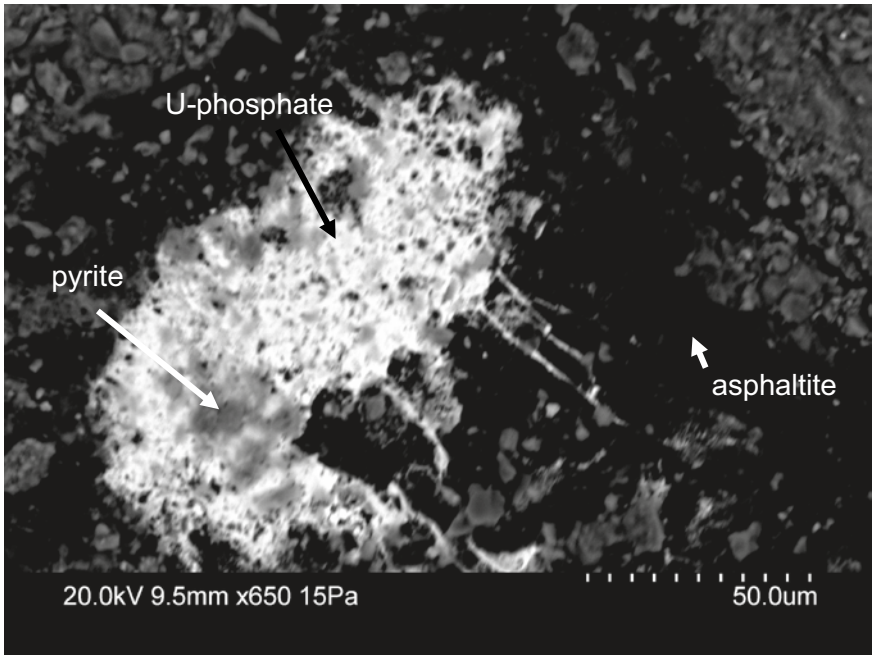

Figure 6-6. *Electron image of uranium mineral cogenetic with pyrite and asphaltite in sample KFR01 47.09–47.46 m.*

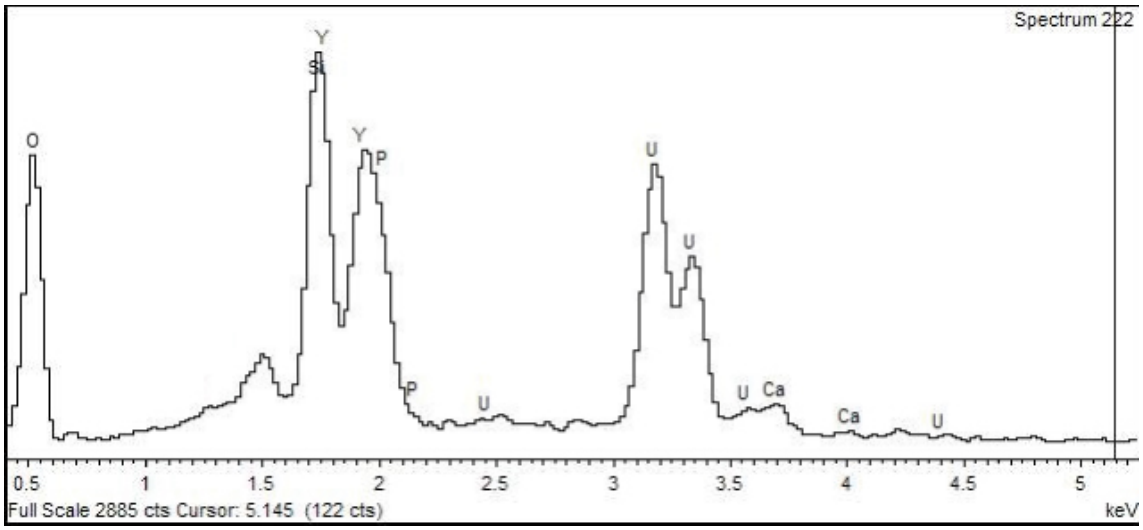

Figure 6-7. *EDS-spectra of uranium mineral in sample KFR01 47.09–47.46 m. The unmarked peak at approximately 1.5 keV represents aluminum.*

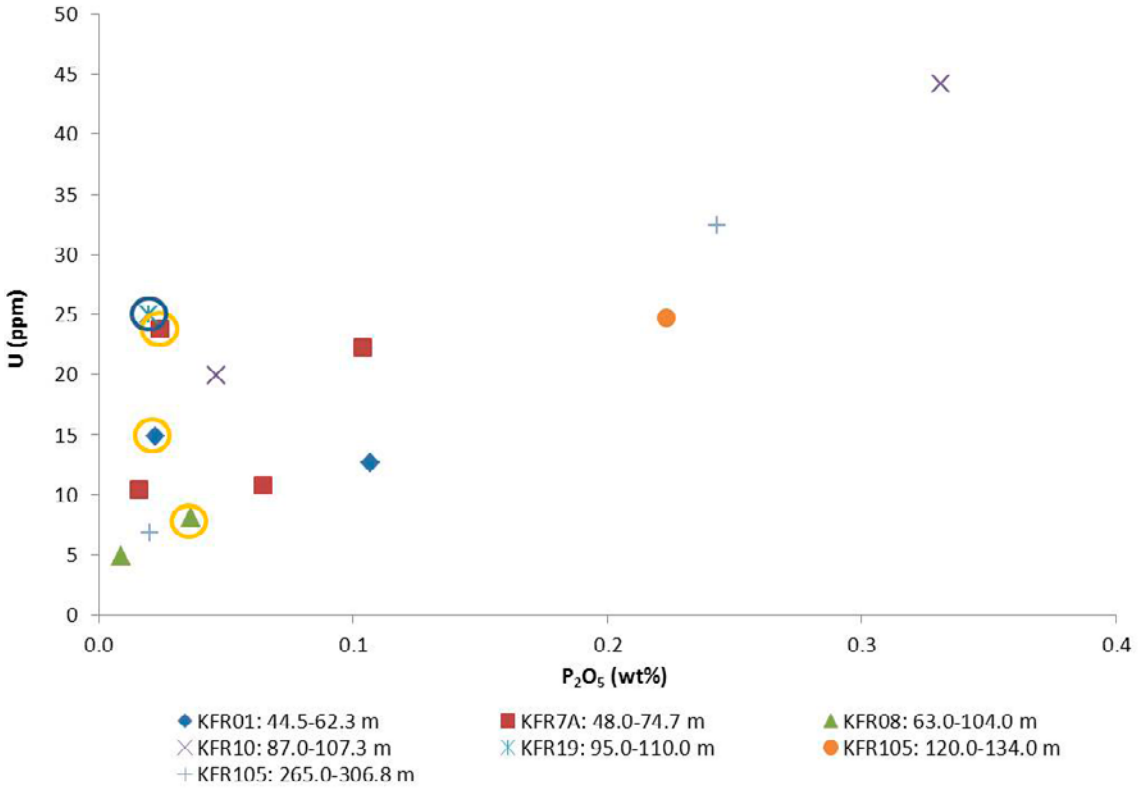

Figure 6-8. *Bivariate plot of P_2O_5 versus U in bulk fracture filling material. Circles represent samples where uranium minerals were detected by SEM-EDS,yellow circle: uranium phosphate, blue circle: uranium silicate.*

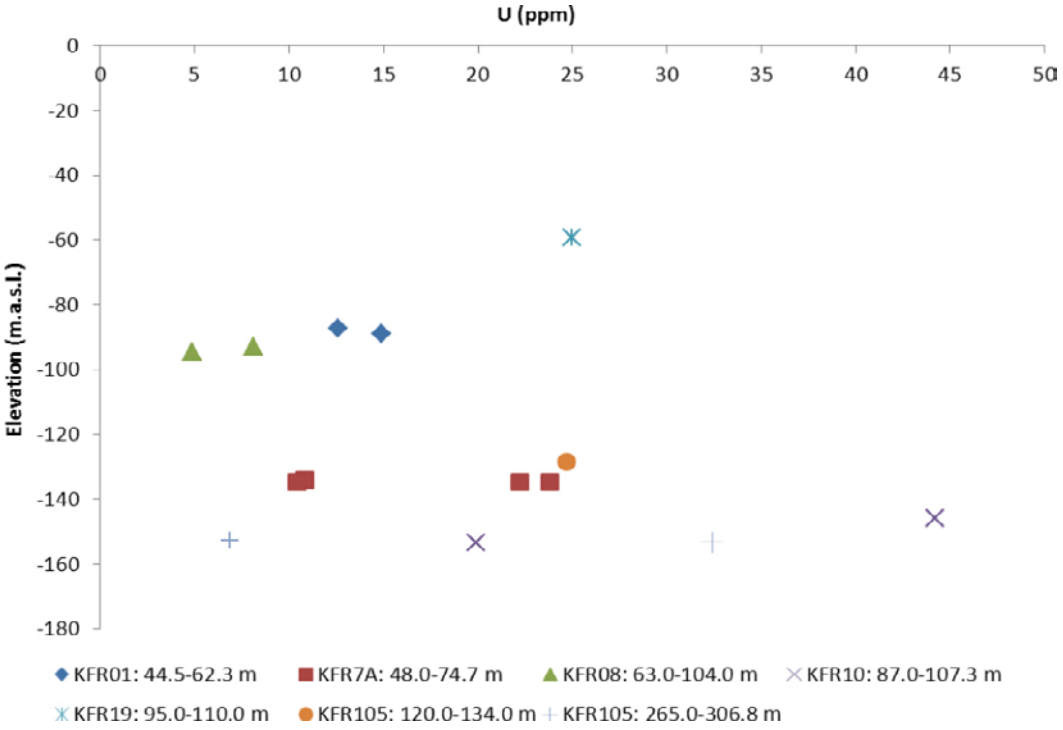

Figure 6-9. *Uranium content in bulk fracture filling material versus elevation.*

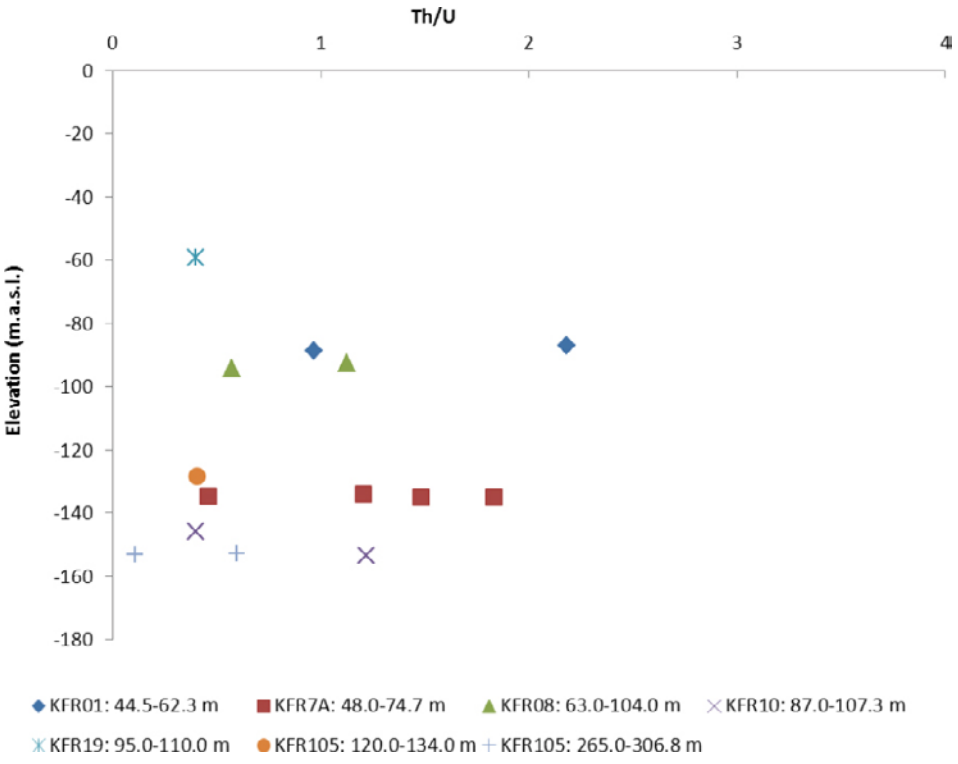

Figure 6-10. *Th/U ratio in bulk fracture filling material versus elevation.*

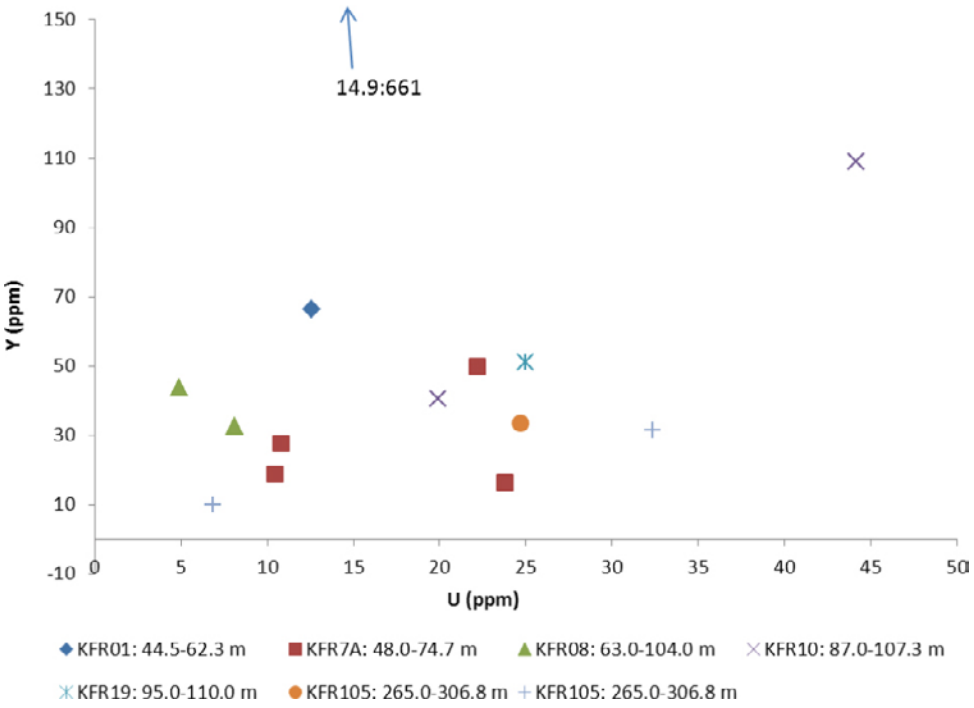

Figure 6-11. *Bivariate plot of uranium versus yttrium in bulk fracture filling material. An outlier with 14.9 ppm U and 661 ppm Y is not plotted but represented by the arrow. The sample with the high yttrium-content is inferred to be contaminated by steel fragments during the drilling or subsequent handling of the drill core.*

7 Concluding remarks

The fracture mineralogy and geochemistry presented in this report is representative for the fracture surfaces in contact with the groundwater in the sampled borehole sections.

The most common fracture minerals in the sampled borehole sections are mixed layer clay (smectite-illite), illite, chlorite, calcite, quartz, adularia and albite. Other minerals identified in the borehole sections include laumontite, pyrite, barite, hematite, Fe-oxy-hydroxide, muscovite, REE-carbonate, allanite, biotite, asphaltite, galena, sphalerite, arsenopyrite, uranium phosphate, uranium silicate, Y-Ca silicate, monazite, xenotime, harmotome and fluorite. Many of the observed PFL-fractures show traces of Palaeozoic generation 3 minerals, indicating that the water conductive fractures are old structures. This is in agreement with the observations made during the Forsmark site investigation /Sandström et al. 2008/.

No indications of a significant inflow of oxygenated waters, such as oxidation and/or dissolution of sulphides, have been identified in the SFR fracture system. However, in water conductive zones, occurrences of Fe-oxy-hydroxides indicate that oxidising conditions have prevailed, at some period, in parts of the fracture system. This is in agreement with the observations from the Forsmark site investigations /Sandström et al. 2008, Sidborn et al. 2010/. No signs of a redox transition zone were detected, also in agreement with observations of the redox system at Forsmark /Sidborn et al. 2010/. No samples have been investigated from above –57 m.a.s.l. in this study. However, based on the drill core mapping, pyrite is only absent in water conductive fractures in the upper 10 meters indicating prevailing reducing conditions. Noteworthy is the presence of iron hydroxide at depths down to about –500 m.a.s.l. as indicated by the drill core mapping. The age of these occurrences is not known and it is also possible that at least some of them are iron oxides that can be difficult to distinguish from iron hydroxides by visual inspection.

No major differences are evident between the fracture mineralogy of the sampled SFR drill cores and samples investigated during the Forsmark site investigation. The four fracture mineral generations distinguished within the Forsmark site investigation are also found at SFR. However, a few minor differences have been identified:

- The relative abundance of different clay minerals; in SFR, a mixed layer clay consisting of smectite-illite dominatestogether with illite in the water conductive fractures. Within the Forsmark site investigationarea, corrensite, a mixed layer clay consisting of smectite-chlorite, was totally dominating. However, only a few occurrences of corrensite were recorded above –100 m.a.s.l. during the Forsmark site investigations /Sandström et al. 2008/, in agreement with the results from SFR.
- REE-carbonate has been identified in many of the SFR drill core samples, no REE-carbonates were identified within the Forsmark site investigations.
- Barite is more common in the SFR drill cores, a few occurrences of a Sr-rich barite have also been identified (solid solution between barite-celestine).
- Uranium minerals have been detected in 20% of the analysed samples from the SFR drill cores. At the Forsmark site investigation, only one uranium mineral was identified in more than 200 sampled fractures.

These observations indicate that fluids rich in REE, barium and uranium have circulated in the area at some period. Based on the association with generation 3 minerals, it is inferred that the main phase of precipitation of minerals from these fluids occurred during the Palaeozoic. However, at least the precipitation of uranium minerals was due to remobilisation of uranium already present in the fracture system.

8 References

SKB's (Svensk Kärnbränslehantering AB) publications can be found at www.skb.se/publications.

Brindley G W, Brown G (eds), 1984. Crustal structure of clay mineral and their X-ray identification. London: Mineralogical Society of Great Brittain and Ireland. (Mineralogical Society Monograph 5)

Claesson Liljedahl L, Munier R, Sandström B, Drake H, Tullborg E-L, 2011. Assessment of fractures classified as non-mineralised in the Sicada database. SKB R-11-02, Svensk Kärnbränslehantering AB.

Curtis P, Markström I, Petersson J, Triumf C-A, Isaksson H, Matsson H, 2010. Site investigation SFR. Geological description of deformation zones and rock domains. Model version 1.0. SKB R-10-49, Svensk Kärnbränslehantering AB.

Deer W A, Howie R A, Zussman J, 1992. An introduction to the rock-forming minerals. 2nd ed. Harlow: Pearson Education Limited.

Drever J I, 1973. The preparation of orientated clay mineral specimens for X-ray diffraction analysis by a filter-membrane peel technique. American Mineralogist, 58, pp 553–554.

Evansen N M, Hamilton P J, O'Nions R K, 1978. Rare-earth abundance ni chondritic meteorites. Geochimica et Cosmoschimica Acta, 42, pp 1199–1212.

ICDD, 1994. Powder diffraction file computer database, set 1-43. Swartmore, PA: International Centre for Diffraction Data.

Jasmund K, Lagaly G (eds), 1993. Tonminerale und Tone: Struktur, Eigenschaften, Anwendungen und Einsatz in Industrie und Umwelt. Darmstadt: Steinkopff.

Nilsson K, 2011. Site investigation SFR. Hydrochemical characterisation of groundwater in the SFR repository. Sampling and analysis during 2010. Extended investigations in KRF7A: 48.0 to 74.7 m, KFR08: 63.0 to 104.0 m and KFR19: 95.6 to 110.0 m. SKB P-11-14, Svensk Kärnbränslehantering AB.

Nilsson A-C, Tullborg E-L, Smellie J, 2010. Preliminary hydrogeochemical site description SFR (version 0.2). SKB R-10-38, Svensk Kärnbränslehantering AB.

Sandström B, Tullborg E-L, 2009. Episodic fluid migration in the Fennoscandian Shield recorded by stable isotopes, rare earth elements and fluid inclusions in fracture minerals at Forsmark, Sweden. Chemical Geology, 266, pp 135–151.

Sandström B, Stephens M, 2009. Mineralogy, geochemistry, porosity and redox properties of rocks from Forsmark. Compilation of data from the regional model volume for SR-Site. SKB R-09-51, Svensk Kärnbränslehantering AB.

Sandström B, Tullborg E-L, de Torres T, Ortiz J E, 2006. The occurrence and potential origin of asphaltite in bedrock fractures, Forsmark, central Sweden. GFF, 128, pp 233–242.

Sandström B, Tullborg E-L, Smellie J, MacKenzie AB, Suksi J, 2008. Fracture mineralogy of the Forsmark site. SDM Forsmark. SKB R-08-102, Svensk Kärnbränslehantering AB.

Sandström B, Tullborg E-L, Larson S Å, Page L, 2009. Brittle tectonothermal evolution in the Forsmark area, central Fennoscandian Shield, recorded by paragenesis, orientation and $^{40}Ar/^{39}Ar$ geochronology of fracture minerals. Tectonophysics, 478, pp 158–174.

Sandström B, Annersten H, Tullborg E-L, 2010. Fracture-related hydrothermal alteration of metagranitic rock and associated changes in mineralogy, geochemistry and degree of oxidation: a case study at Forsmark, central Sweden. International Journal of Earth Sciences, 99, pp 1–25.

Sidborn M, Sandström B, Tullborg E-L, Salas J, Maia F, Delos A, Molinero J, Hallbeck L, Pedersen K, 2010. SR-Site: Oxygen ingress in the rock at Forsmark during a glacial cycle. SKB TR-10-57, Svensk Kärnbränslehantering AB.

Starkey H C, Blackmon P D, Hauff P L, 1984. The routine mineralogical analysis of clay-bearing samples. Washington: U.S. Government Printing Office. (USGS Bulletin 1563)

Stephens M B, Fox A, La Pointe P, Isaksson H, Simeonov A, Hermansson J, Öhman J, 2007. Geology Forsmark. Site descriptive modelling Forsmark stage 2.2. SKB R-07-45, Svensk Kärnbränslehantering AB.

Welin E, 1964. Uranium dissemination and vein fillings in iron ores of northern Uppland, central Sweden. Geologiska Föreningens i Stockholm Förhandlingar, 86, pp 51–82.

Appendix 1

Sample descriptions

Borehole: KFR01
Secup: 45.18 m
Seclow: 45.42 m
Deformation zone: ZFMWNW0001
Groundwater type: Transition + Littorina
Identified minerals: Chlorite, illite, quartz, allanite, pyrite

Figure A1-1. Photograph of the sampled drill core box. The sampled section is marked with a black line under the drill core.

Figure A1-2. Photograph of the sampled fracture filling material.

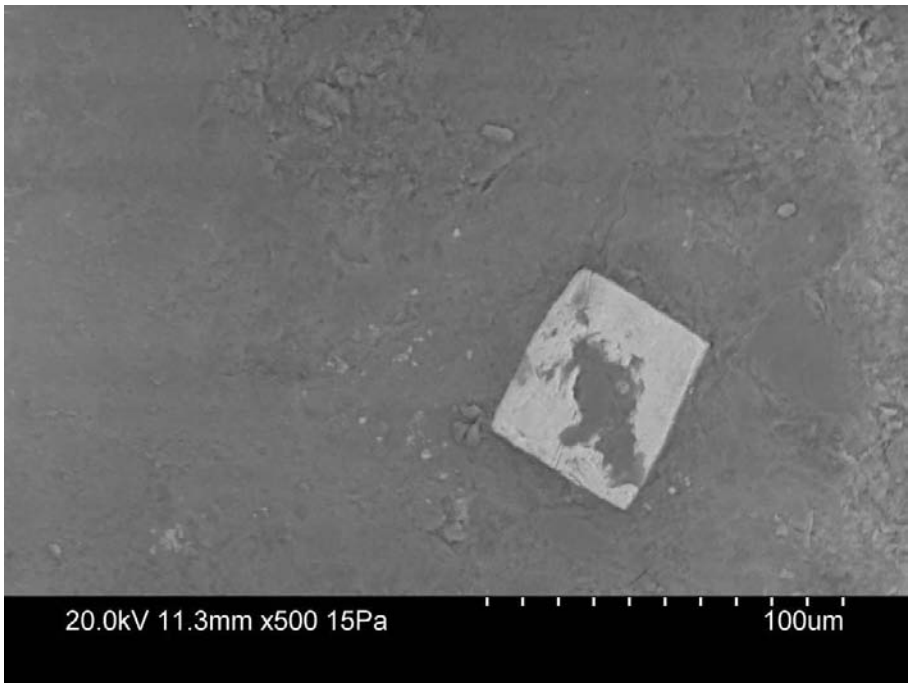

Figure A1-3. Electron image of pyrite crystal on Mg-Fe chlorite.

Borehole: KFR01
Secup: 47.09 m
Seclow: 47.46 m
Deformation zone: ZFMWNW0001
Groundwater type: Transition + Littorina
Identified minerals: Mixed layer clay (illite-smectite), illite, adularia, calcite, pyrite, barite, asphaltite, U-phosphate**.**

Figure A1-4. Photograph of the sampled drill core box. The sampled section is marked with a black line under the drill core.


Figure A1-5. Photograph of the sampled fractures.

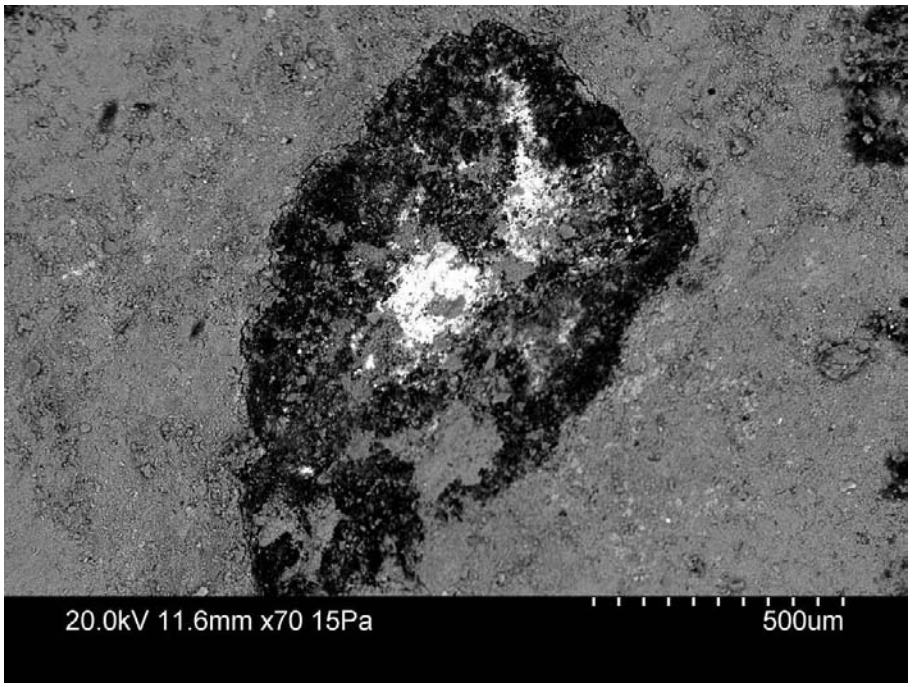

Figure A1-6. Electron image of uranium-mineral (white) together with asphaltite (black). The grey areas are dominated by adularia.

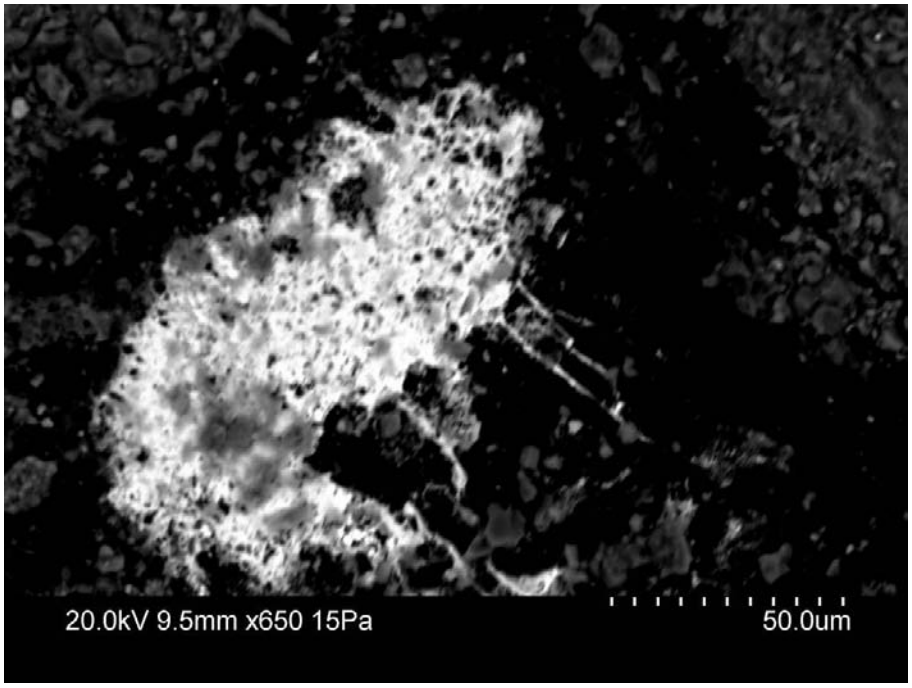

Figure A1-7. Electron image of uranium-mineral (white/grey) together with asphaltite (black).

Borehole: KFR01
Secup: 49.37 m
Seclow: 49.47 m
Deformation zone: ZFMWNW0001
Groundwater type: Transition + Littorina
Identified minerals: Pyrite, galena, calcite, Y-Ca-silicate.

Figure A1-8. Photograph of the sampled drill core box. The sampled section is marked with a black line under the drill core.


Figure A1-9. Photograph of the sampled fractures.

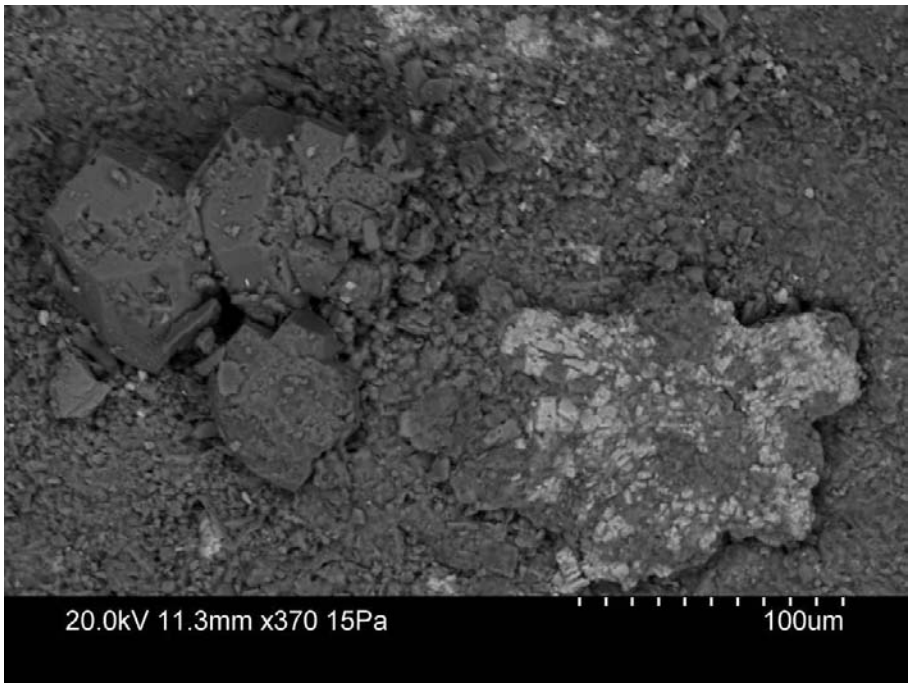

Figure A1-10. Electron image of calcite (euhedral crystals to the right) and Y-Ca silicate (light grey) on a fracture surface coated with clay mineral (grey).

Borehole: KFR01
Secup: 49.99 m
Seclow: 50.03 m
Deformation zone: ZFMWNW0001
Groundwater type: Transition + Littorina
Identified minerals: Calcite, mixed layer clay, adularia, quartz, pyrite, galena, barite-celestine, Y-Ca-silicate.

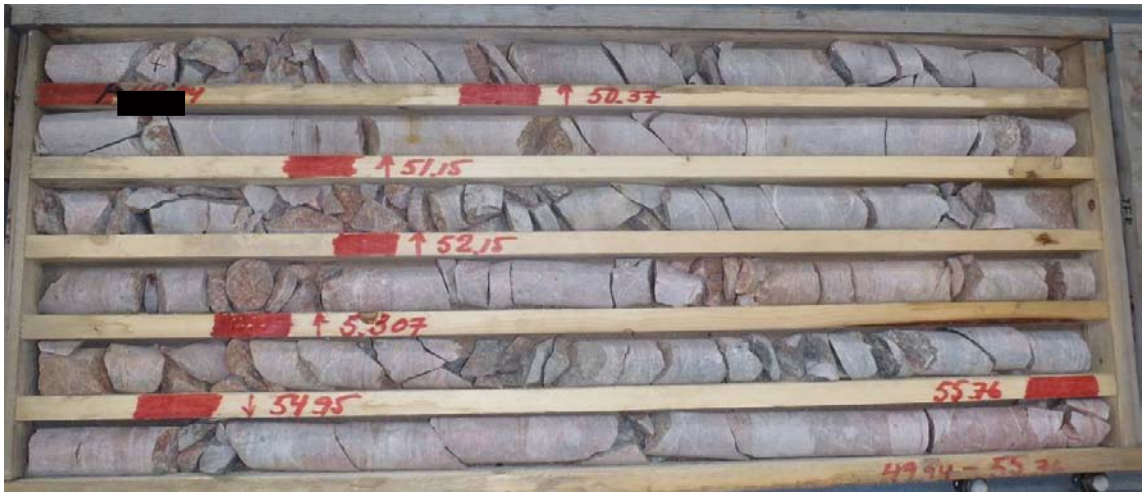

Figure A1-11. Photograph of the sampled drill core box. The sampled section is marked with a black under the drill core.


Figure A1-12. Photograph of the sampled fractures.

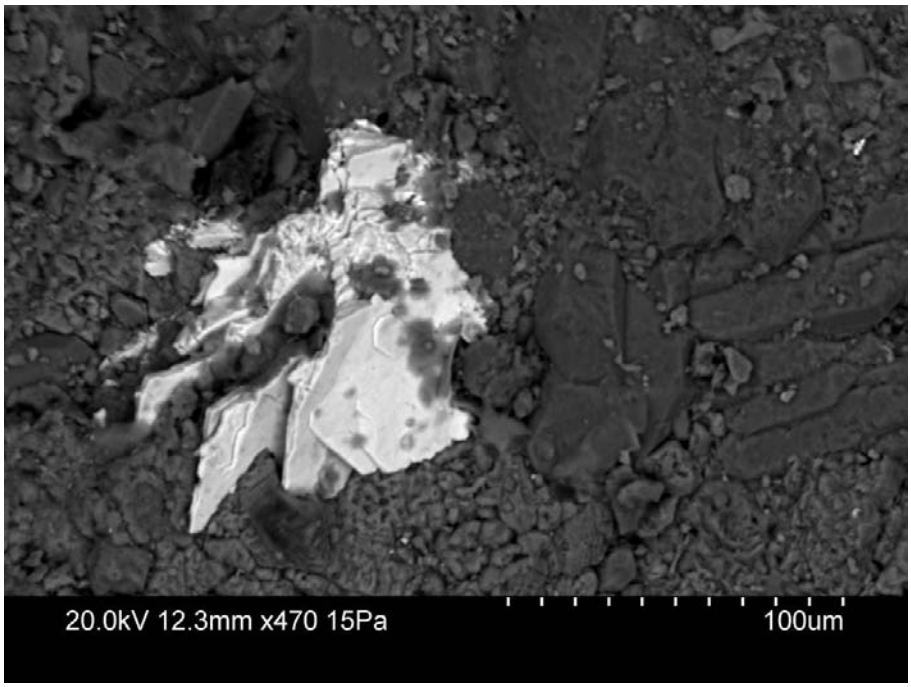

Figure A1-13. Electron image of barite-celestine (white) together with euhedral quartz crystals (upper right part of the image) and calcite (lower part of the image).

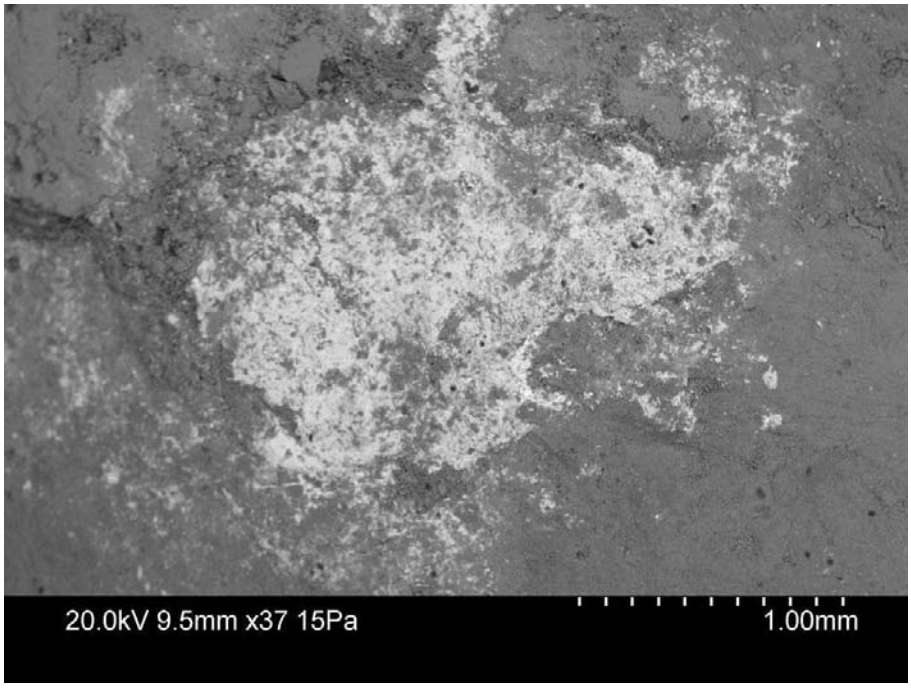

Figure A1-14. Electron image of Ca-Y silicate.

Borehole: KFR01
Secup: 61.10 m
Seclow: 61.12 m
Deformation zone: ZFMWNW0001
Groundwater type: Transition + Littorina
Identified minerals: Quartz, calcite, asphaltite, pyrite, barite.

Figure A1-15. Photograph of the sampled drill core box. The sampled section is marked with a black line under the drill core.


Figure A1-16. Photograph of the sampled fractures.

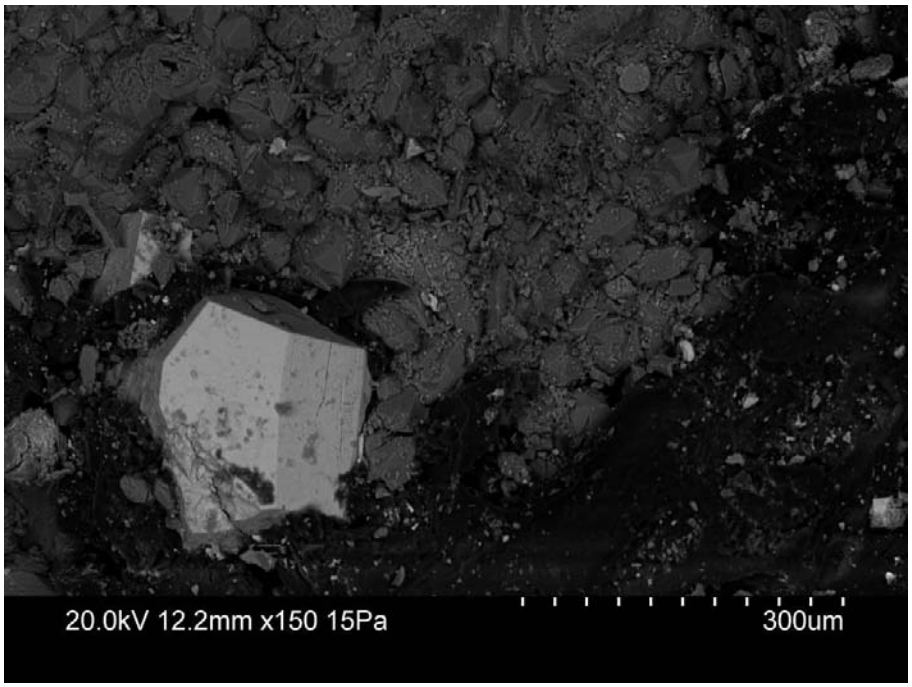

Figure A1-17. Electron image of pyrite crystal (light grey) on quartz (dark grey) together with asphaltite (black).

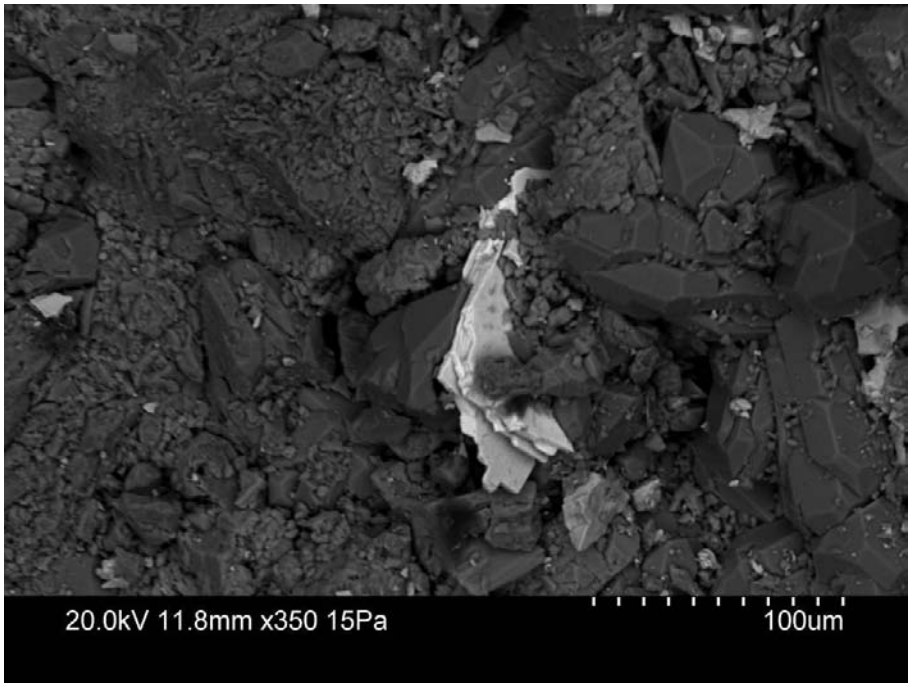

Figure A1-18. Electron image of barite crystal (bright) together with euhedral quartz.

Borehole: KFR7A
Secup: 49.60 m
Seclow: 50.04 m
Deformation zone: ZFMNE0805a, ZFM871
Groundwater type: Littorina
Identified minerals: Mixed layer clay (smectite-illite), illite, Fe-oxy-hydroxide.

Figure A1-19. Photograph of the sampled drill core box. The sampled section is marked with a black line under the drill core.


Figure A1-20. Photograph of the sampled fractures.

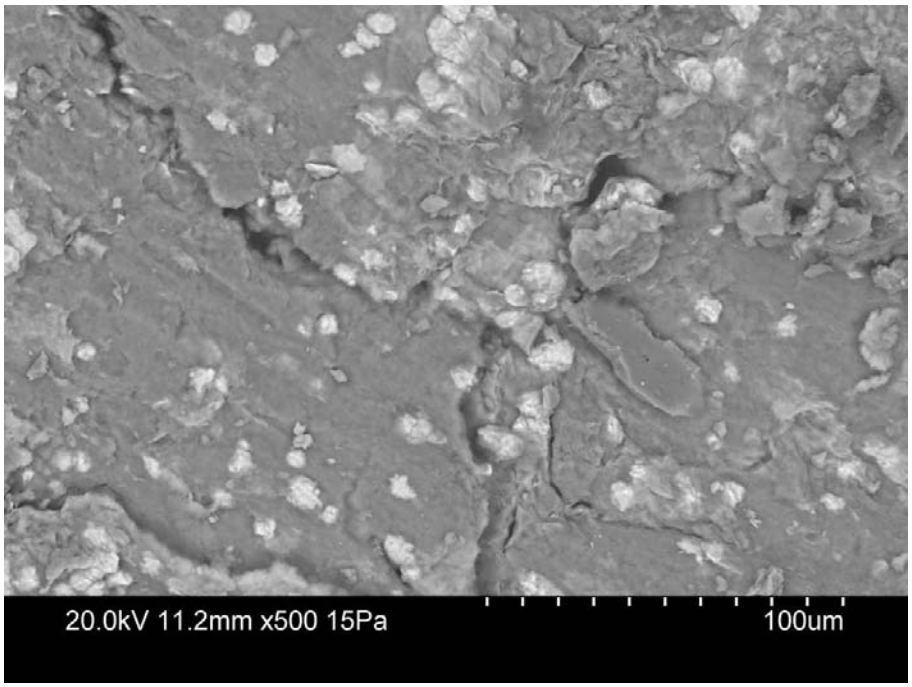

Figure A1-21. Electron image of Fe-rich clay minerals on surface coated with mixed layer clay.

Borehole: KFR7A
Secup: 68.80 m
Seclow: 68.90 m
Deformation zone: ZFMNE0805a, ZFM871
Groundwater type: Littorina
Identified minerals: Mixed layer clay (smectite-illite), adularia, albite, REE-carbonate, U-phosphate.

Figure A1-22. Photograph of the sampled drill core box. The sampled section is marked with a black line under the drill core


Figure A1-23. Photograph of the sampled fractures.

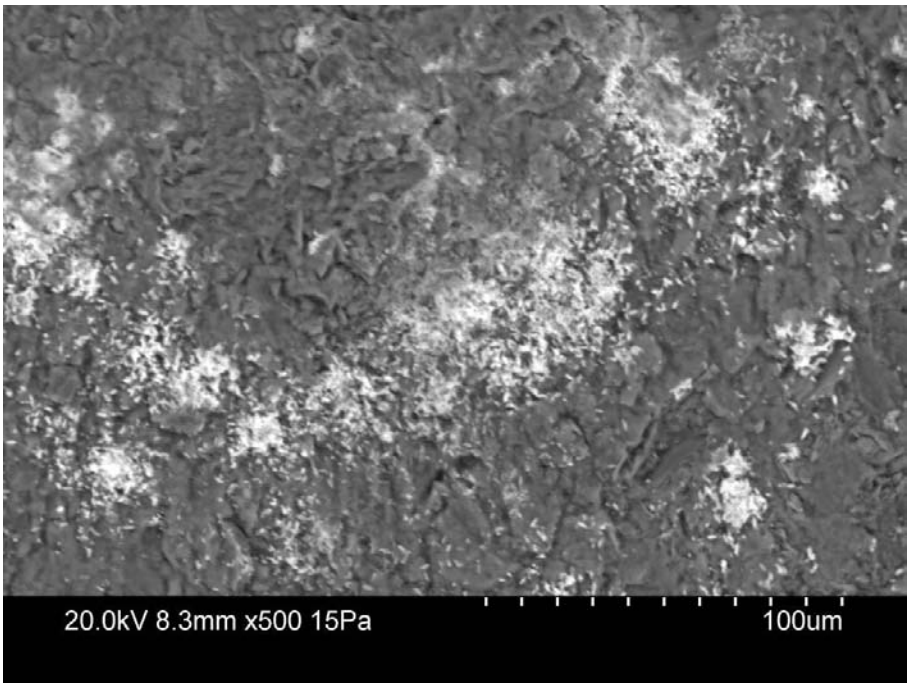

Figure A1-24. Electron image of uranium-phosphate on adularia surface.

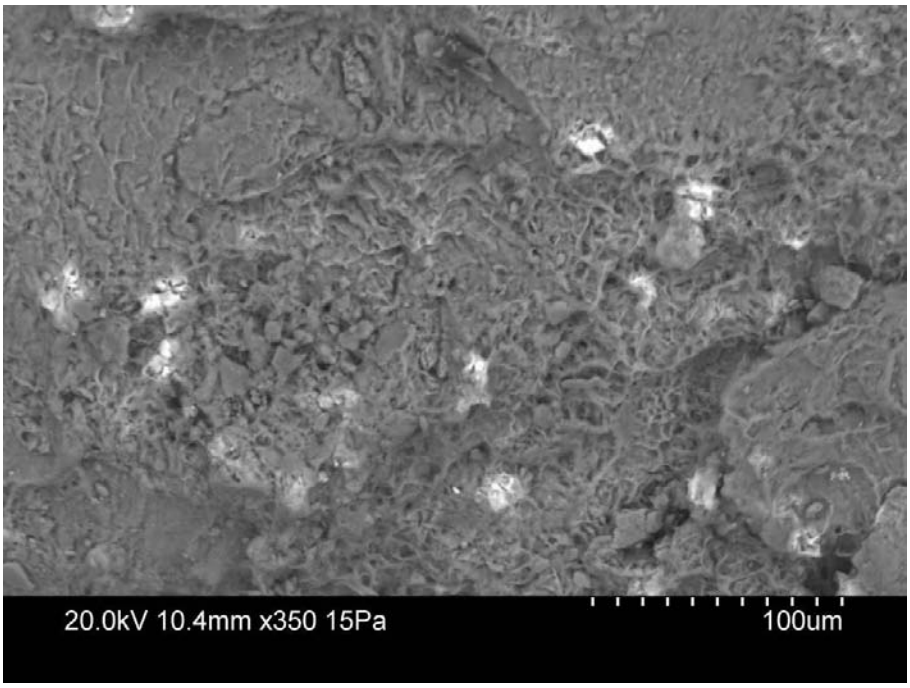

Figure A1-25. Electron image of uranium-phosphate on mixed layer clay surface.

Borehole: KFR7A
Secup: 70.05 m
Seclow: 70.12 m
Deformation zone: ZFMNE0805a, ZFM871
Groundwater type: Littorina
Identified minerals: Mixed layer clay (smectite-illite)**,** illite, quartz, adularia, albite, barite, Fe-oxy-hydroxide.

Figure A1-26. Photograph of the sampled drill core box. The sampled section is marked with a black line under the drill core.


Figure A1-27. Photograph of the sampled fractures.

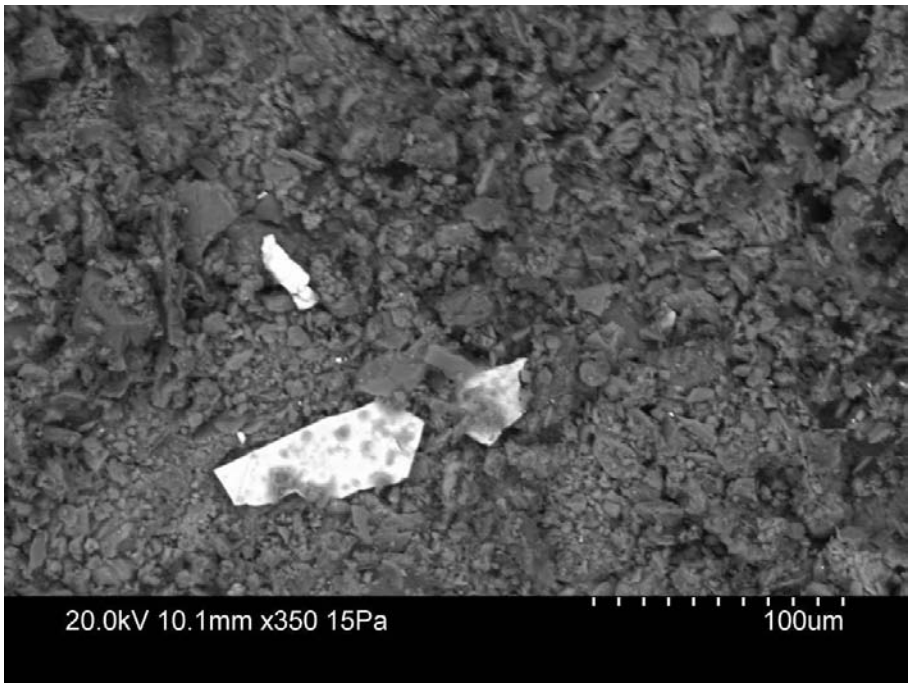

Figure A1-28. Electron image of barite crystals (bright) on a fracture surface coated with clay mineral.

Borehole: KFR7A
Secup: 70.47 m
Seclow: 70.52 m
Deformation zone: ZFMNE0805a, ZFM871
Groundwater type: Littorina
Identified minerals: Quartz, adularia, albite, illite, calcite.

Figure A1-29. Photograph of the sampled drill core box. The sampled section is marked with a black line under the drill core.


Figure A1-30. Photograph of the sampled fractures.

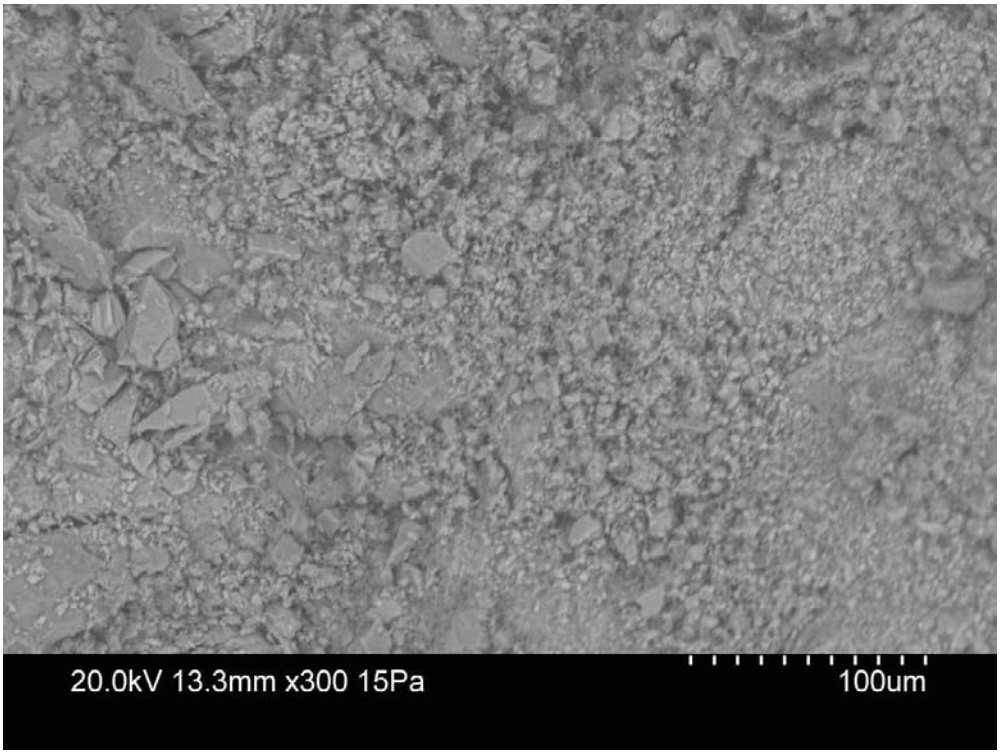

Figure A1-31. Electron image of fine-grained adularia.

Borehole: KFR7A
Secup: 73.74 m
Seclow: 73.91 m
Deformation zone: ZFMNE0805a, ZFM871
Groundwater type: Littorina
Identified minerals: Adularia, albite, quartz, barite, REE-carbonate, U-phosphate.

Figure A1-32. Photograph of the sampled drill core box. The sampled section is marked with a black line under the drill core.


Figure A1-33. Photograph of the sampled fractures.

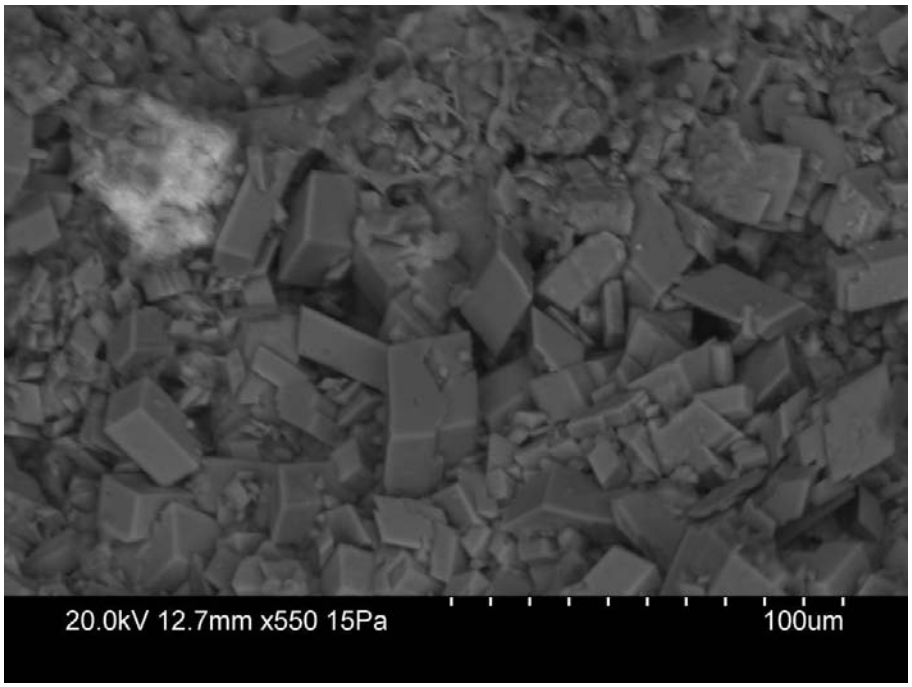

Figure A1-34. Electron image of REE-carbonate (bright) together with euhedral adularia.

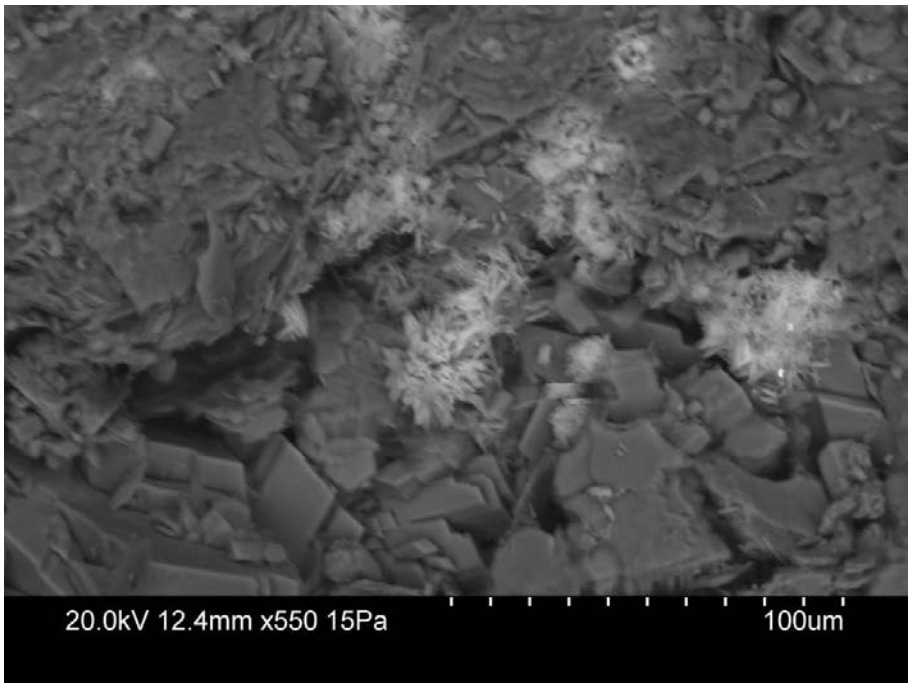

Figure A1-35. Electron image of uranium-silicate (bright) together with euhedral adularia.

Borehole: KFR08
Secup: 69.22 m
Seclow: 69.50 m
Deformation zone: ZFMNW0805a, ZFMNNW0999, ZFMWNW0836
Groundwater type: Baltic
Identified minerals: Mixed layer clay (smectite-illite), albite, hematite, barite, REE-carbonate, xenotime, galena.

Figure A1-36. Photograph of the sampled drill core box. The sampled section is marked with a black line under the drill core.


Figure A1-37. Photograph of the sampled fractures.

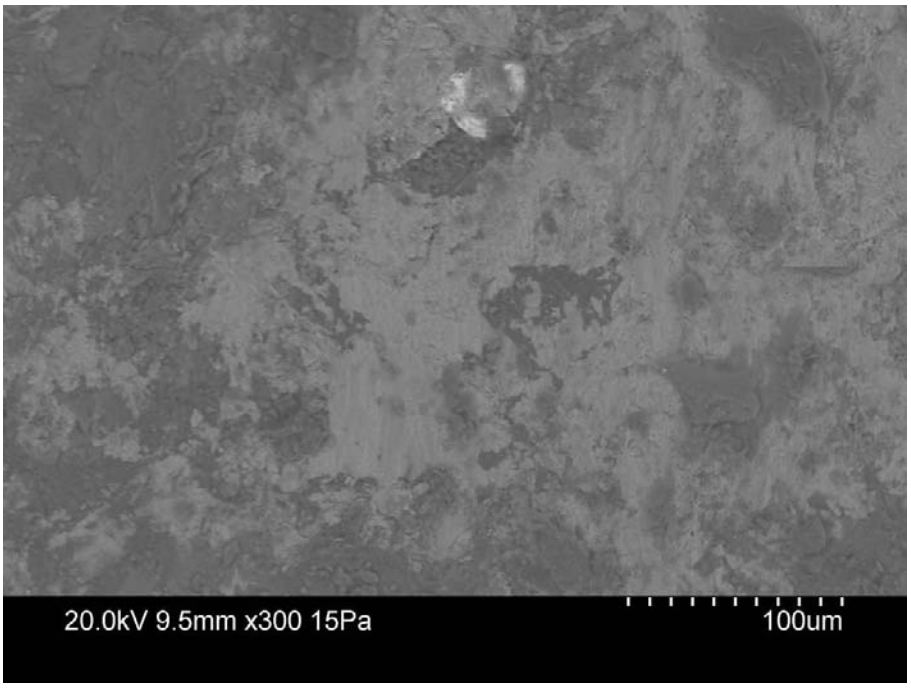

Figure A1-38. Electron image of a thin layer of REE-carbonate (light grey) precipitated on clay mineral. The bright grain in the upper part of the figure is a galena crystal.

Borehole: KFR08
Secup: 76.77 m
Seclow: 77.27 m
Deformation zone: ZFMNW0805a, ZFMNNW0999, ZFMWNW0836
Groundwater type: Baltic
Identified minerals: Mixed layer clay (smectite-illite), illite, chlorite, quartz, adularia, albite, calcite, hematite, pyrite, galena, chalcopyrite, U-phosphate.

Figure A1-39. Photograph of the sampled drill core box. The sampled section is marked with a black line under the drill core.


Figure A1-40. Photograph of the sampled fractures.

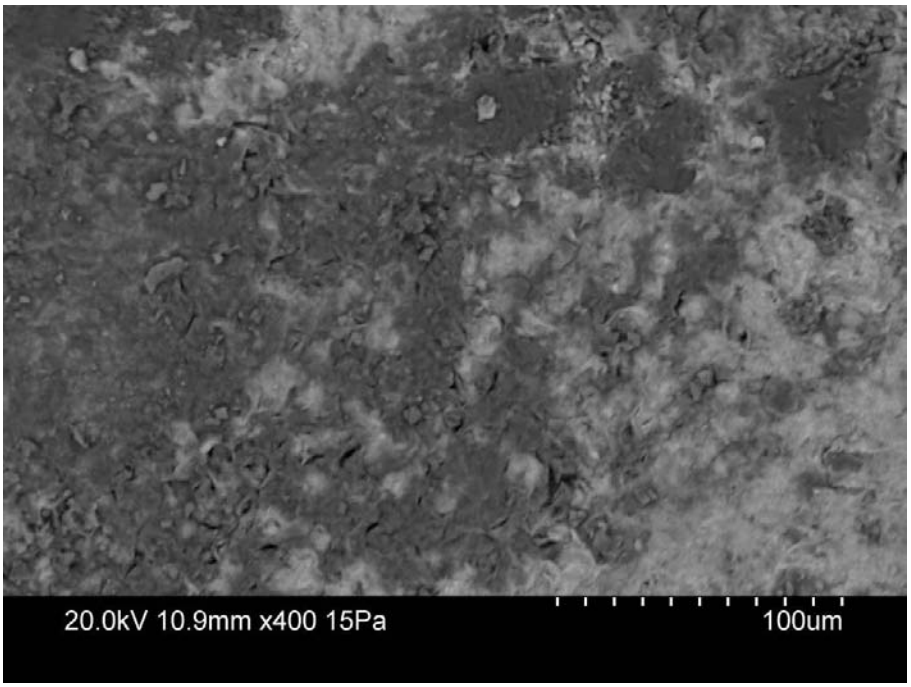

Figure A1-41. Electron image of Fe-oxide (light grey) together with clay mineral.

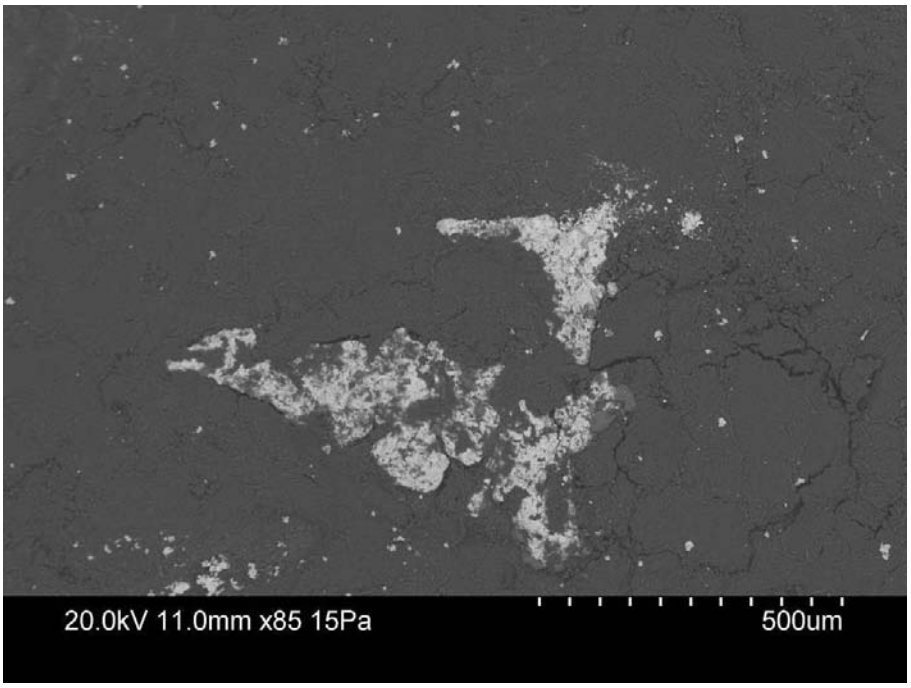

Figure A1-42. Electron image of galena (bright) on fracture surface together with clay mineral.

Borehole: KFR08
Secup: 79.13 m
Seclow: 79.41 m
Deformation zone: ZFMNW0805a, ZFMNNW0999, ZFMWNW0836
Groundwater type: Baltic
Identified minerals: Quartz, adularia, albite, calcite, hematite, pyrite, corrensite, barite, chalcopyrite, possibly allanite.

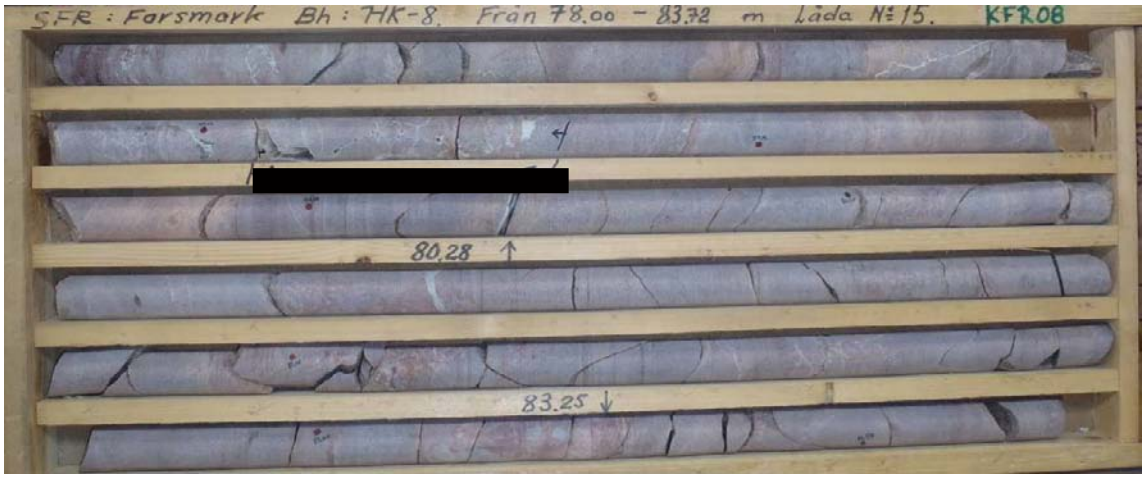

Figure A1-43. Photograph of the sampled drill core box. The sampled section is marked with a black line under the drill core.


Figure A1-44. Photograph of the sampled fractures.

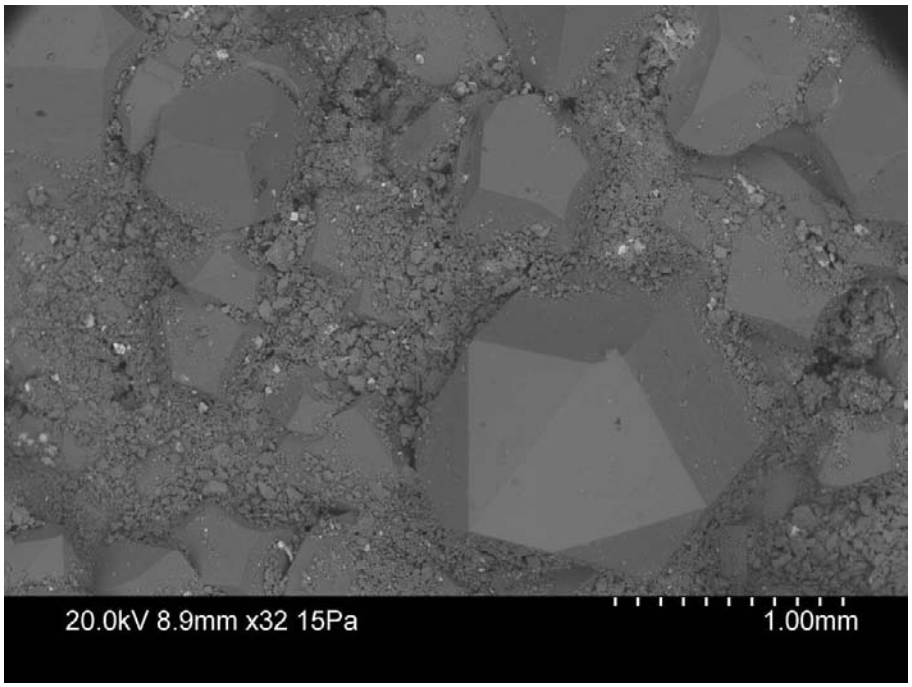

Figure A1-45. Electron image of euhedral quartz crystals, the small bright spots are pyrite crystal. The fine-grained material between the quartz crystals consists of adularia and albite.

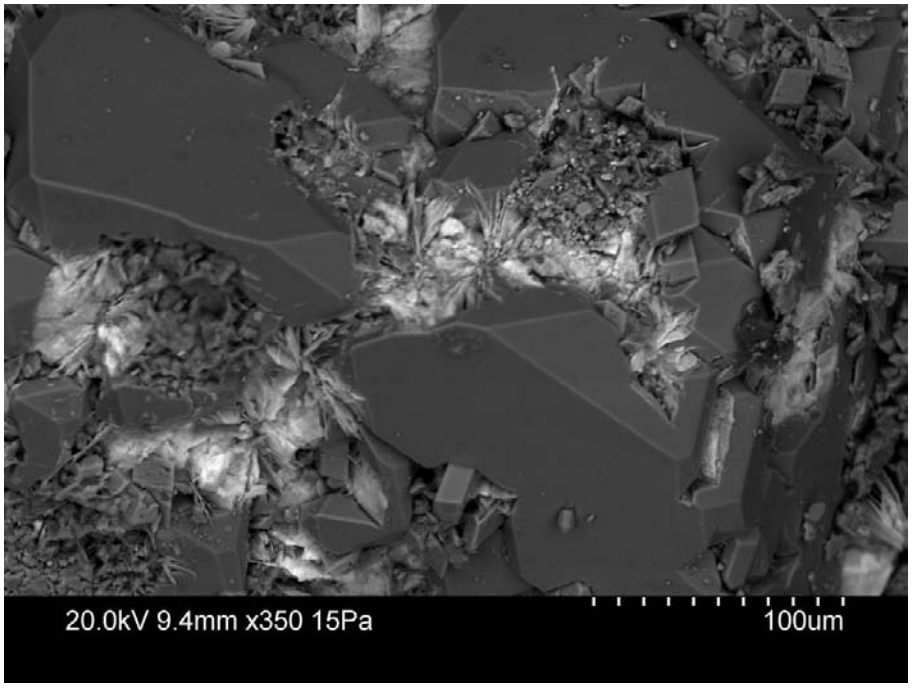

Figure A1-46. Electron image of unknown blady REE-silicate, possibly allanite, precipitated on an euhedral quartz crystal.

Borehole: KFR08
Secup: 85.96 m
Seclow: 86.16 m
Deformation zone: ZFMNW0805a, ZFMNNW0999, ZFMWNW0836
Groundwater type: Baltic
Identified minerals: Illite, corrensite, quartz, calcite, hematite, pyrite, monazite, arsenopyrite, sphalerite.

Figure A1-47. Photograph of the sampled drill core box. The sampled section is marked with a black line under the drill core.


Figure A1-48. Photograph of the sampled fractures.

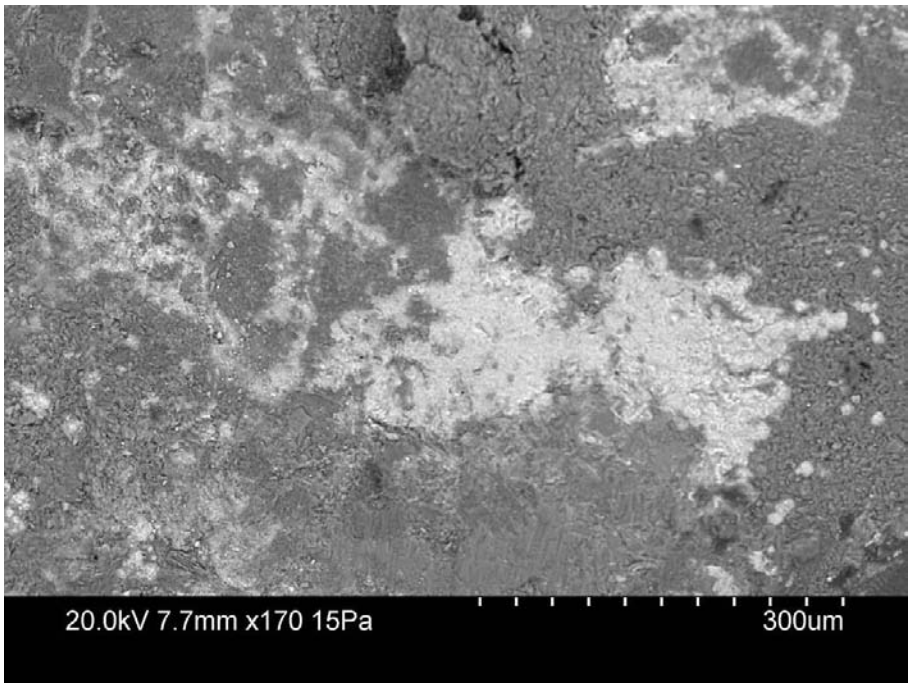

Figure A1-49. Electron image of Fe-oxide (bright) together with clay mineral (grey).

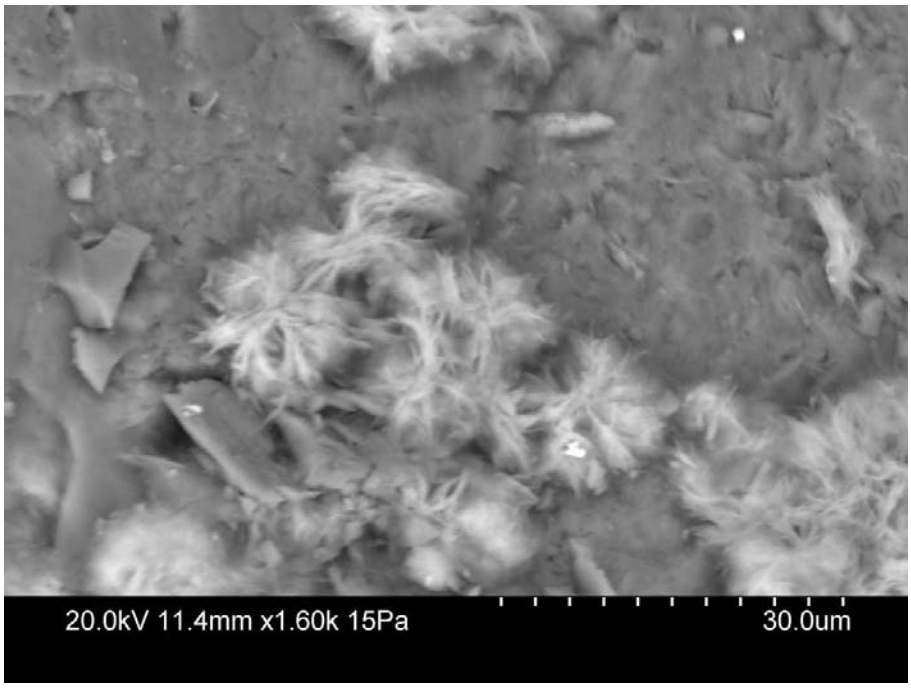

Figure A1-50. Electron image of corrensite aggregates on fracture surface with mixed layer clay.

Borehole: KFR08
Secup: 95.29 m
Seclow: 95.54 m
Groundwater type: Baltic
Deformation zone: ZFMNW0805a, ZFMNNW0999, ZFMWNW0836
Identified minerals: Calcite, adularia, albite, mixed layer clay (smectite-illite), hematite, apatite, REE-carbonate.

Figure A1-51. Photograph of the sampled drill core box. The sampled section is marked with a black line under the drill core.


Figure A1-52. Photograph of the sampled fractures.

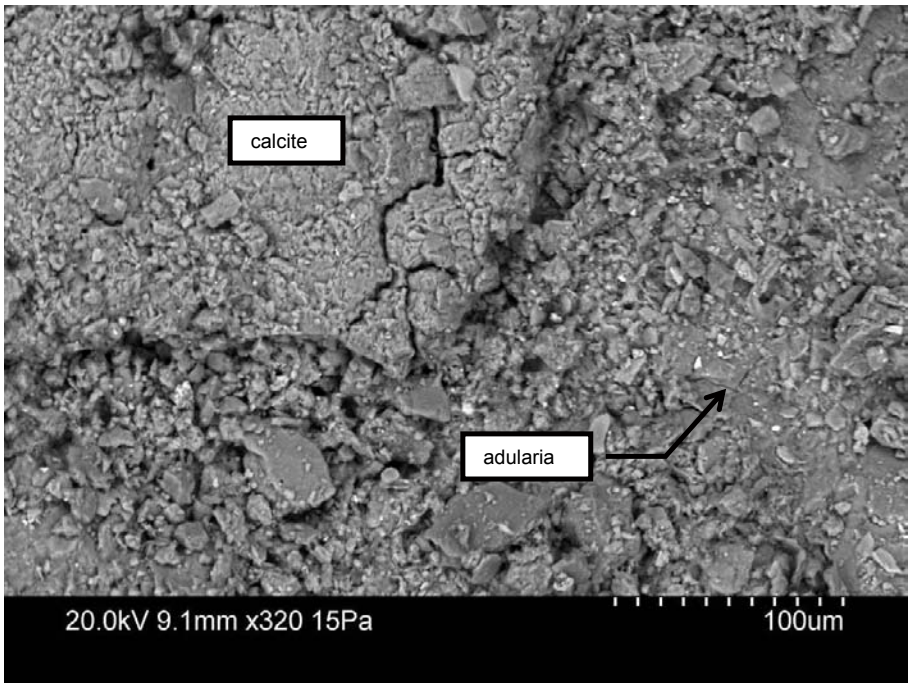

Figure A1-53. Electron image of calcite together with adularia and albite.

Borehole: KFR10
Secup: 95.65 m
Seclow: 95.80 m
Deformation zone: ZFMNNE0869
Groundwater type: Baltic
Identified minerals: Hematite, biotite, illite, chlorite, laumontite, quartz, adularia, albite, pyrite, allanite.

Figure A1-54. Photograph of the sampled drill core box. The sampled section is marked with a black line under the drill core.


Figure A1-55. Photograph of the sampled fractures.

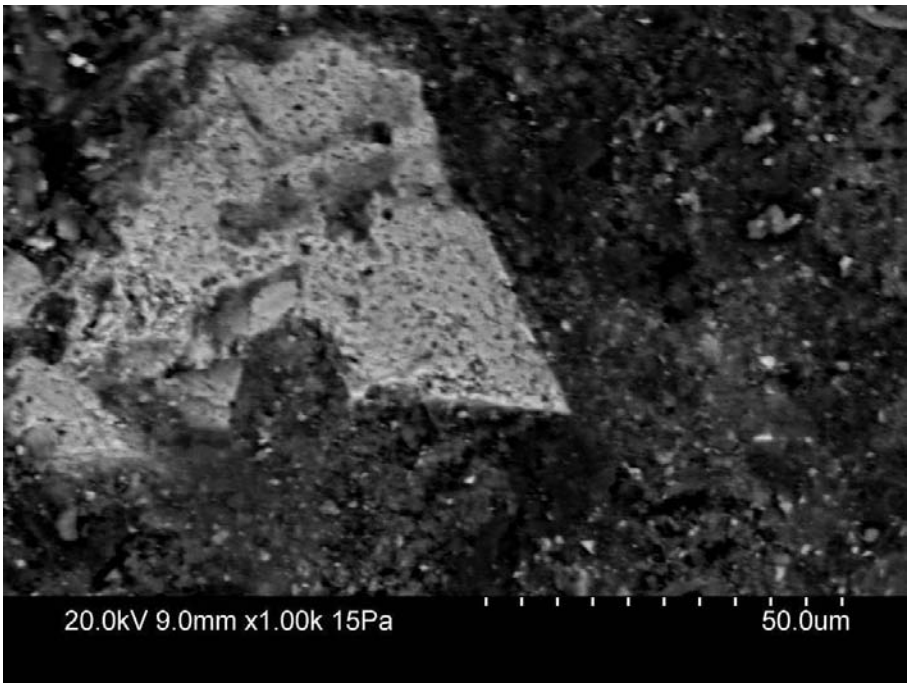

Figure A1-56. Electron image of Fe-oxide (bright) with clay mineral on fracture surface.

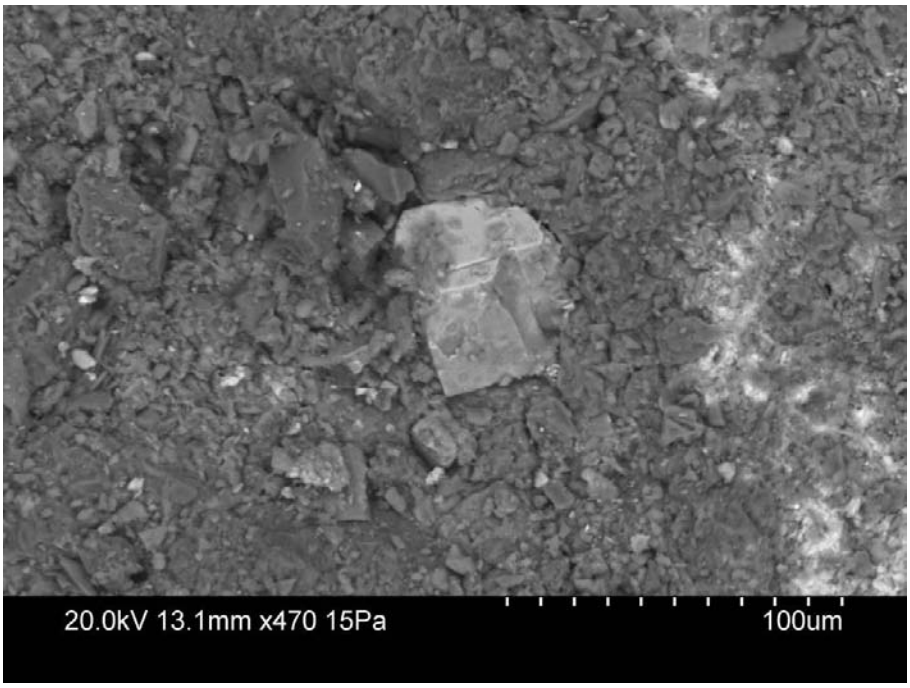

Figure A1-57. Electron image of euhedral pyrite (bright crystal) with clay mineral on fracture surface. The bright band to the right in the image consists of allanite.

Borehole: KFR10
Secup: 101.85 m
Seclow: 101.92 m
Deformation zone: Not modelled as deformation zone in the geological model, but close to ZFMNNE0869
Groundwater type: Littorina
Identified minerals: Calcite, quartz, pyrite, galena.

Figure A1-58. Photograph of the sampled drill core box. The sampled section is marked with a black line under the drill core.


Figure A1-59. Photograph of the sampled fractures.

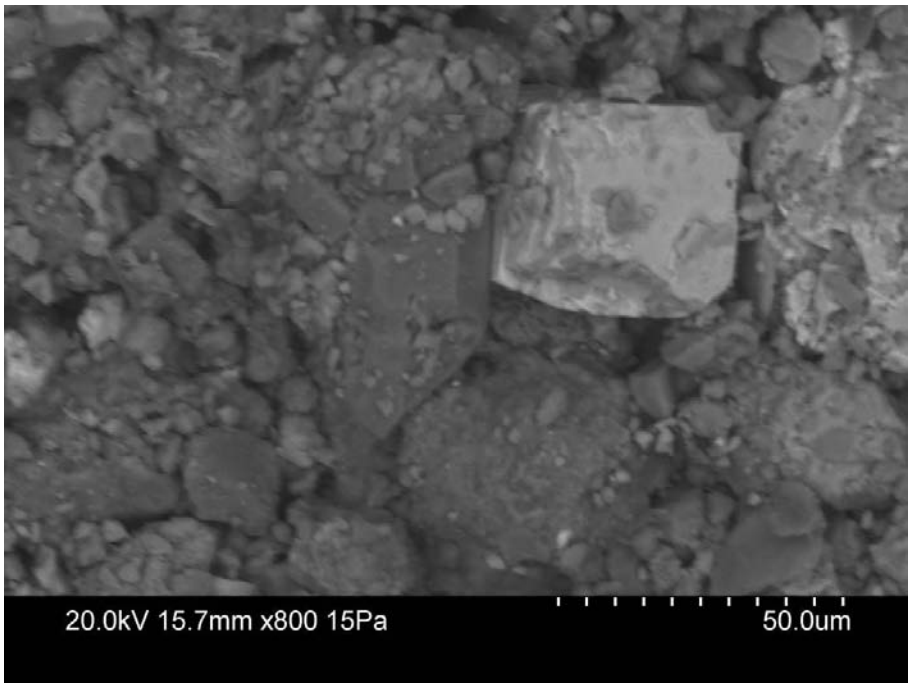

Figure A1-60. Electron image of pyrite (light grey) with quartz on fracture surface.

Borehole: KFR10
Secup: 106.30 m
Seclow: 106.50 m
Deformation zone: Not modelled as deformation zone in the geological model, but close to ZFMNNE0869
Groundwater type: Littorina
Identified minerals: Quartz, adularia, albite, mixed layer clay (smectite-illite), pyrite, corrensite, barite, allanite.

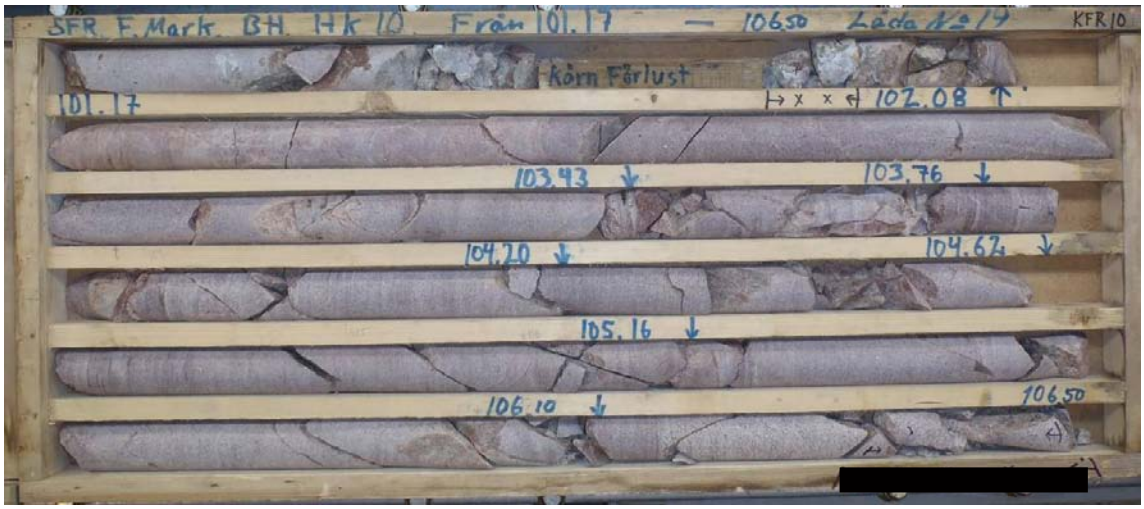

Figure A1-61. Photograph of the sampled drill core box. The sampled section is marked with a black line under the drill core.


Figure A1-62. Photograph of the sampled fractures.

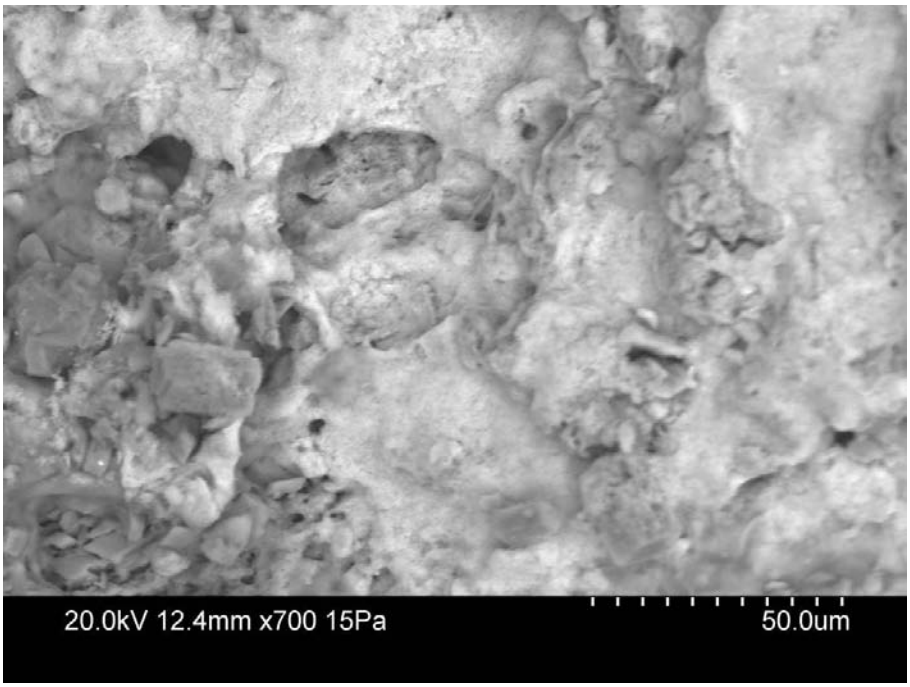

Figure A1-63. Electron image of Fe-oxide (bright) with clay mineral on fracture surface.

Borehole: KFR19
Secup: 90.56 m
Seclow: 90.74 m
Deformation zone: Not modelled as deformation zone in the geological model
Groundwater type: Baltic
Identified minerals: Illite, mixed layer clay (smectite-illite), quartz, calcite, adularia, hematite, U-silicate.

Figure A1-64. Photograph of the sampled drill core box. The sampled section is marked with a black line under the drill core.


Figure A1-65. Photograph of the sampled fractures.

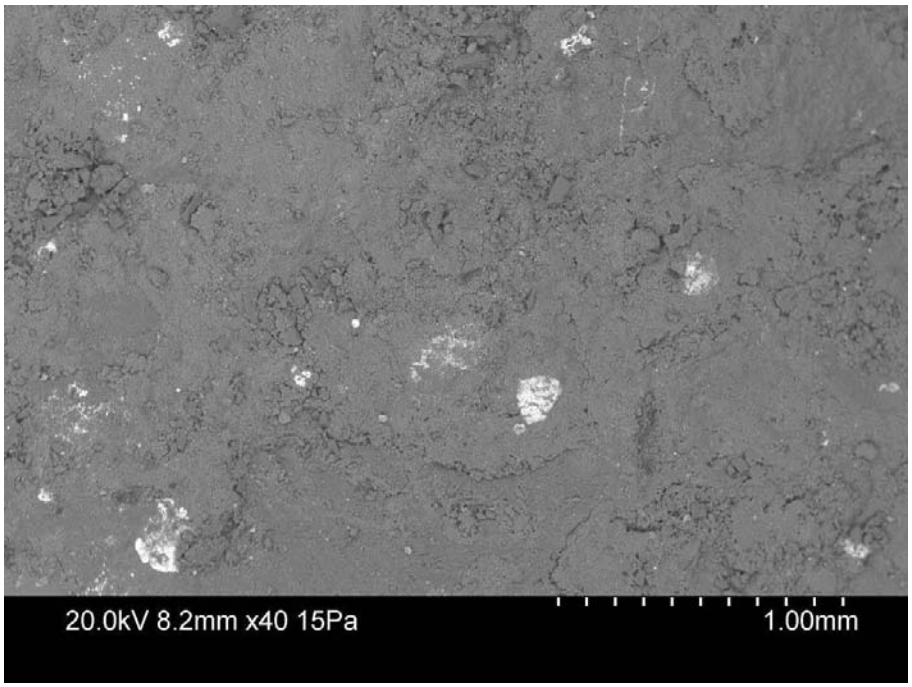

Figure A1-66. Electron image of uranium-silicate (bright) on surface coated with clay mineral

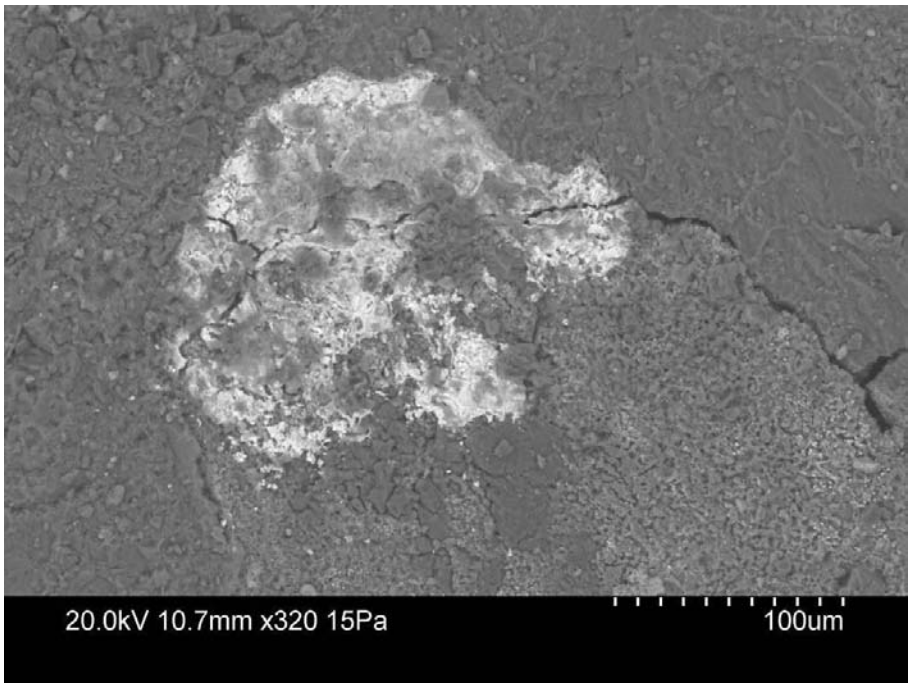

Figure A1-67. Electron image of uranium-silicate (bright) on surface coated with clay mineral, calcite and quartz.

Borehole: KFR19
Secup: 91.05 m
Seclow: 91.14 m
Deformation zone: Not modelled as deformation zone in the geological model
Groundwater type: Baltic
Identified minerals: Illite, mixed layer clay (smectite-illite), quartz, albite, adularia, calcite, U-silicate.

Figure A1-68. Photograph of the sampled drill core box. The sampled section is marked with a black line under the drill core.


Figure A1-69. Photograph of the sampled fractures

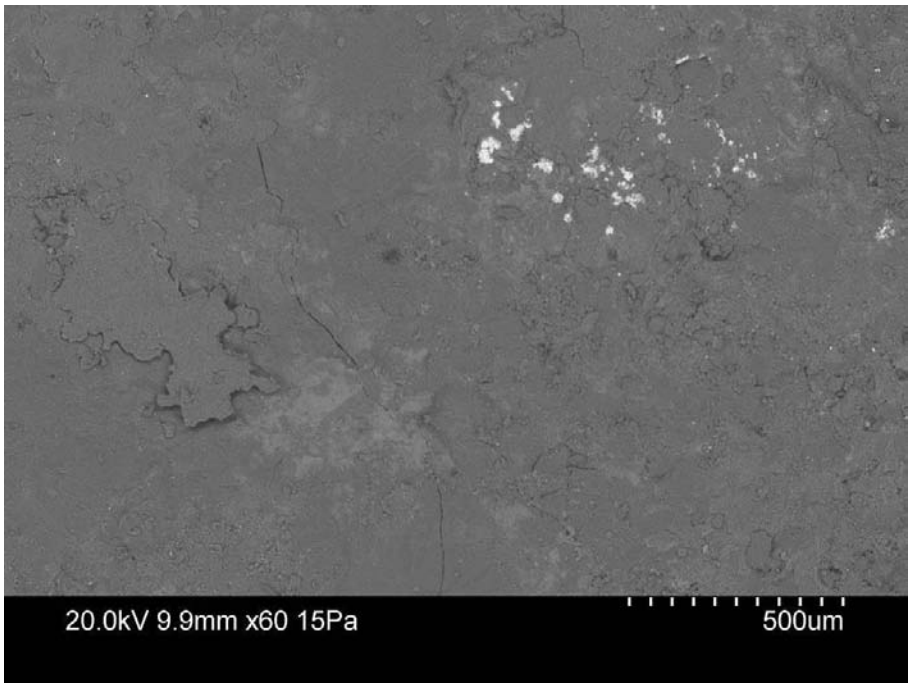

Figure A1-70. Electron image of uranium-silicate (bright) on surface coated with clay mineral and quartz.

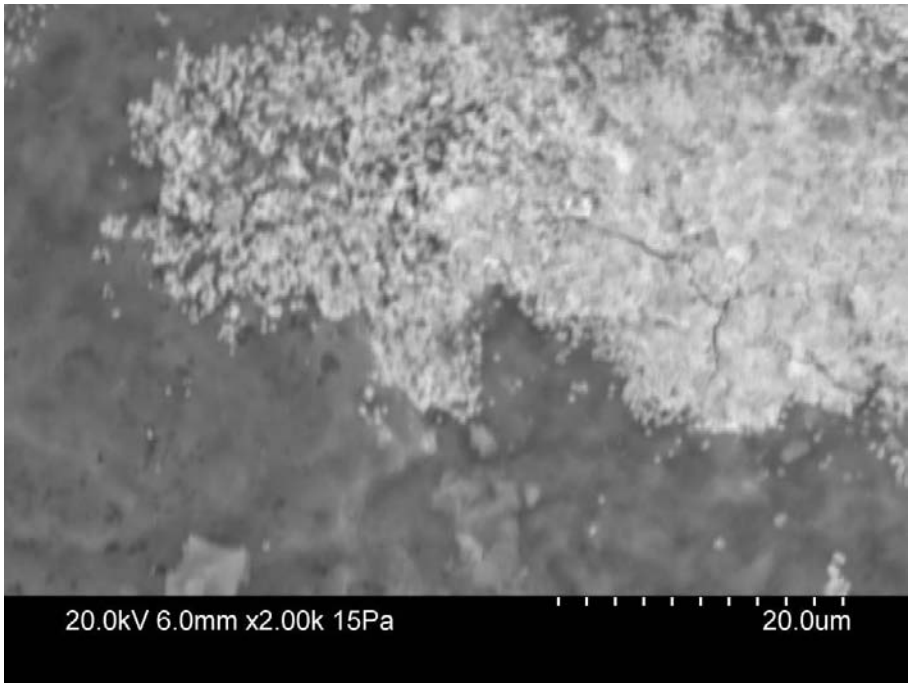

Figure A1-71. Electron image of uranium-silicate (bright) on surface coated with clay mineral.

Borehole: KFR19
Secup: 96.97 m
Seclow: 97.26 m
Deformation zone: Not modelled as deformation zone in the geological model
Groundwater type: Baltic
Identified minerals: Chlorite, mixed layer clay, adularia, allanite, calcite, quartz.

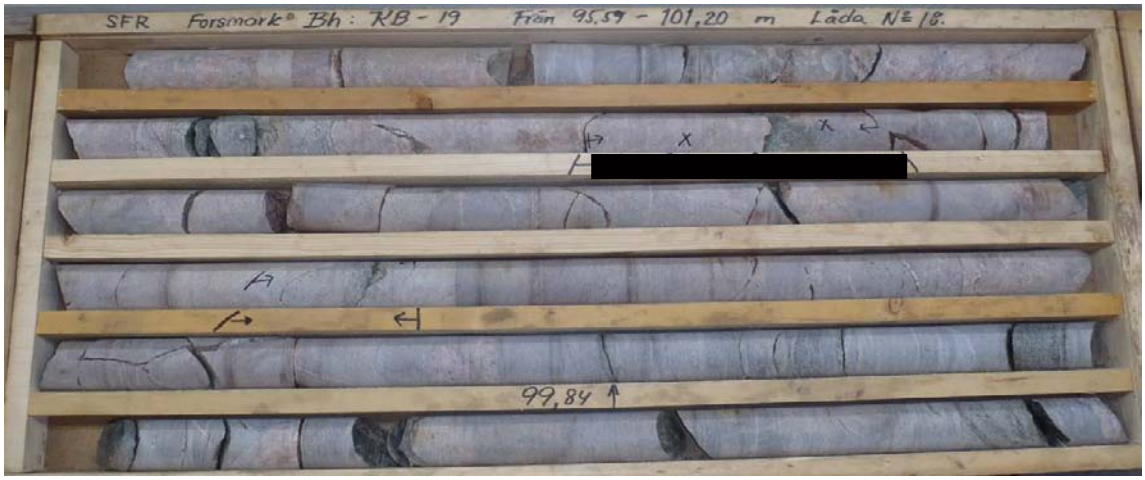

Figure A1-72. Photograph of the sampled drill core box. The sampled section is marked with a black line under the drill core.


Figure A1-73. Photograph of the sampled fractures.

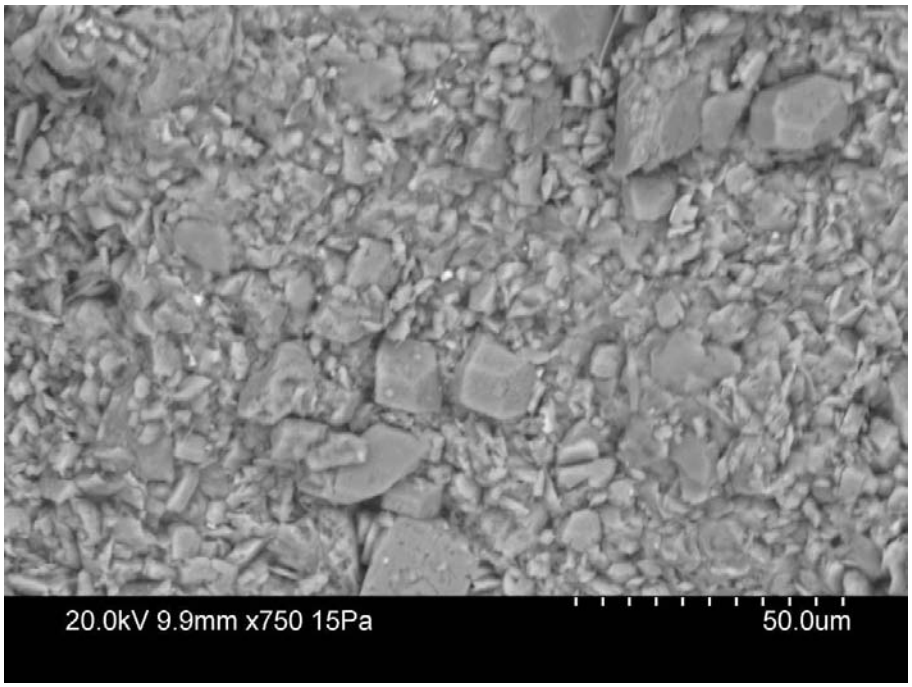

Figure A1-74. Electron image of euhedral calcite crystals on fracture surface coated with clay mineral.

Borehole: KFR19
Secup: 98.56 m
Seclow: 98.71 m
Deformation zone: Not modelled as deformation zone in the geological model.
Groundwater type: Baltic
Identified minerals: Calcite, quartz, albite, adularia, illite, barite, REE-carbonate, Fe-oxy-hydroxide, chalcopyrite.

Figure A1-75. Photograph of the sampled drill core box. The sampled section is marked with a black line under the drill core.


Figure A1-76. Photograph of the sampled fractures.

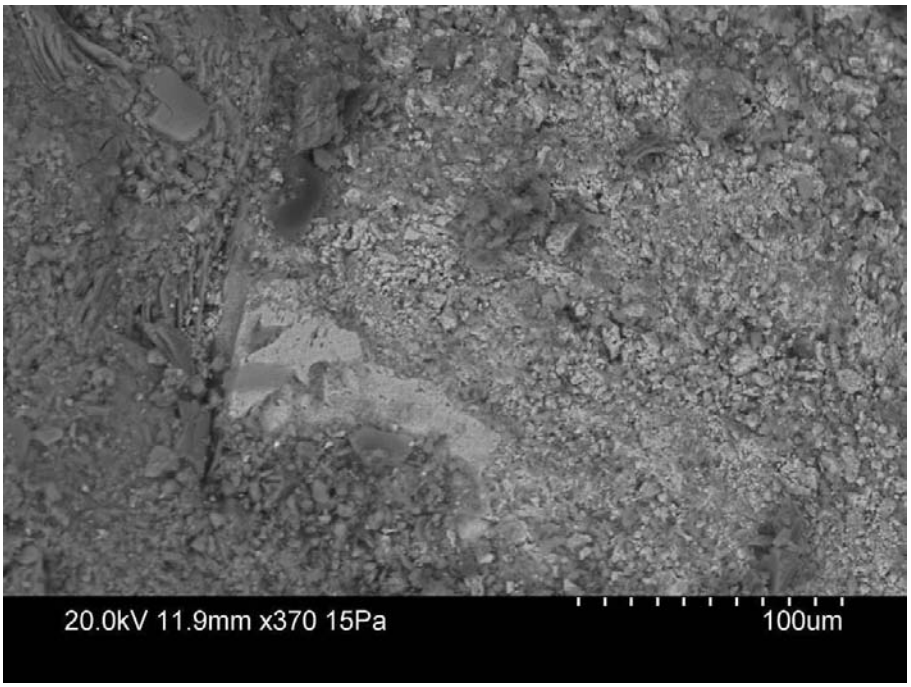

Figure A1-77. Electron image of Fe-oxy-hydroxide together with clay mineral.

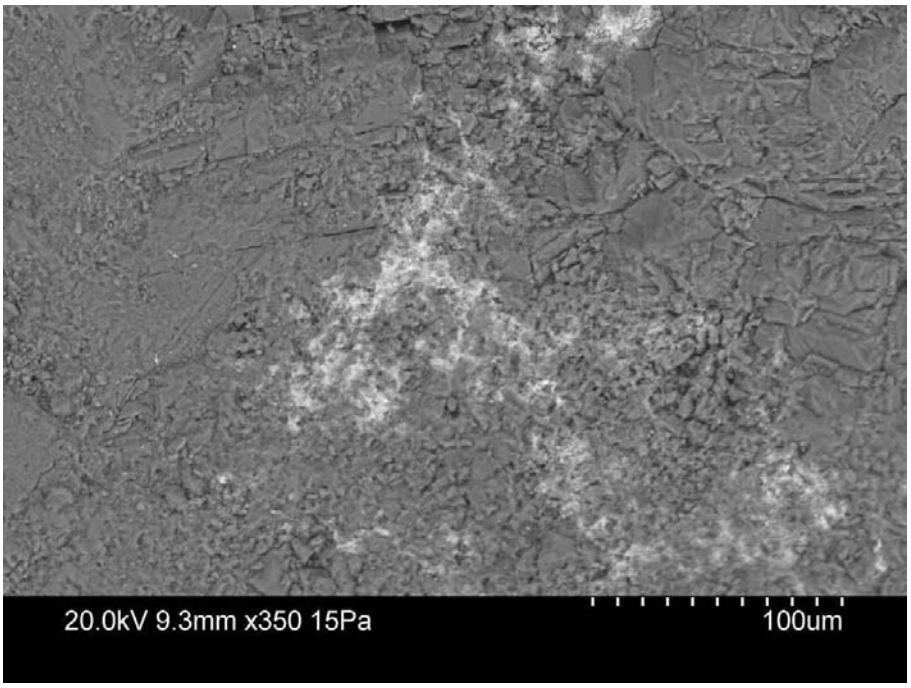

Figure A1-78. Electron image of REE-carbonate (bright) together with clay mineral.

Borehole: KFR105
Secup: 124.05 m
Seclow: 124.32 m
Deformation zone: Not modelled as deformation zone in the geological model
Groundwater type: Transition
Identified minerals: Mixed layer clay (smectite-illite), chlorite, quartz, adularia, pyrite, barite, fluorite.

Figure A1-79. Photograph of the sampled drill core box. The sampled section is marked with a black line under the drill core.


Figure A1-80. Photograph of the sampled fractures.

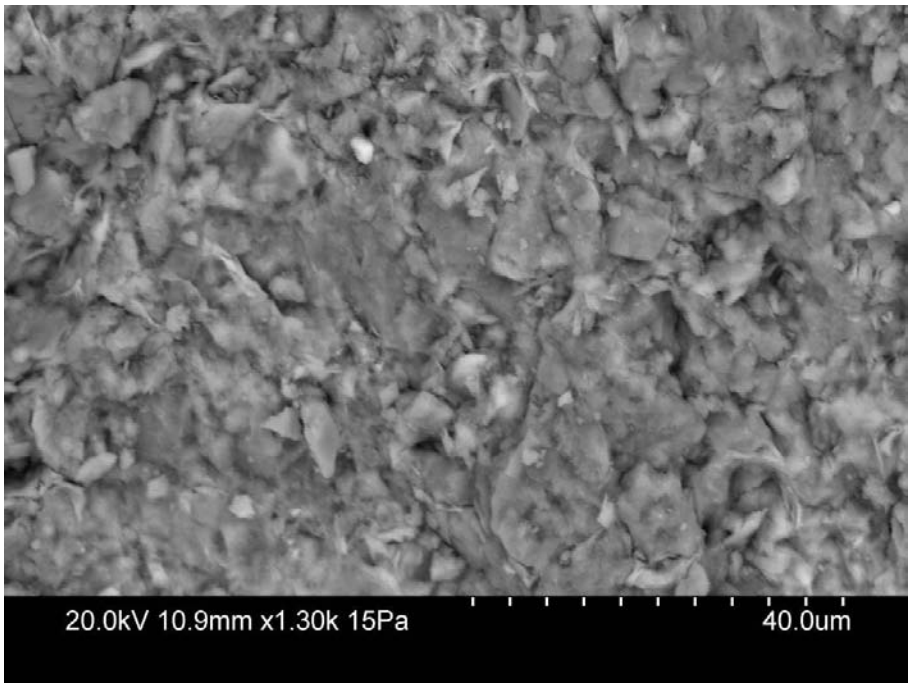

Figure A1-81. Electron image of clay mineral.

Borehole: KFR105
Secup: 126.90 m
Seclow: 127.08 m
Deformation zone: Not modelled as deformation zone in the geological model
Groundwater type: Transition
Identified minerals: Illite, mixed layer clay (smectite-illite), chlorite, albite, quartz, adularia, biotite, barite, hematite.

Figure A1-82. Photograph of the sampled drill core box. The sampled section is marked with a black line under the drill core.


Figure A1-83. Photograph of the sampled fractures.

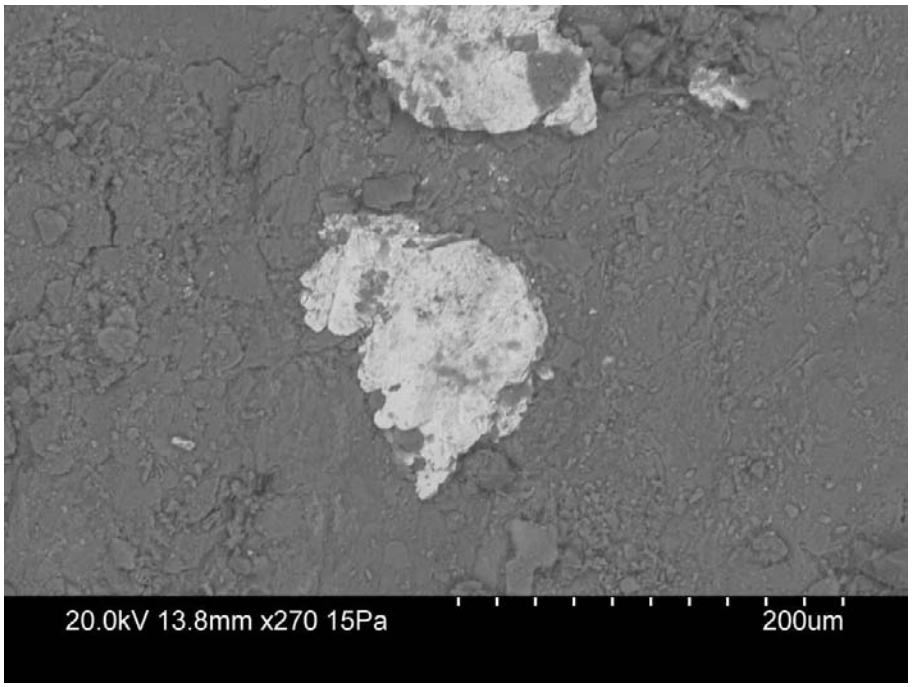

Figure A1-84. Electron image of barite (bright on surface coated with clay mineral.

Borehole: KFR105
Secup: 133.50 m
Seclow: 133.75 m
Deformation zone: Not modelled as deformation zone in the geological model
Groundwater type: Transition
Identified minerals: Mixed layer clay, adularia, quartz, albite, celestine-barite, Ca-Y-silicate.

Figure A1-85. Photograph of the sampled drill core box. The sampled section is marked with a black line under the drill core.


Figure A1-86. Photograph of the sampled fractures.

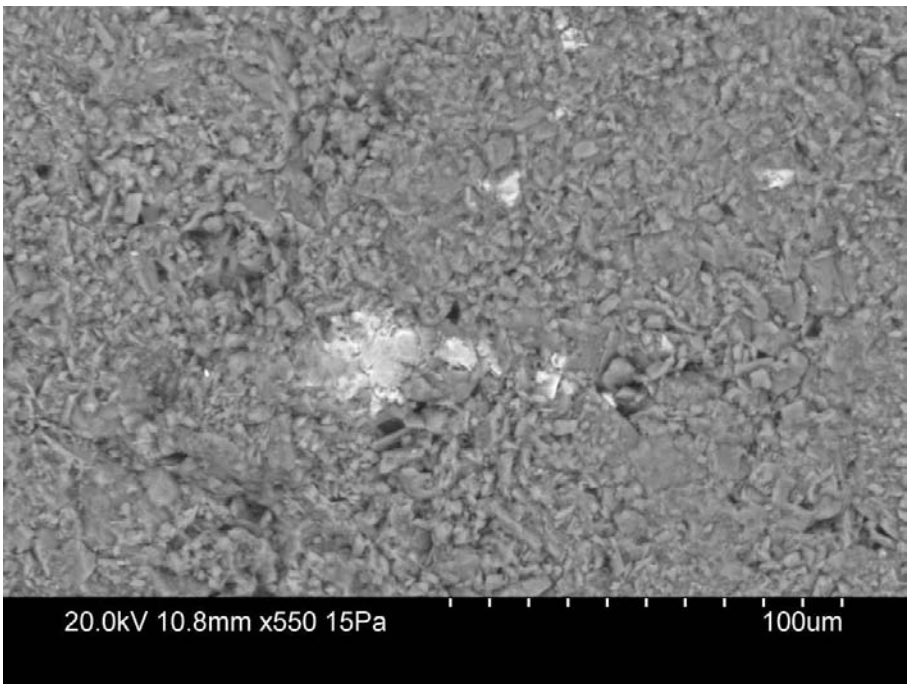

Figure A1-87. Electron image of Ca-Y-silicate (bright) together with clay mineral.

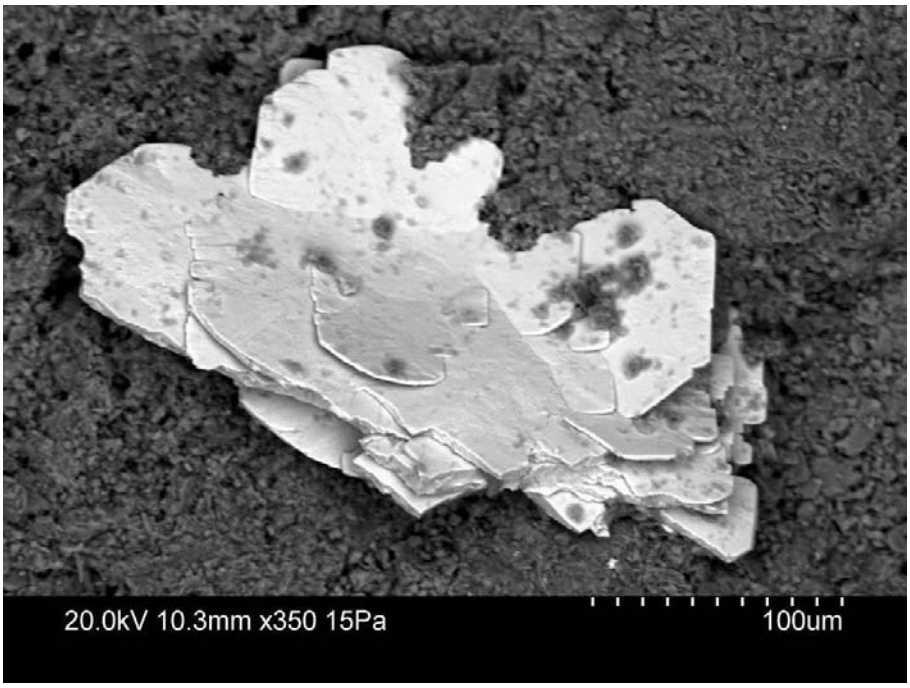

Figure A1-88. Electron image of celestine-barite (bright) on surface coated with clay mineral.

Borehole: KFR105
Secup: 267.80 m
Seclow: 268.05 m
Deformation zone: ZFMWNW3267
Groundwater type: Glacial
Identified minerals: Laumontite, muscovite, allanite, REE-carbonate, barite
.

Figure A1-89. Photograph of the sampled drill core box. The sampled section is marked with a black line under the drill core.


Figure A1-90. Photograph of the sampled fractures.

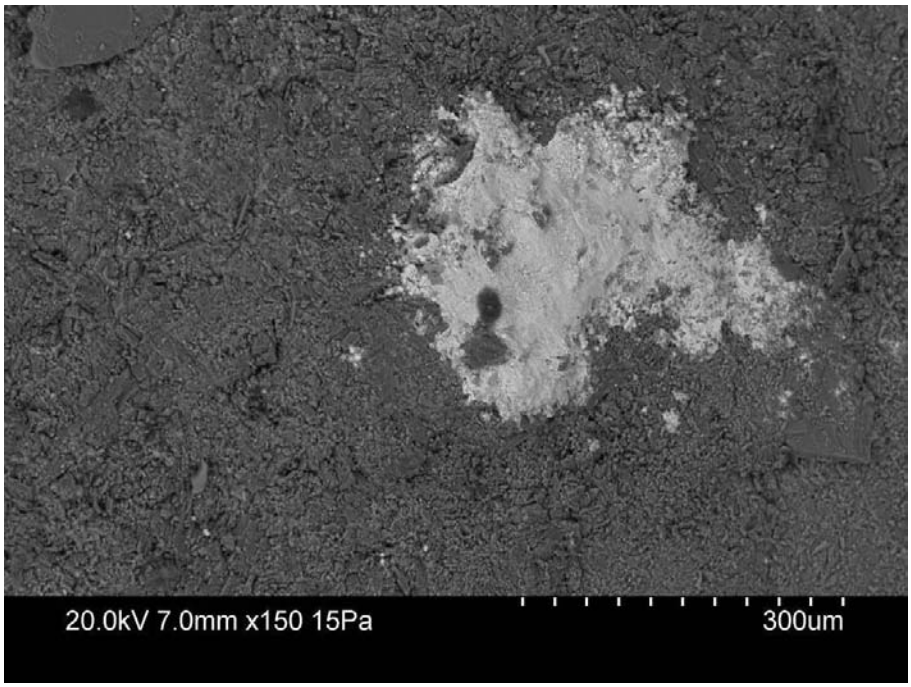

Figure A1-91. Electron image of REE-carbonate (bright) on laumontite surface.

Borehole: KFR105
Secup: 280.07 m
Seclow: 280.13 m
Deformation zone: ZFMWNW3267
Groundwater type: Glacial
Identified minerals: Illite, laumontite, quartz, adularia, albite, biotite, harmotome, galena.

Figure A1-92. Photograph of the sampled drill core box. The sampled section is marked with a black line under the drill core.


Figure A1-93. Photograph of the sampled fractures.

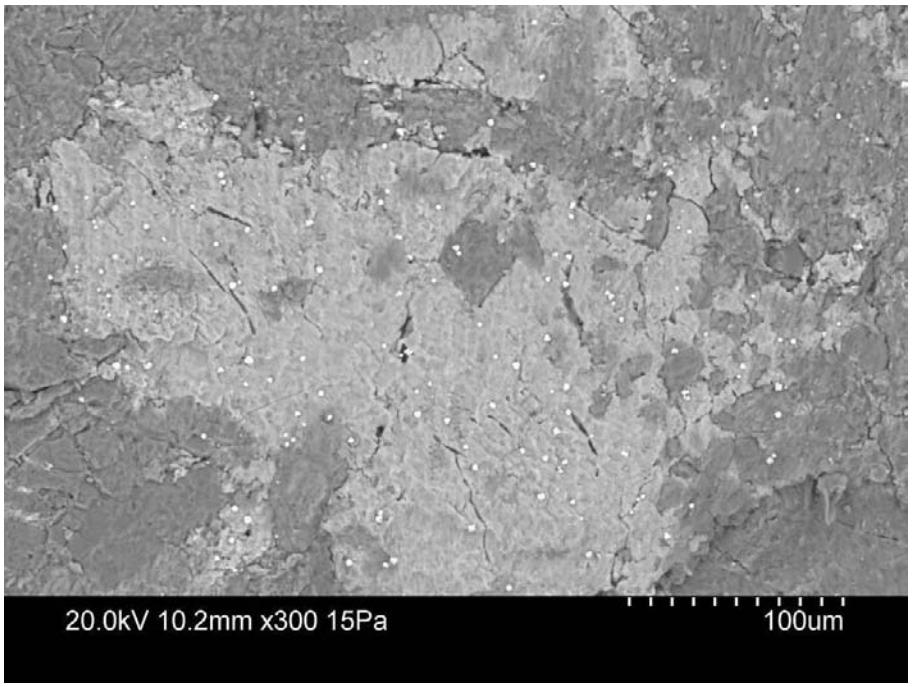

Figure A1-94. Electron image of harmotome crystals (small white grains) on pyrite (light grey) surrounded by quartz (grey).

Borehole: KFR105
Secup: 283.38 m
Seclow: 283.57 m
Deformation Zone: Not modelled as deformation zone in the geological model, but close to ZFMWNW3267
Groundwater type: Glacial
Identified minerals: Corrensite, laumontite, calcite, quartz, hematite, pyrite.

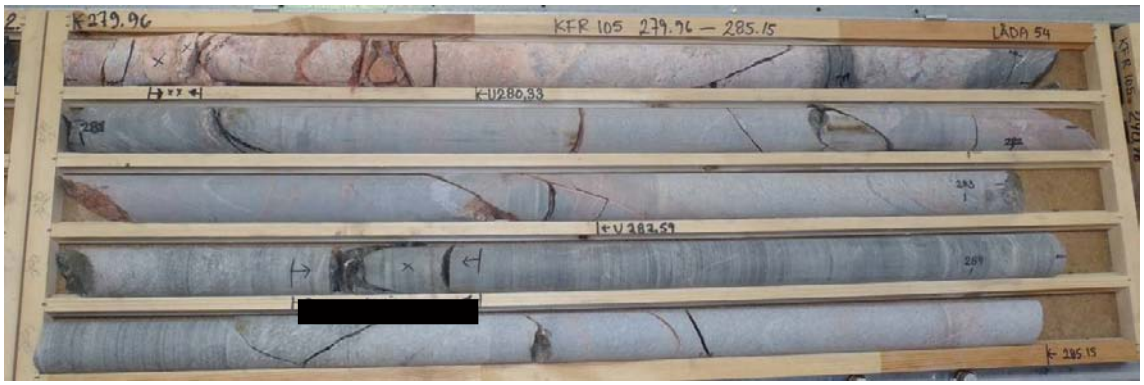

Figure A1-95. Photograph of the sampled drill core box. The sampled section is marked with a black line under the drill core.


Figure A1-96. Photograph of the sampled fractures.

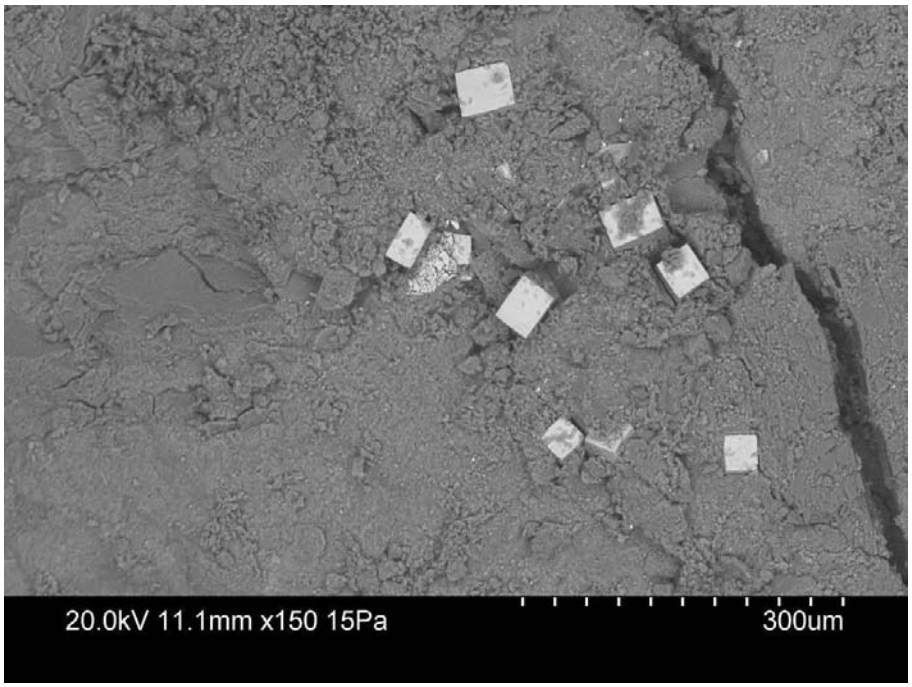

Figure A1-97. Electron image of euhedral pyrite crystals (bright) on fracture surface coated with illite and quartz.

Borehole: KFR105
Secup: 298.35 m
Seclow: 298.46 m
Deformation zone: Not modelled as deformation zone in the geological model
Groundwater type: Glacial
Identified minerals: Laumontite, quartz, U-silicate, pyrite, adularia.

Figure A1-98. Photograph of the sampled drill core box. The sampled section is marked with a black line under the drill core.


Figure A1-99. Photograph of the sampled fractures.

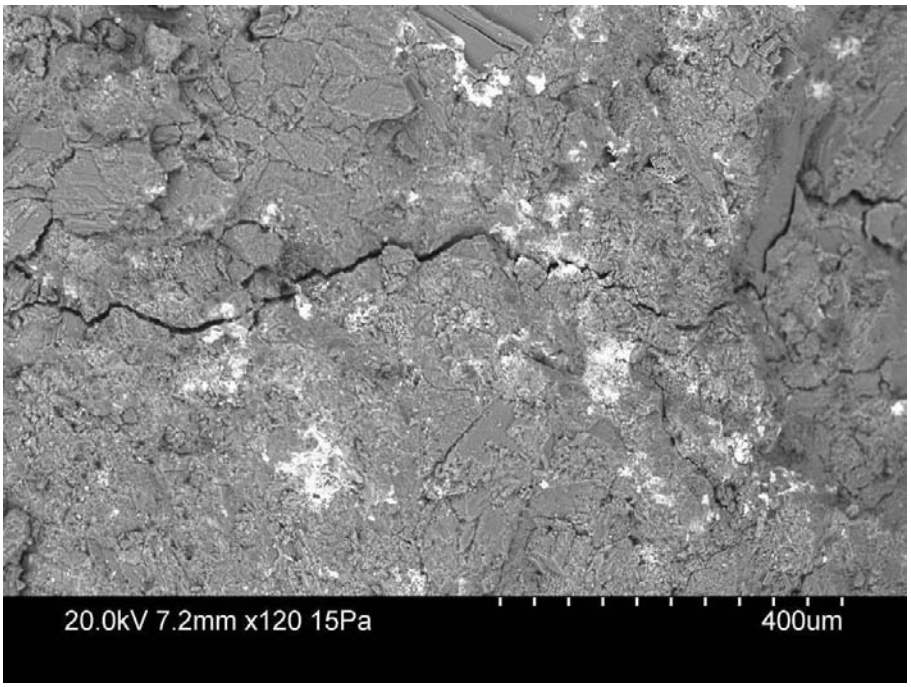

Figure A1-100. Electron image of uranium-silicate (bright) together with laumontite and quartz..

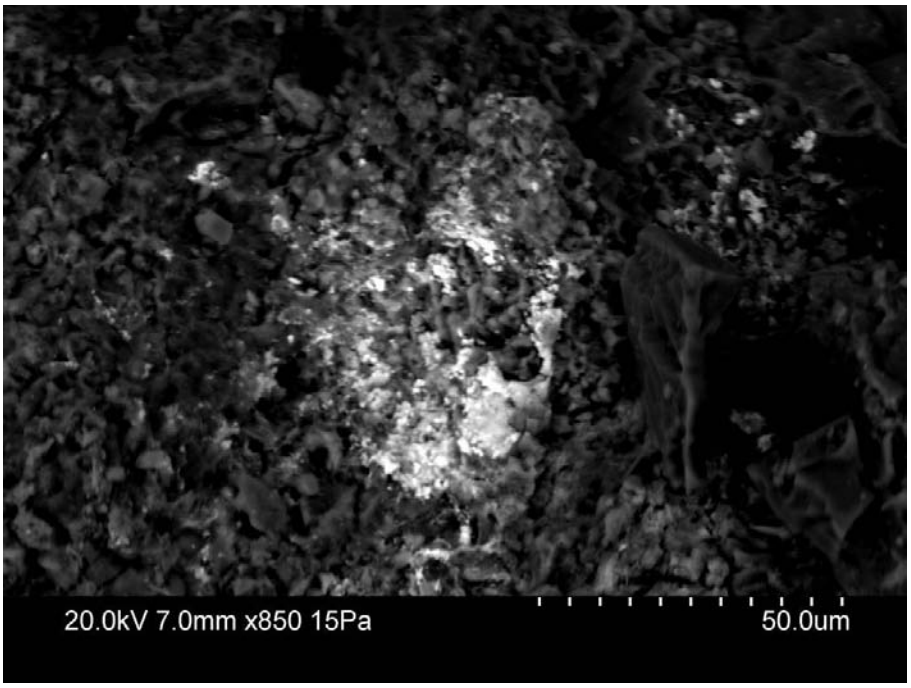

Figure A1-101. Electron image of uranium-silicate (bright) together with laumontite.

XRD Spectras

KFR01 45.18 WR

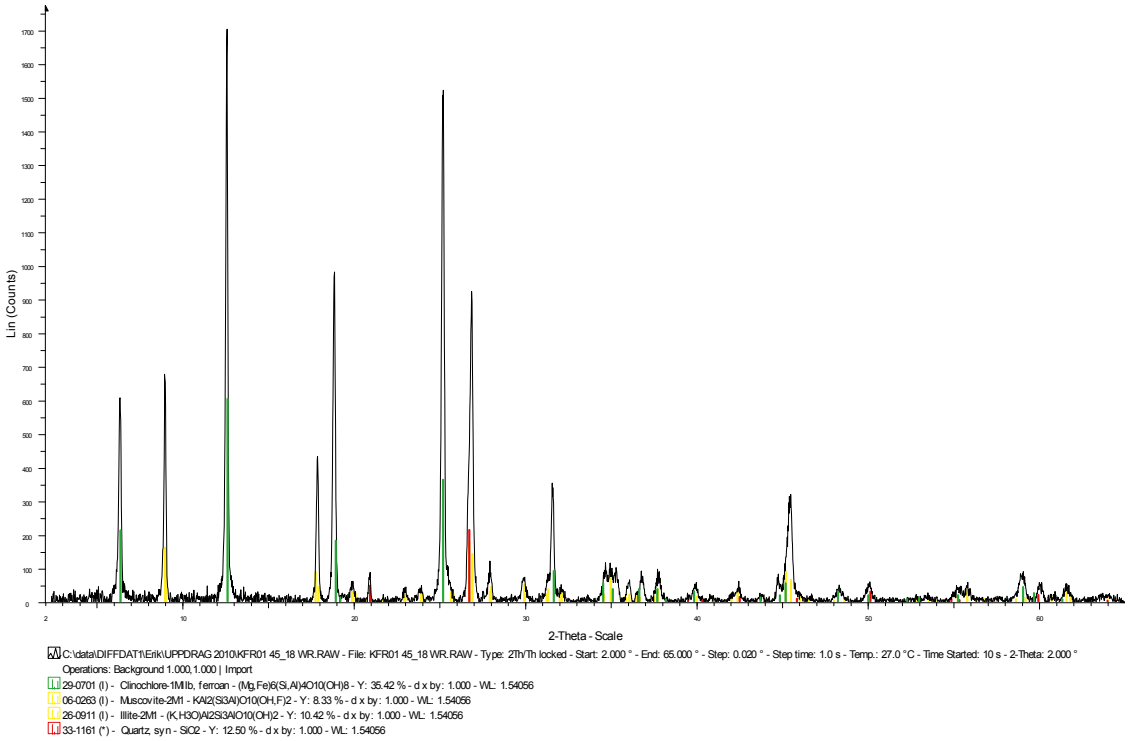

KFR7A 49.60 WR

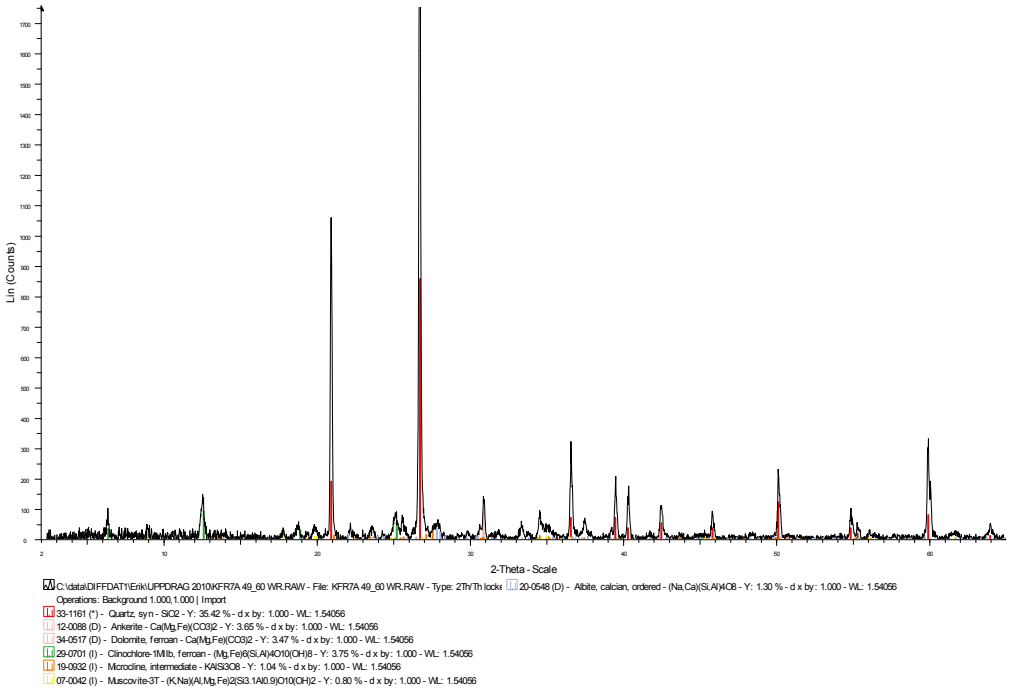

KFR7A 70.05 WR

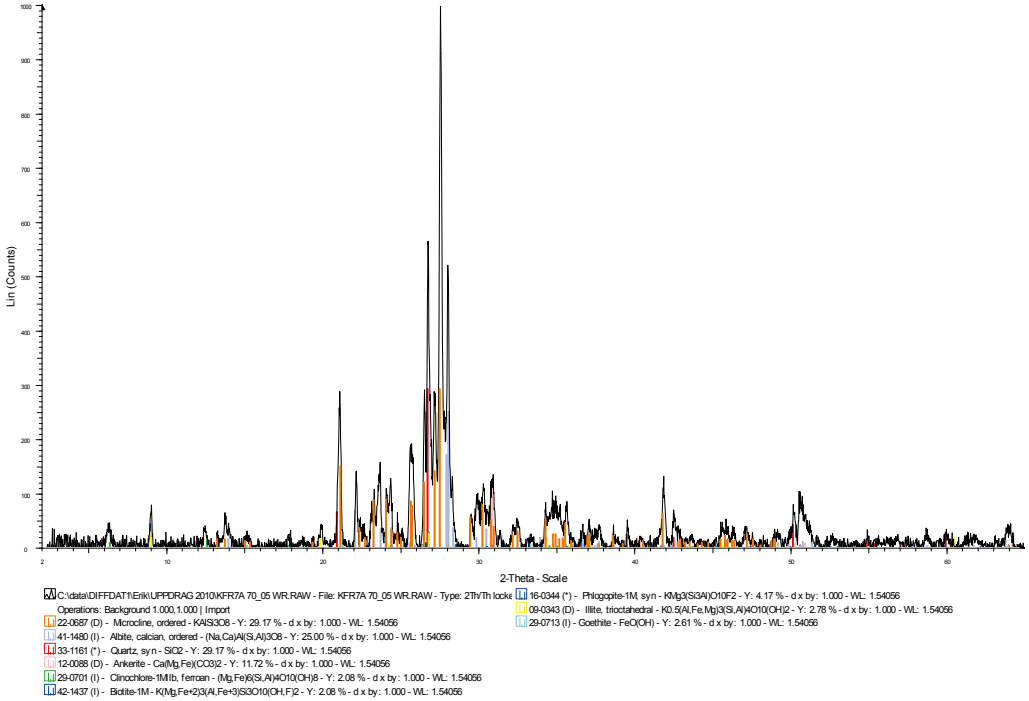

KFR7A 70.47 WR

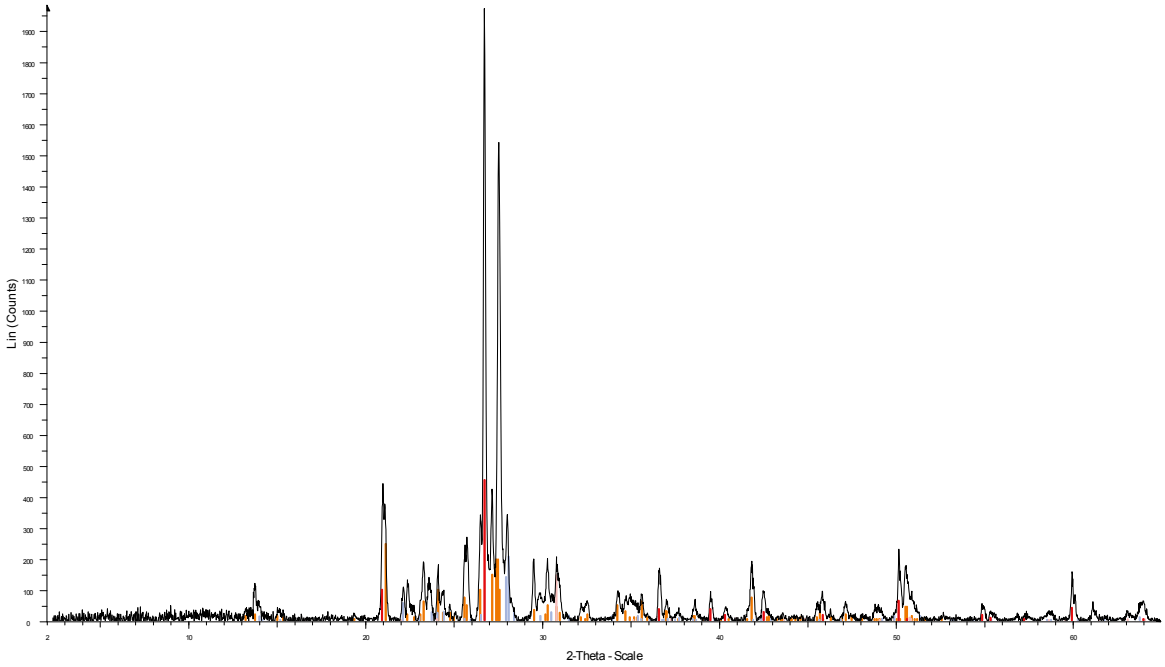

KFR08 76.77 WR

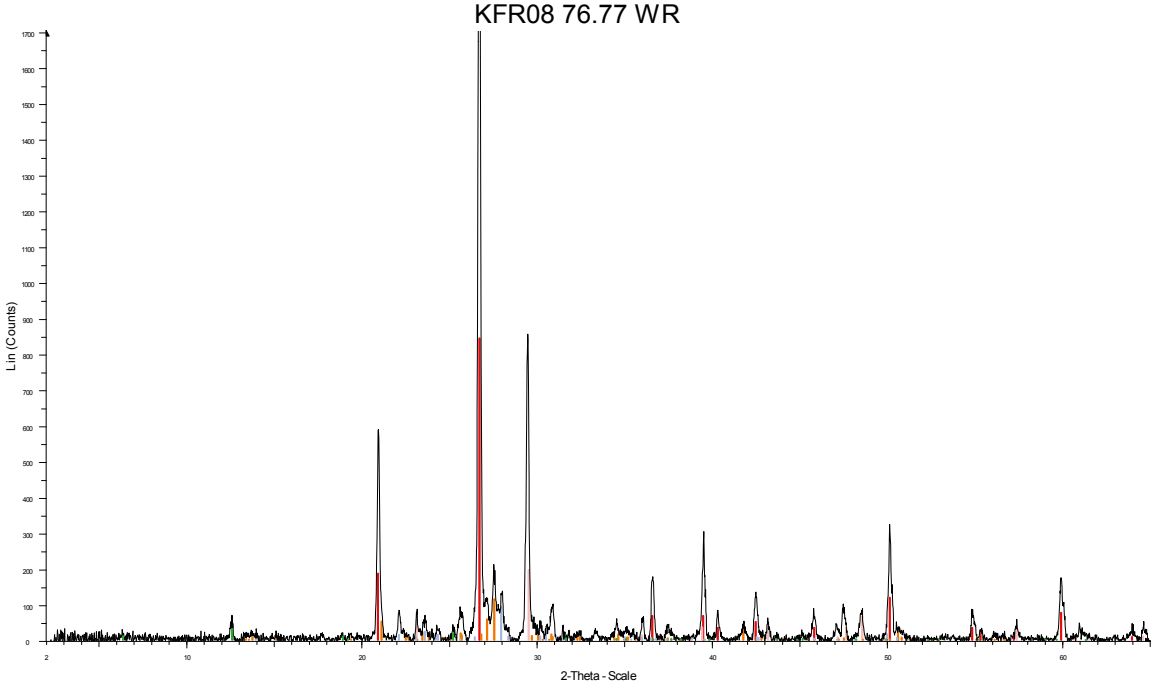

C:\data\DIFFDAT1\Erik\UPPDRAG 2010\KFR08 76_77 WR.RAW - File: KFR08 76_77 WR.RAW - Type: 2Th/Th locked - Start: 2.000 ° - End: 65.000 ° - Step: 0.020 ° - Step time: 1.0 s - Temp.: 27.0 °C - Time Started: 3 s - 2-Theta: 2.000 ° -
Operations: Background 1.000,1.000 | Import

33-1161 (*) - Quartz, syn - SiO2 - Y: 31.25 % - d x by: 1.000 - WL: 1.54056
24-0027 (D) - Calcite - CaCO3 - Y: 7.29 % - d x by: 1.000 - WL: 1.54056
19-0932 (I) - Microcline, intermediate - KAlSi3O8 - Y: 4.25 % - d x by: 1.000 - WL: 1.54056
09-0466 (*) - Albite, ordered - NaAlSi3O8 - Y: 3.47 % - d x by: 1.000 - WL: 1.54056
29-0701 (I) - Clinochlore-1MIb, ferroan - (Mg,Fe)6(Si,Al)4O10(OH)8 - Y: 1.17 % - d x by: 1.000 - WL: 1.54056

KFR08 79.13 WR

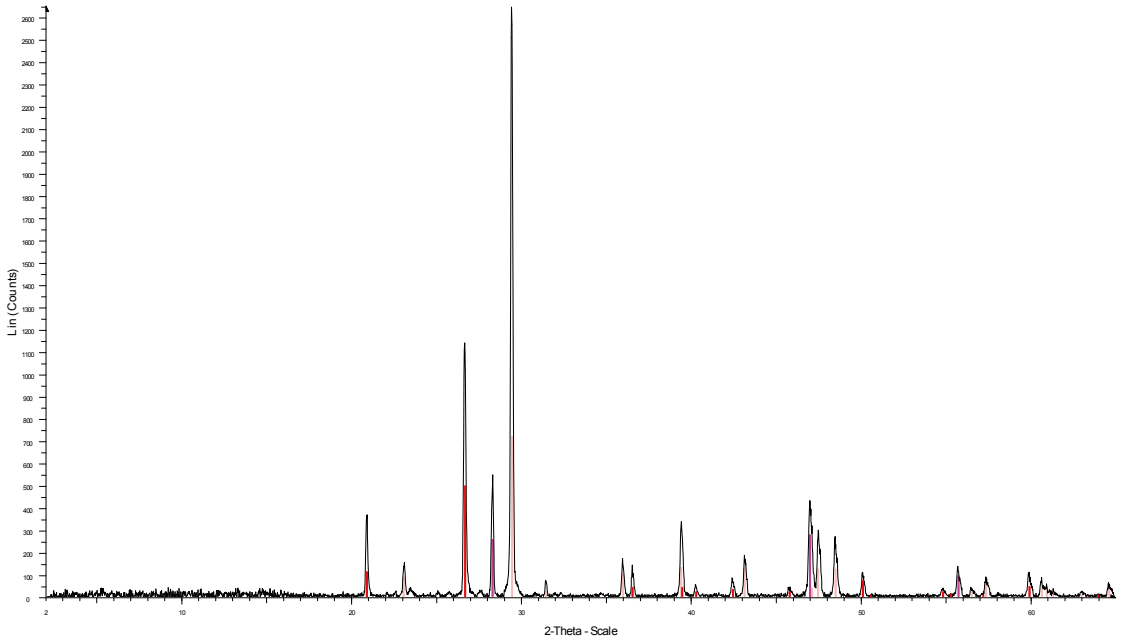

C:\data\DIFFDAT1\Erik\UPPDRAG 2010\KFR08 79_13 WR.RAW - File: KFR08 79_13 WR.RAW - Type: 2Th/Th locked - Start: 2.000 ° - End: 65.000 ° - Step: 0.020 ° - Step time: 1.0 s - Temp.: 27.0 °C - Time Started: 3 s - 2-Theta: 2.000 ° -
Operations: Background 1.000,1.000 | Import

05-0586 (*) - Calcite, syn - CaCO3 - Y: 27.08 % - d x by: 1.000 - WL: 1.54056
33-1161 (*) - Quartz, syn - SiO2 - Y: 18.75 % - d x by: 1.000 - WL: 1.54056
35-0816 (*) - Fluorite, syn - CaF2 - Y: 10.42 % - d x by: 1.000 - WL: 1.54056

KFR08 95.29 WR

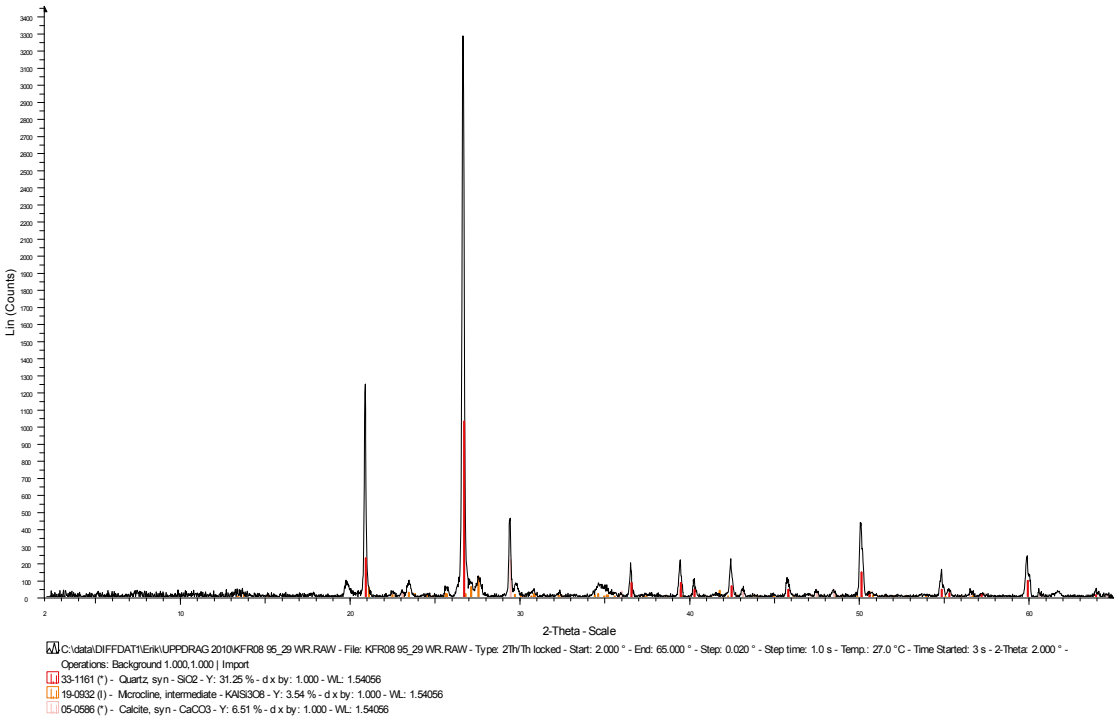

C:\data\DIFFDAT\Erik\UPPDRAG 2010\KFR08 95_29 WR.RAW - File: KFR08 95_29 WR.RAW - Type: 2Th/Th locked - Start: 2.000 ° - End: 65.000 ° - Step: 0.020 ° - Step time: 1.0 s - Temp.: 27.0 °C - Time Started: 3 s - 2-Theta: 2.000 ° -
Operations: Background 1.000,1.000 | Import
33-1161 (*) - Quartz, syn - SiO2 - Y: 31.25 % - d x by: 1.000 - WL: 1.54056
19-0932 (I) - Microcline, intermediate - KAlSi3O8 - Y: 3.54 % - d x by: 1.000 - WL: 1.54056
05-0586 (*) - Calcite, syn - CaCO3 - Y: 6.51 % - d x by: 1.000 - WL: 1.54056

KFR10 95.65 WR

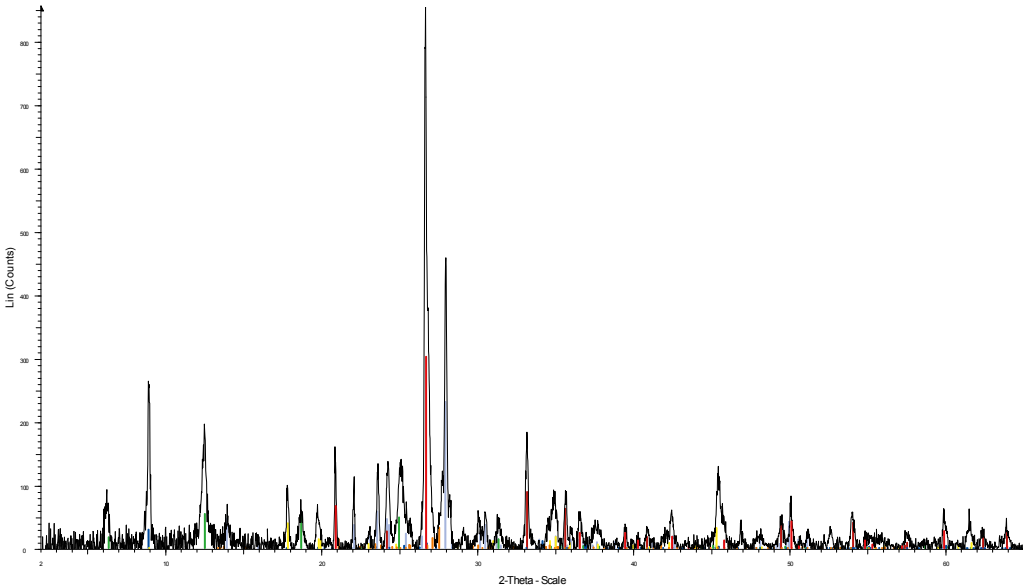

C:\data\DIFFDAT\Erik\UPPDRAG 2010\KFR10 95_65 WR.RAW - File: KFR10 95_65 WR.RAW - Type: 2Th/Th locke 19-0932 (I) - Microcline, intermediate - KAlSi3O8 - Y: 3.82 % - d x by: 1.000 - WL: 1.54056
Operations: Background 1.000,1.000 | Import
33-1161 (*) - Quartz, syn - SiO2 - Y: 35.42 % - d x by: 1.000 - WL: 1.54056
09-0466 (*) - Albite, ordered - NaAlSi3O8 - Y: 27.08 % - d x by: 1.000 - WL: 1.54056
33-0664 (*) - Hematite, syn - Fe2O3 - Y: 10.42 % - d x by: 1.000 - WL: 1.54056
12-0185 (D) - Clinochlore - (Mg,Fe,Al)6(Si,Cr)4O10(OH)8 - Y: 6.68 % - d x by: 1.000 - WL: 1.54056
42-1339 (C) - Biotite-2M1 - KMg3(Si3Al)O10(OH)2 - Y: 3.47 % - d x by: 1.000 - WL: 1.54056
07-0042 (I) - Muscovite-3T - (K,Na)(Al,Mg,Fe)2(Si3.1Al0.9)O10(OH)2 - Y: 4.58 % - d x by: 1.000 - WL: 1.54056

KFR19 90.56 WR

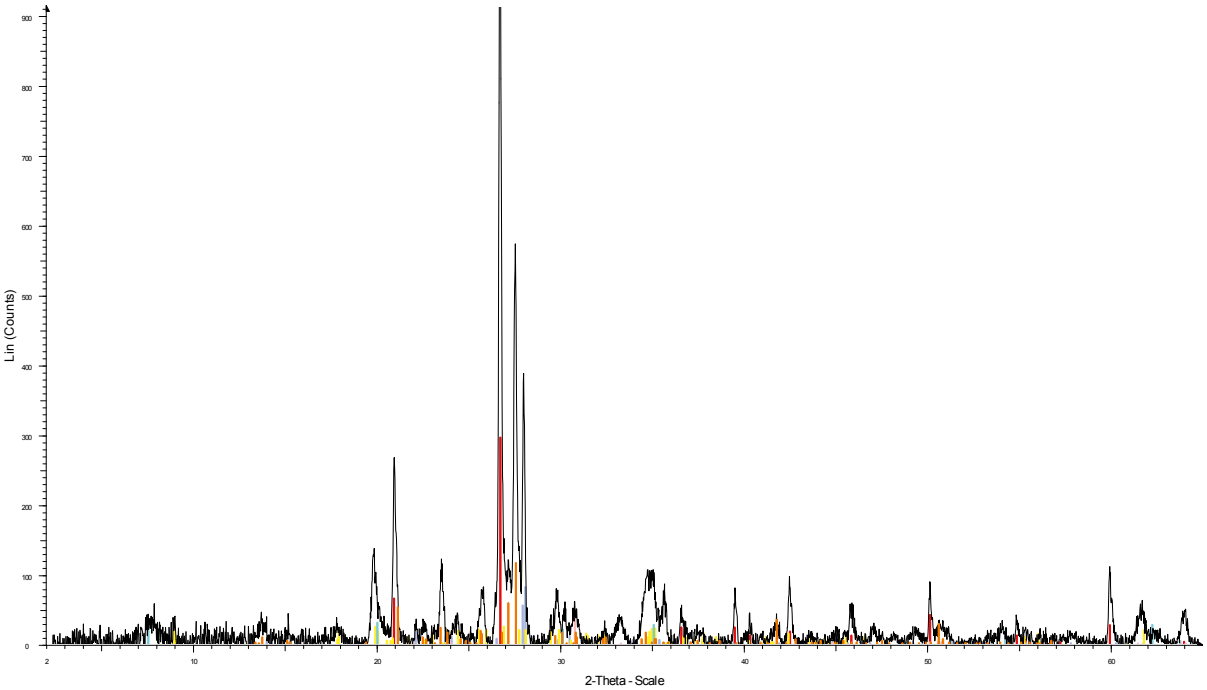

C:\data\DIFFDAT1\Erik\UPPDRAG 2010\KFR19 90_56 WR.RAW - File: KFR19 90_56 WR.RAW - Type: 2Th/Th locke 02-0037 (D) - Montmorillonite - Al5i2O6(OH)2 - Y: 3.04 % - d x by: 1.000 - WL: 1.54056
Operations: Background 1.000,1.000 | Import
33-1161 (*) - Quartz, syn - SiO2 - Y: 26.56 % - d x by: 1.000 - WL: 1.54056
19-0932 (I) - Microcline, intermediate - KAlSi3O8 - Y: 10.42 % - d x by: 1.000 - WL: 1.54056
41-1480 (I) - Albite, calcian, ordered - (Na,Ca)Al(Si,Al)3O8 - Y: 7.29 % - d x by: 1.000 - WL: 1.54056
34-0175 (C) - Muscovite-2M2 - (K,Na)Al2(Si,Al)4O10(OH)2 - Y: 2.23 % - d x by: 1.000 - WL: 1.54056
41-0586 (*) - Ankerite - Ca(Fe,Mg)(CO3)2 - Y: 3.47 % - d x by: 1.000 - WL: 1.54056
02-0056 (D) - Illite - KAl2Si3AlO10(OH)2 - Y: 2.22 % - d x by: 1.000 - WL: 1.54056

KFR19 91.05 WR

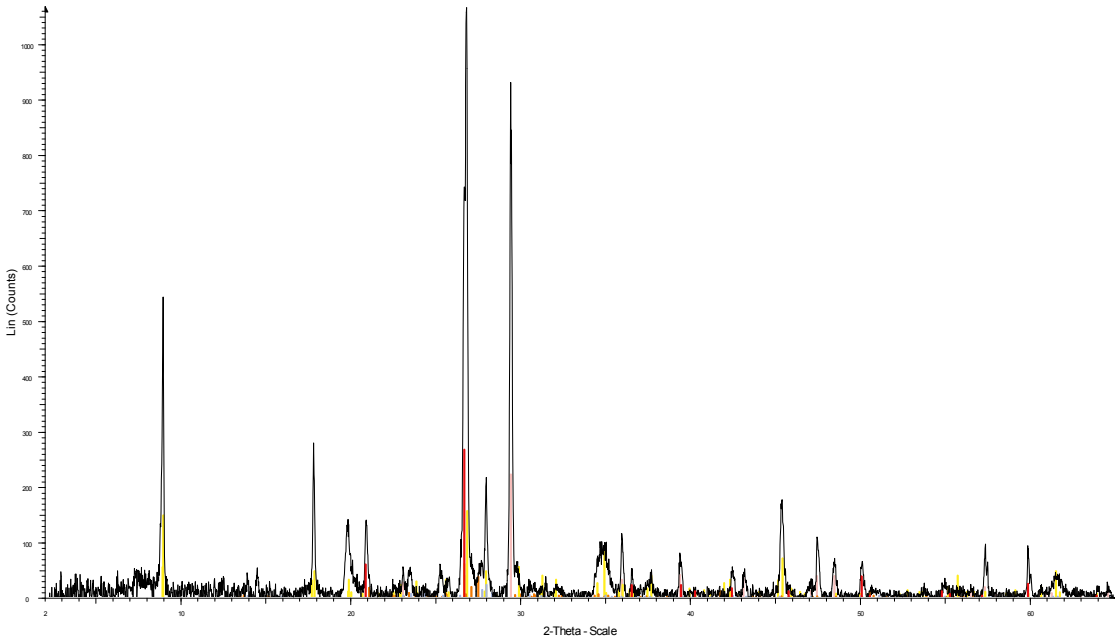

C:\data\DIFFDAT1\Erik\UPPDRAG 2010\KFR19 91_05 WR.RAW - File: KFR19 91_05 WR.RAW - Type: 2Th/Th locked - Start: 2.000 ° - End: 65.000 ° - Step: 0.020 ° - Step time: 1.0 s - Temp.: 27.0 °C - Time Started: 3 s - 2-Theta: 2.000 ° -
Operations: Background 1.000,1.000 | Import
33-1161 (*) - Quartz, syn - SiO2 - Y: 25.00 % - d x by: 1.000 - WL: 1.54056
05-0586 (*) - Calcite, syn - CaCO3 - Y: 20.83 % - d x by: 1.000 - WL: 1.54056
06-0263 (I) - Muscovite-2M1 - KAl2(Si3Al)O10(OH,F)2 - Y: 14.58 % - d x by: 1.000 - WL: 1.54056
19-0932 (I) - Microcline, intermediate - KAlSi3O8 - Y: 3.47 % - d x by: 1.000 - WL: 1.54056
26-0911 (I) - Illite-2M1 - (K,H3O)Al2Si3AlO10(OH)2 - Y: 5.64 % - d x by: 1.000 - WL: 1.54056
20-0554 (D) - Albite, ordered - NaAlSi3O8 - Y: 2.08 % - d x by: 1.000 - WL: 1.54056

KFR105 126.90 WR

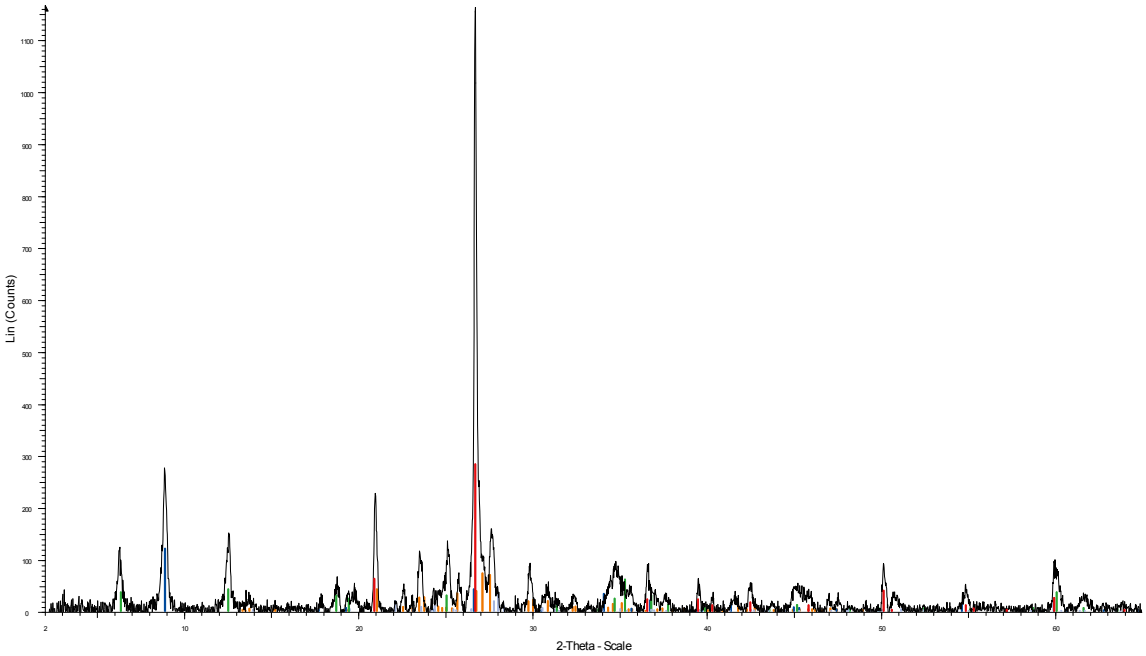

C:\data\DIFFDAT1\Erik\UPPDRAG 2010\KFR105 126_90 WR.RAW - File: KFR105 126_90 WR.RAW - Type: 2Th/Th locked - Start: 2.000 ° - End: 65.000 ° - Step: 0.020 ° - Step time: 1.0 s - Temp.: 27.0 °C - Time Started: 3 s - 2-Theta: 2.0(
Operations: Background 1.000,1.000 | Import
33-1161 (*) - Quartz, syn - SiO2 - Y: 24.31 % - d x by: 1.000 - WL: 1.54056
22-0675 (D) - Microcline, intermediate - KAlSi3O8 - Y: 6.25 % - d x by: 1.000 - WL: 1.54056
42-1437 (I) - Biotite-1M - K(Mg,Fe+2)3(Al,Fe+3)Si3O10(OH,F)2 - Y: 10.33 % - d x by: 1.000 - WL: 1.54056
07-0077 (D) - Clinoclore - Mg-Fe-Al-Si-Al-O-OH - Y: 5.21 % - d x by: 1.000 - WL: 1.54056
20-0554 (D) - Albite, ordered - NaAlSi3O8 - Y: 2.73 % - d x by: 1.000 - WL: 1.54056

KFR105 280.07 WR

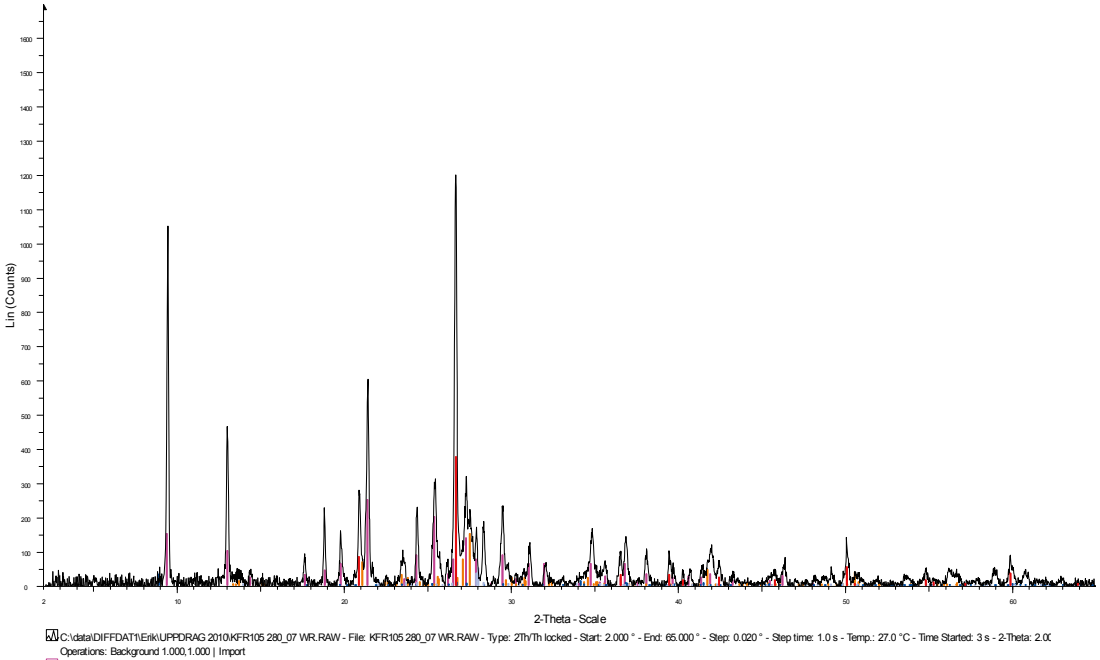

C:\data\DIFFDAT1\Erik\UPPDRAG 2010\KFR105 280_07 WR.RAW - File: KFR105 280_07 WR.RAW - Type: 2Th/Th locked - Start: 2.000 ° - End: 65.000 ° - Step: 0.020 ° - Step time: 1.0 s - Temp.: 27.0 °C - Time Started: 3 s - 2-Theta: 2.0(
Operations: Background 1.000,1.000 | Import
26-1047 (I) - Laumontite, syn - CaAl2Si4O12.4H2O - Y: 20.83 % - d x by: 1.000 - WL: 1.54056
33-1161 (*) - Quartz, syn - SiO2 - Y: 31.25 % - d x by: 1.000 - WL: 1.54056
19-0932 (I) - Microcline, intermediate - KAlSi3O8 - Y: 12.50 % - d x by: 1.000 - WL: 1.54056
42-1339 (C) - Biotite-2M1 - KMg3(Si3Al)O10(OH)2 - Y: 2.61 % - d x by: 1.000 - WL: 1.54056
41-1480 (I) - Albite, calcian, ordered - (Na,Ca)Al(Si,Al)3O8 - Y: 4.17 % - d x by: 1.000 - WL: 1.54056

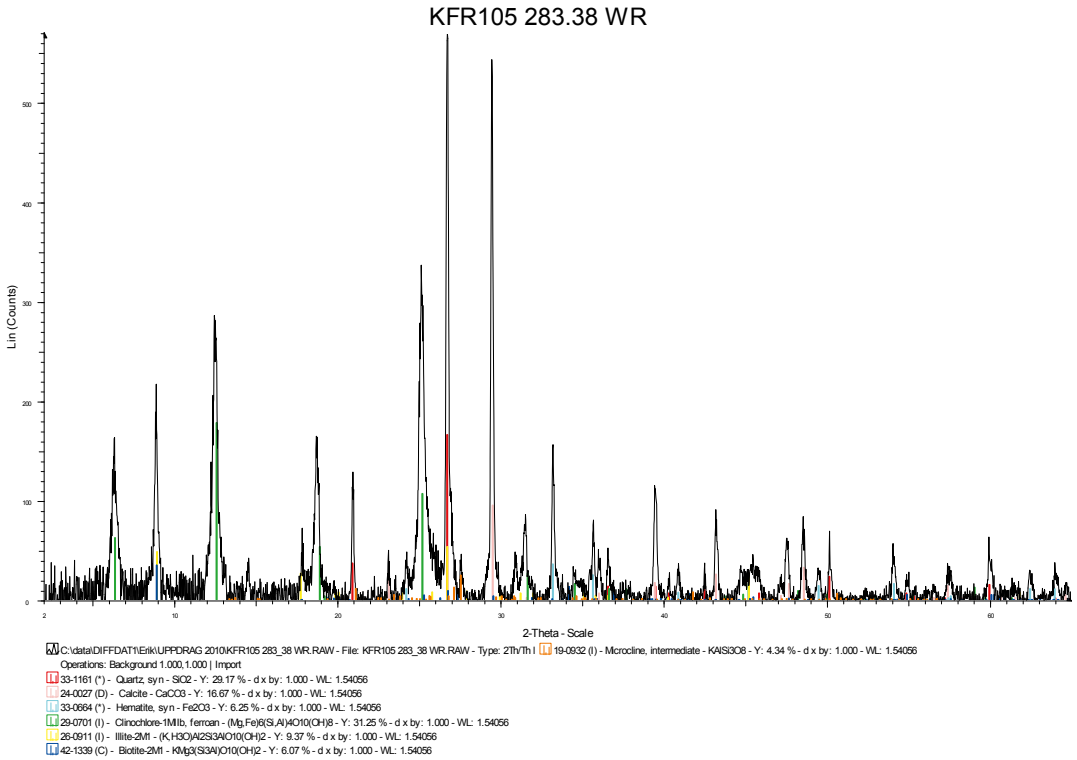
KFR105 283.38 WR
Lin (Counts)
0
100
200
300
400
500
2
10
20
30
40
50
60
2-Theta - Scale
C:\data\DIFFDAT\1\Erik\UPPDRAG 2010\KFR105 283_38 WR.RAW - File: KFR105 283_38 WR.RAW - Type: 2Th/Th l
19-0932 (I) - Microcline, intermediate - KAlSi3O8 - Y: 4.34 % - d x by: 1.000 - WL: 1.54056
Operations: Background 1.000,1.000 | Import
33-1161 (*) - Quartz, syn - SiO2 - Y: 29.17 % - d x by: 1.000 - WL: 1.54056
24-0027 (D) - Calcite - CaCO3 - Y: 16.67 % - d x by: 1.000 - WL: 1.54056
33-0664 (*) - Hematite, syn - Fe2O3 - Y: 6.25 % - d x by: 1.000 - WL: 1.54056
29-0701 (I) - Clinochlore-1M1b, ferroan - (Mg,Fe)6(Si,Al)4O10(OH)8 - Y: 31.25 % - d x by: 1.000 - WL: 1.54056
26-0911 (I) - Illite-2M1 - (K,H3O)Al2Si3AlO10(OH)2 - Y: 9.37 % - d x by: 1.000 - WL: 1.54056
42-1339 (C) - Biotite-2M1 - KMg3(Si3Al)O10(OH)2 - Y: 6.07 % - d x by: 1.000 - WL: 1.54056

XRD SPECTRAS
CLAY MINERAL ANALYSIS (ORIENTED SAMPLES)

Black line: dry sample Blue line: ethyleneglycol saturated Red line: after heating to 400°C

KFR01 45.18 orienterat prov. Svart kurva=torrt prov, blå=EG-mättat, röd=upphettat

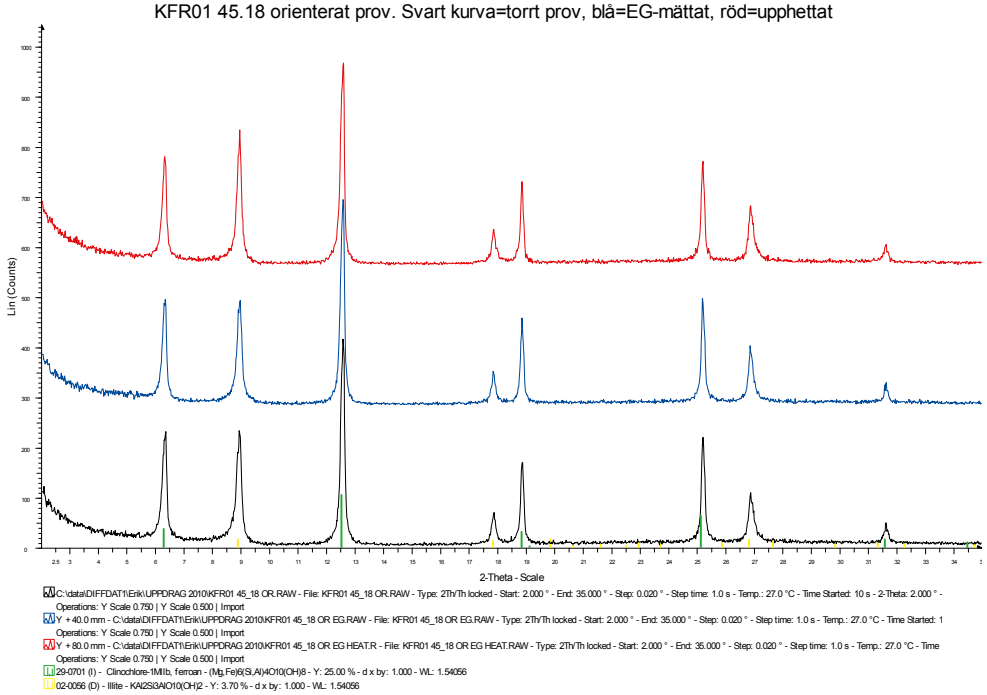

KFR07A 49.6 orienterat prov. Svart kurva=torrt prov, blå=EG-mättat, röd=upphettat

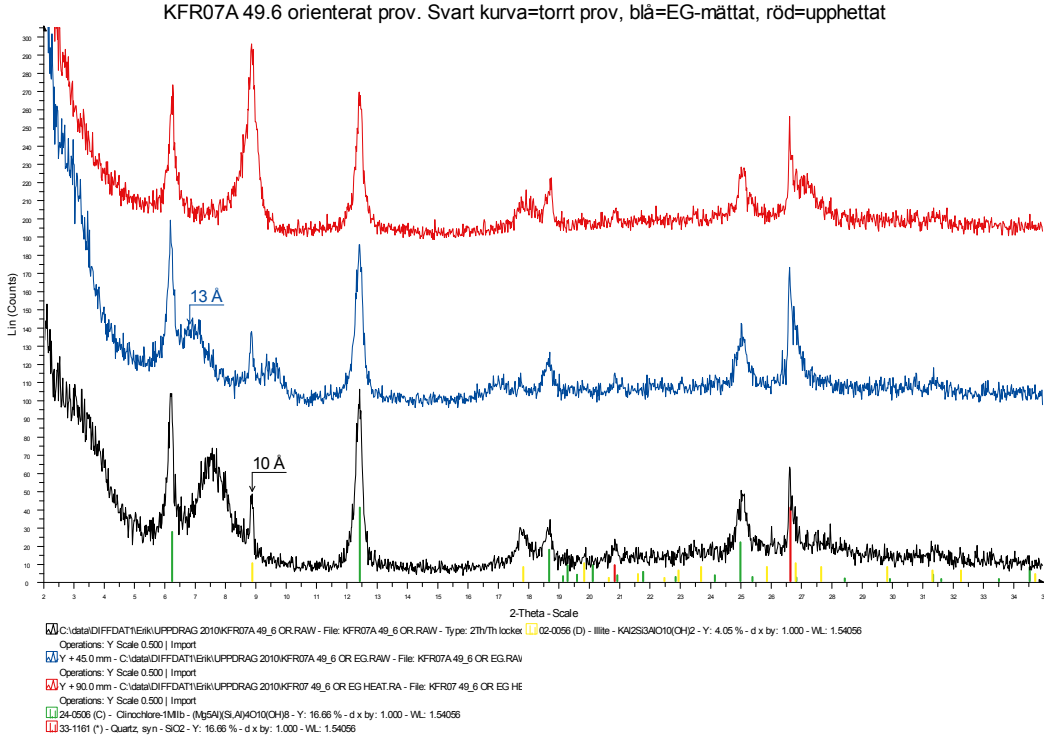

Black line: dry sample
Blue line: ethyleneglycol saturated
Red line: after heating to 400°C

KFR07A 70.05 orienterat prov. Svart kurva=torrt prov, blå=EG-mättat, röd=upphettat

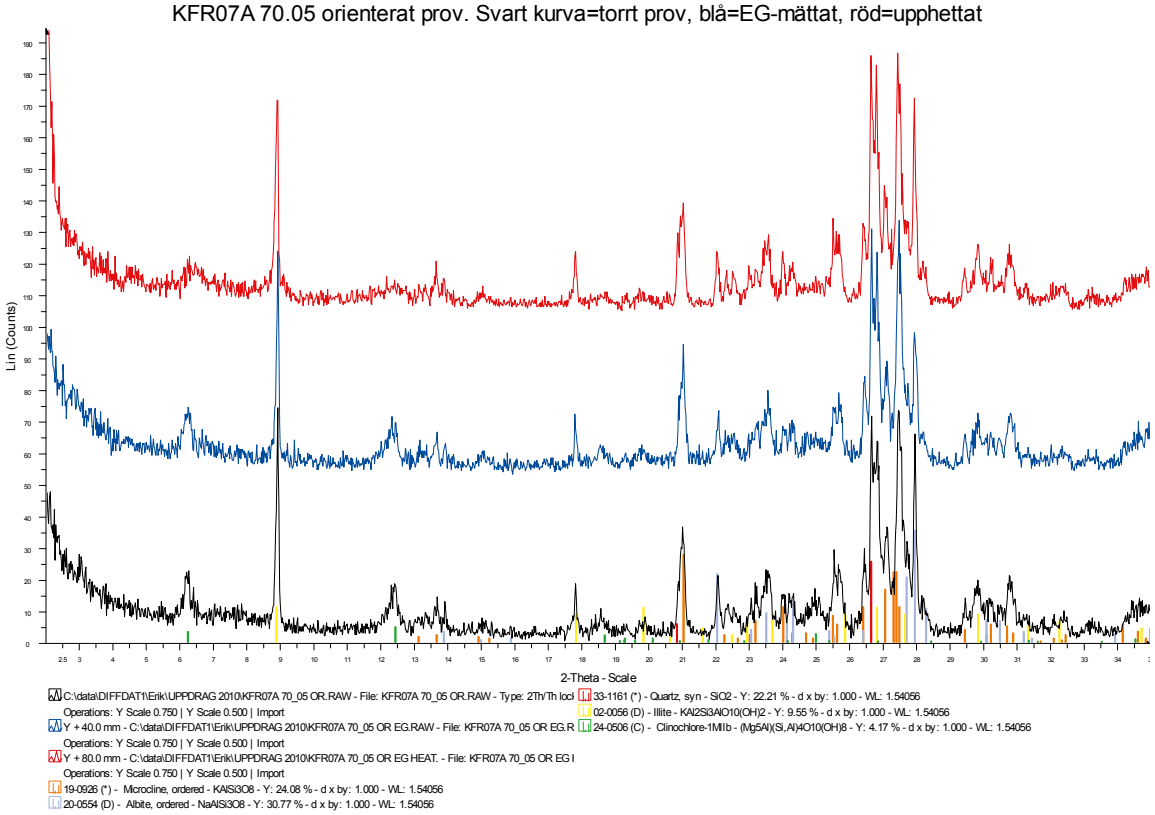

KFR07A 70.47 orienterat prov. Svart kurva=torrt prov, blå=EG-mättat, röd=upphettat

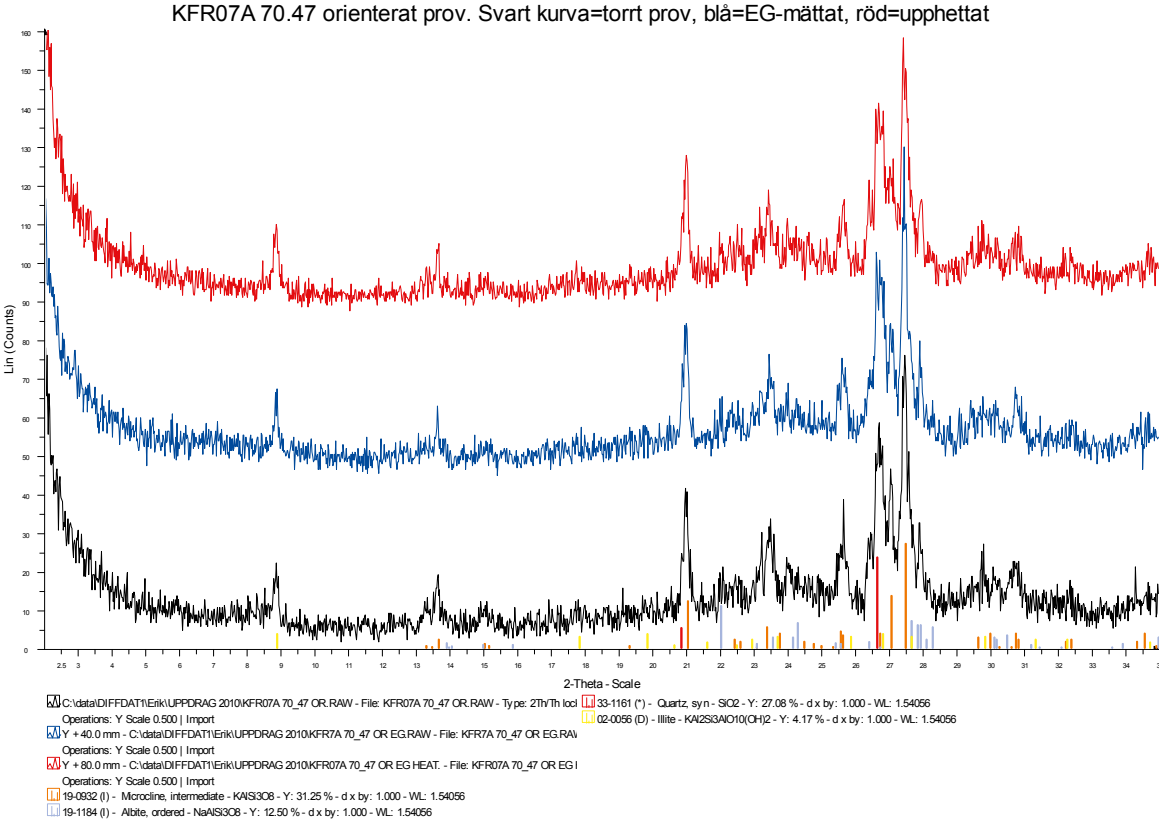

Black line: dry sample
Blue line: ethyleneglycol saturated
Red line: after heating to 400°C

KFR08 76.77 orienterat prov. Svart kurva=torrt prov, blå=EG-mättat, röd=upphettat

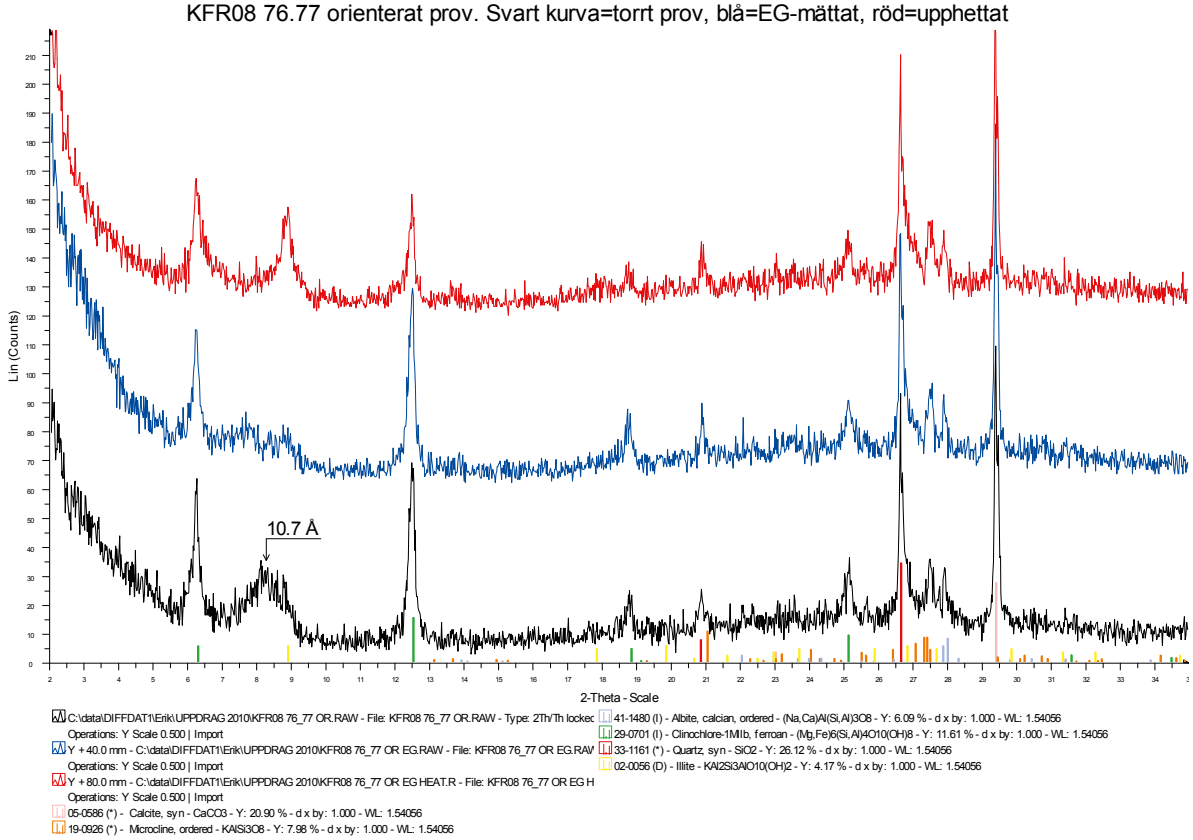

KFR08 79.13 orienterat prov. Svart kurva=torrt prov, blå=EG-mättat, röd=upphettat

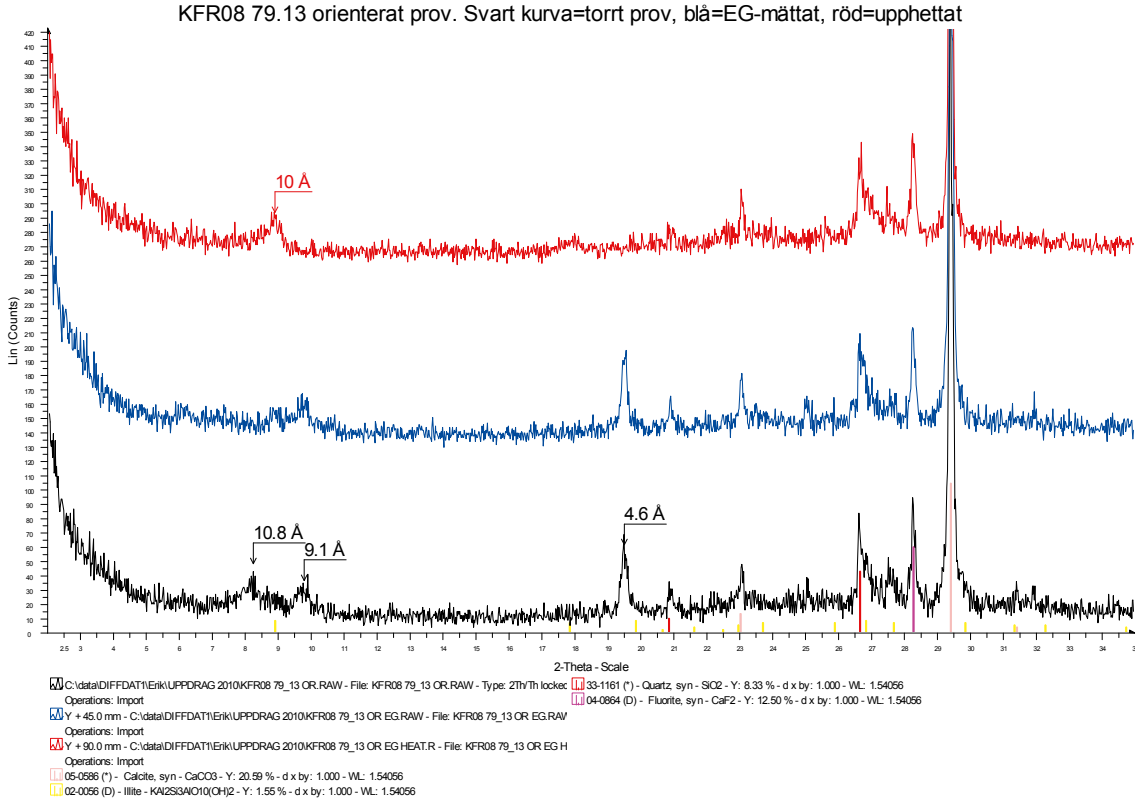

Black line: dry sample
Blue line: ethyleneglycol saturated
Red line: after heating to 400°C

KFR08 95.29 orienterat prov. Svart kurva=torrt prov, blå=EG-mättat, röd=upphettat

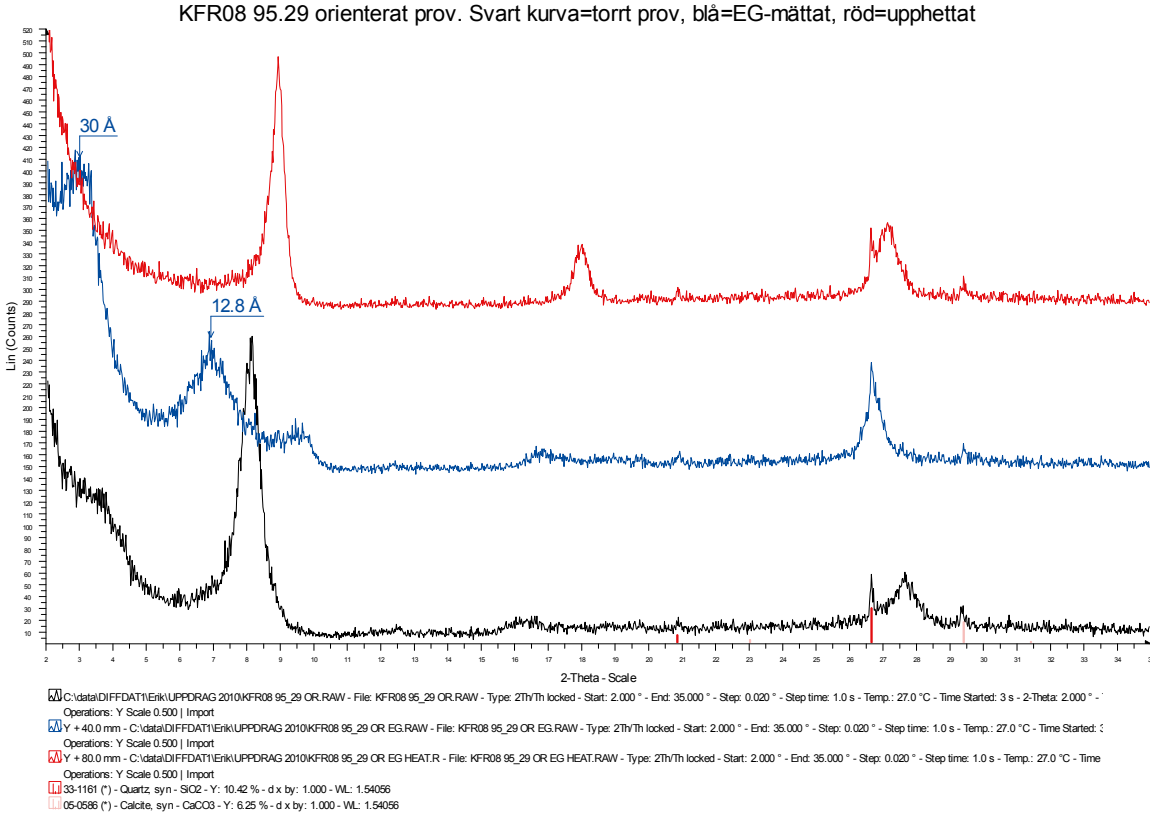

KFR10 95.65 orienterat prov. Svart kurva=torrt prov, blå=EG-mättat, röd=upphettat

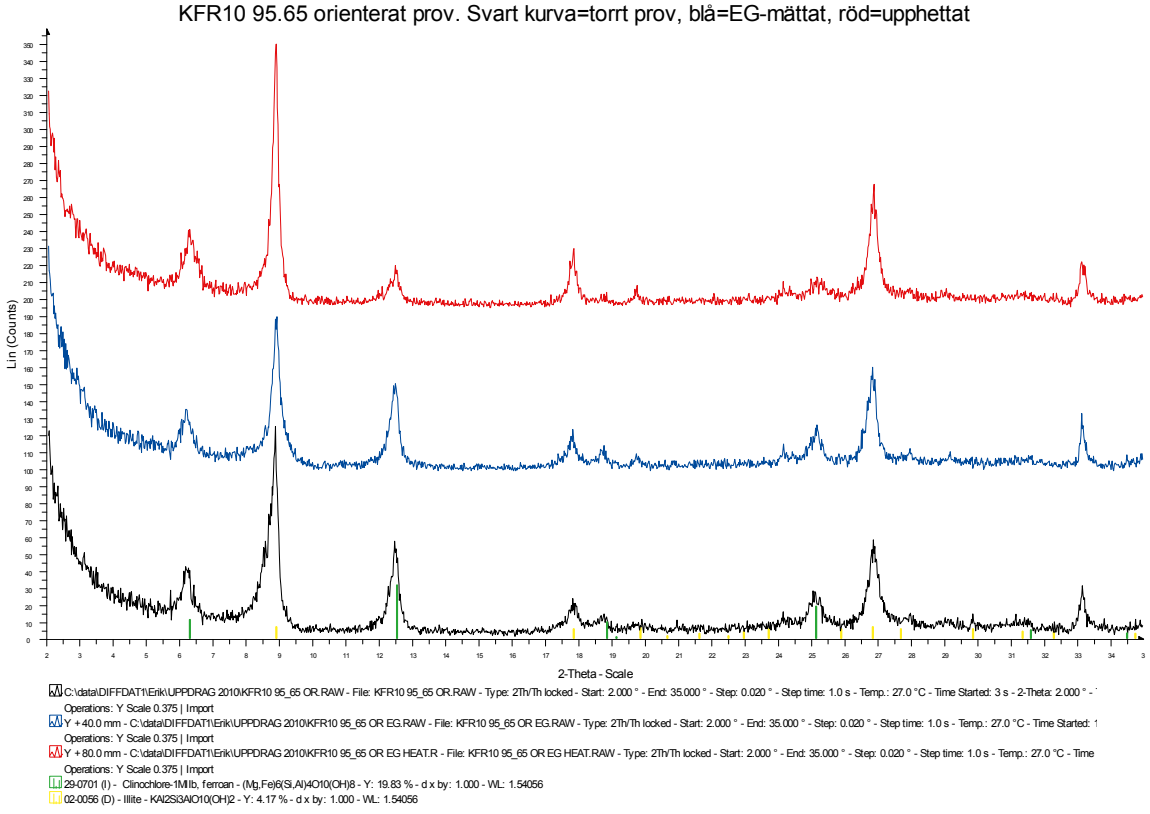

Black line: dry sample
Blue line: ethyleneglycol saturated
Red line: after heating to 400°C

KFR19 90.56 orienterat prov. Svart kurva=torrt prov, blå=EG-mättat, röd=upphettat

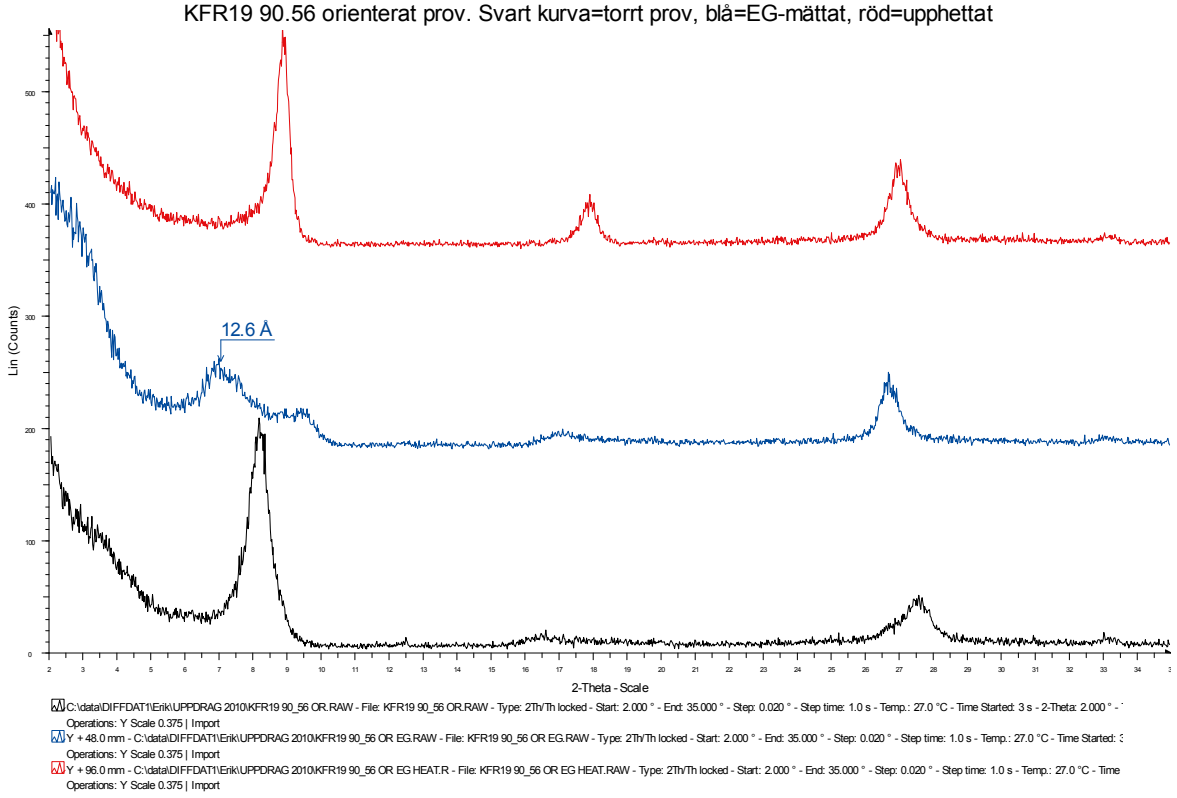

KFR19 91.05 orienterat prov. Svart kurva=torrt prov, blå=EG-mättat, röd=upphettat

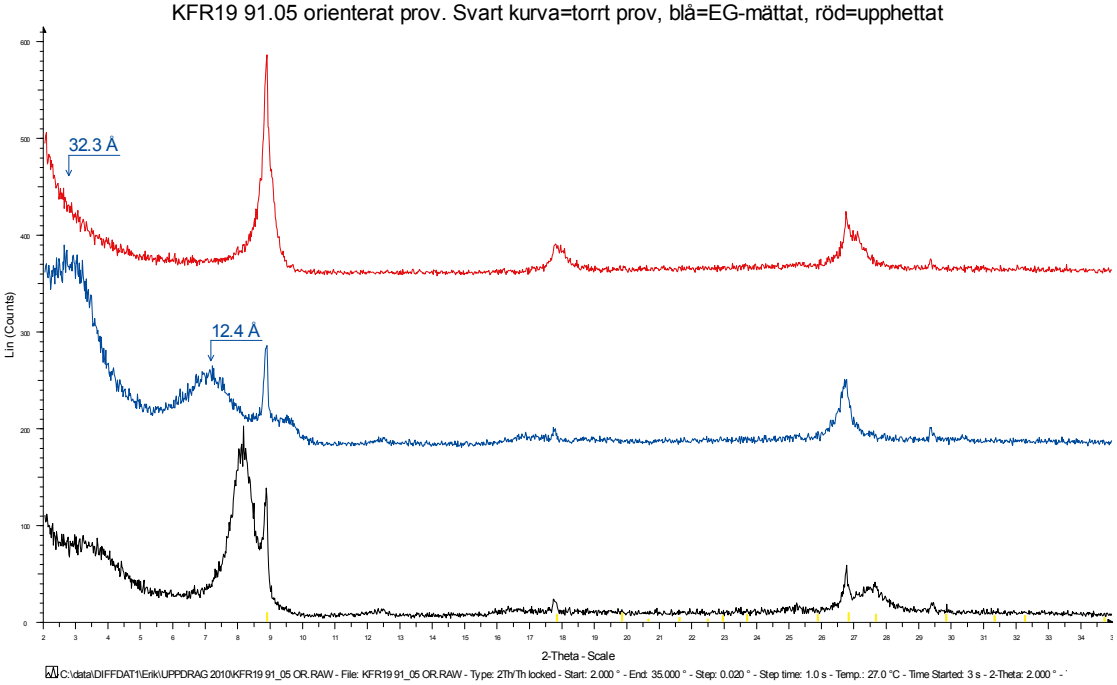

Black line: dry sample
Blue line: ethyleneglycol saturated
Red line: after heating to 400°C

KFR105 126.90 orienterat prov. Svart kurva=torrt prov, blå=EG-mättat, röd=upphettat

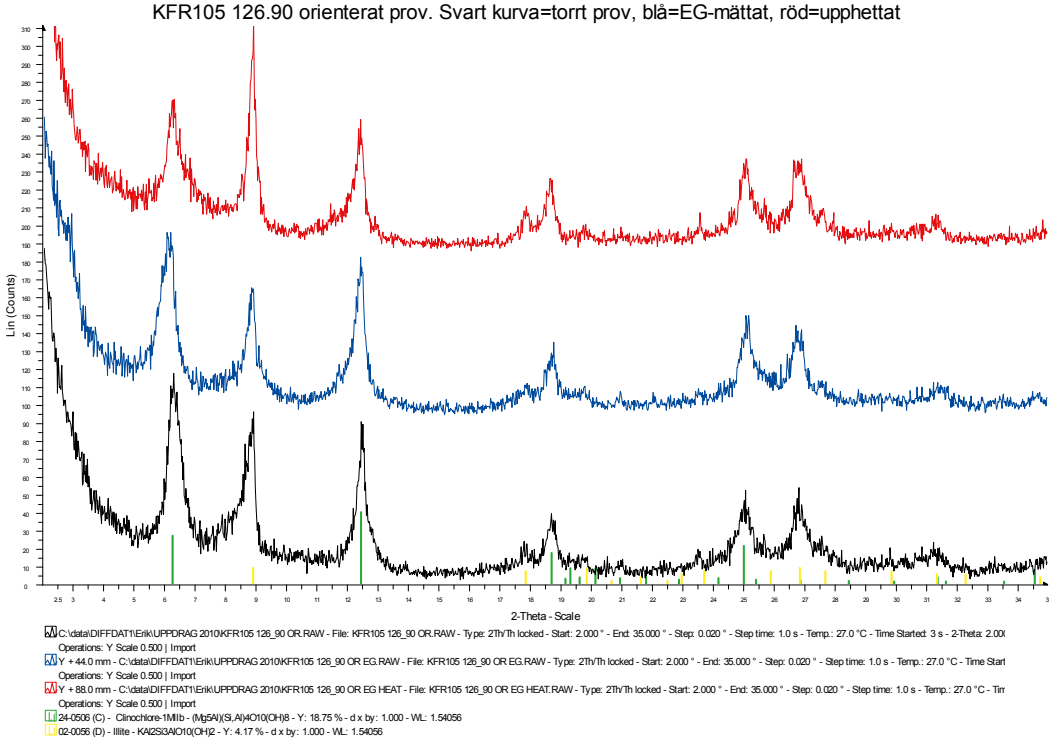

KFR 105 280.07 orienterat prov. Svart kurva=torrt prov, blå=EG-mättat, röd=upphettat

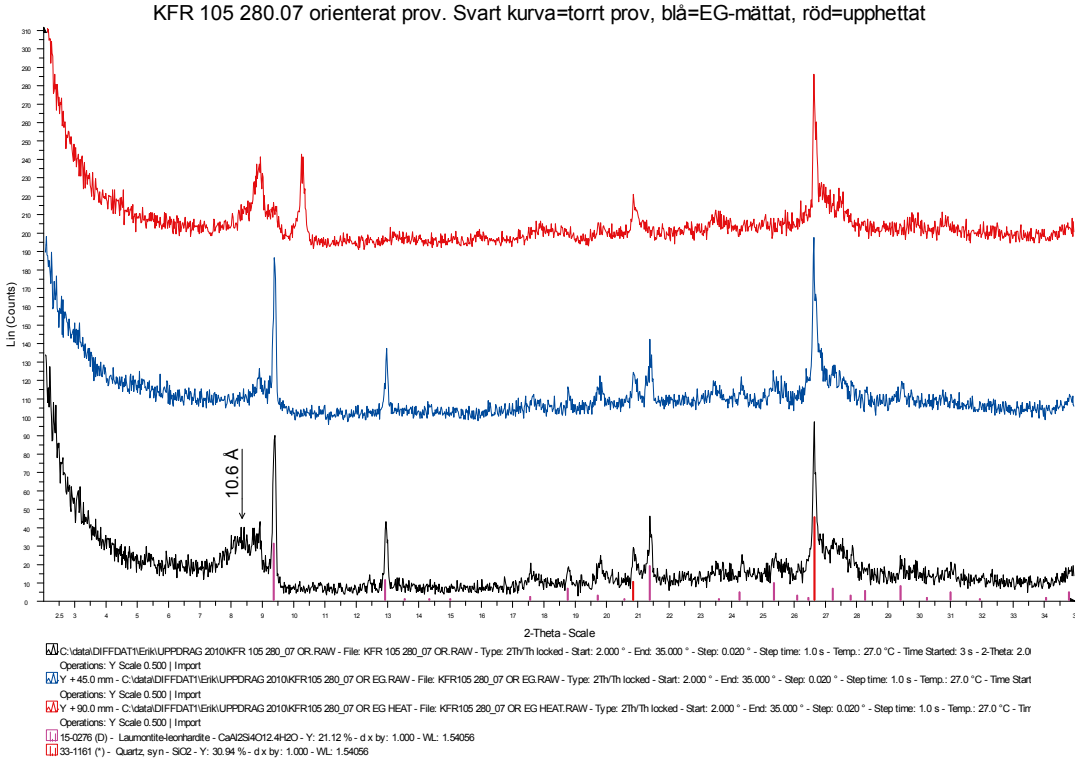

Black line: dry sample
Blue line: ethyleneglycol saturated
Red line: after heating to 400°C

KFR105 283.38 orienterat prov. Svart kurva=torrt prov, blå=EG-mättat, röd=upphettat